SLAC-PUB-1152

Photoproduction and Electroproduction

F. J. Gilman

Stanford Linear Accelerator Center, Stanford University, Stanford, California U.S.A.

Published in Physics Reports 4C, No. 3 (1972).

F. GILMAN

F. J. GILMAN

Stanford Linear Accelerator Center, Stanford University, Stanford, California

I Introduction

Electromagnetism has long been an important tool in investigating the structure of matter. Whether one thinks of the experiments of Rutherford on alpha particle scattering which led to the discovery of the nucleus, the classification of optical spectral lines and the discovery of discrete atomic energy levels, or the experiments of Stern and Gerlach and the quantization of spin, just to cite a few examples, many of the most important conceptual advances in physics during this century have involved experiments which used the electromagnetic interaction as a probe. With the advent of high energy electron accelerators in the past few decades, the structure of the strongly interacting particles, the hadrons, is now also being examined in detail with an electromagnetic probe through study of the interactions of high energy photon and electron beams with nucleons and nuclei.

In these lectures we will discuss some of the knowledge and theoretical understanding that has been gained, and that we could hope to gain, from the study of photoproduction and electroproduction of hadrons. As we proceed we will emphasize in turn two different aspects of (real or virtual) photon-hadron reactions: (1) Photon-hadron collisions as just another kind of hadron-hadron

reaction, with cross sections smaller by roughly a factor of $\alpha = e^2/4\pi \simeq 1/137$ to be sure, but with all the essential features of hadron-hadron collisions and all the attendant successes and failures in our theoretical understanding.

(2) Photon-hadron reactions, or more exactly, matrix elements of the electromagnetic current between hadron states, considered to lowest order in the electromagnetic coupling constant but to all orders in the strong interactions as a unique way of obtaining the algebraic properties of the electromagnetic current under commutation with other currents or operators, of probing hadron structure in general, and of searching for possible hadron substructure. The first of these aspects will be the central theme in the lectures on photoproduction, while the second aspect will be emphasized more in the later lectures on electroproduction.

In the case of photoproduction, we shall see that the total cross section for hadron production and the various two body and quasi-two body final state processes generally behave very much as their hadronic analogs do. Thus the theoretical considerations involved are very much the same as in strong interactions, and we have chosen to concentrate on certain specific photon induced reactions as illustrative of the application of dispersions relations, finite energy sum rules, Regge poles and cuts, duality, etc., which are used in the theoretical treatment of strong interactions processes. From a phenomenological point of view, photoproduction processes offer the advantage that many photon induced two body or quasi-two body reactions are more systematically measured over large ranges of energy and momentum transfer in single experiments than their hadronic analogs, and, given existence of high energy polarized photon beams, the dependence on photon polarization of many photon induced reactions is accessible to measurement. These measurements have

revealed both interesting simplicities and complications which were almost totally unexpected from the differential cross section measurements alone, and which provide strong restrictions on theories of two body processes.

II The Electromagnetic Interaction

A Classical and Quantum Electrodynamics

The development of classical electrodynamics is, perhaps, the greatest triumph of nineteenth century physics. As summarized in Maxwell's equations, it provides a theory of the electromagnetic field and its interaction with stationary and moving charges, i.e. currents. It was quite logical that after the development of quantum mechanics, which involved the change of the classical position and momentum variables into operators with specified commutation relations, the same rules would be applied to the electromagnetic field [1]. With the application of the quantization rules ("second quantization") the fields become operators with associated quanta, photons. The quantized electromagnetic field, together with the quantized electron (and positron) field and the Dirac theory of their electromagnetic interaction forms the basic part of the theory of quantum electrodynamics. Its development may be traced in the original papers collected in reference 1.

Quantum Electrodynamics, as extended into a systematic, perturbative calculational scheme with a renormalization procedure by Feynman, Tomonaga and Schwinger, is presently in magnificent agreement with experiment[2]. Particularly the recent calculation[3] of the photon-photon scattering contributions to the sixth order contributions to the muon magnetic moment, and the recalculation[4] of the slope of the Dirac from factor of the electron in fourth order as it contributes to the Lamb shift, have resolved any remaining discrepancies between theory and experiment. Present precision experiments on atomic systems and high energy experiments with large momentum transfers indicate agreement with theory to an accuracy[2], which, when expressed as a momentum

cut-off in the theory corresponds to several GeV, and when expressed as a distance corresponds to roughly 10^{-14}cm. Moreover, the most recent tests of Coulomb's law by the Cavendish method give[5]

$$q = (2.7 \pm 3.1) \times 10^{-16}$$

if the deviation of Coulomb's law is of the form $1/r^{2+q}$, which corresponds to a limit on the photon rest mass,

$$m_\gamma < 1.6 \times 10^{-47}\ g,$$

and is comparable to the limit[6]

$$m_\gamma < 4 \times 10^{-48}\ g,$$

obtained from the agreement of the earth's magnetic field with Ampere's law out to distances of order 5×10^{10}cm. As emphasized by Brodsky and Drell in their review[2], the combination of classical and quantum electrodynamics thus works for lengths ranging over 25 orders of magnitude, an incredible domain spanning the subnuclear as well as cosmic.

B The Electromagnetic Current of Hadrons

In complete analogy to Quantum Electrodynamics, where the quantized electromagnetic field interacts with the electromagnetic current of the leptons, $j_\mu^{\text{leptons}}(x)$, the electromagnetic interaction of hadrons is also to be formulated in terms of the electromagnetic field interacting with a local vector current, $J_\mu^{\text{hadrons}}(x)$. To lowest order in the electromagnetic coupling, e, it is then matrix elements of this current, taken between the appropriate hadron states, which are measured in experiments involving the electromagnetic interactions

of hadrons. The corresponding charge operator of the hadrons is given by the space integral over the charge density[7]:

$$Q = Q(t) = -i\int d^3x\, J_4(\vec{x}, t). \tag{1}$$

The charge is of course conserved and independent of time, corresponding to a conserved current,

$$\frac{\partial}{\partial x_\mu} J_\mu(x) = 0. \tag{2}$$

Conventionally the internal quantum numbers of the electromagnetic current are taken to be the same as those of the charge. These can be read off from the Gell-Mann - Nishijima formula[8],

$$Q = e(I_3 + \frac{Y}{2}) \tag{3}$$

where e is the proton charge, I_3 is the third component of isotopic spin, and Y is the hypercharge equal to the sum of B (baryon number) and S (strangeness), all of which are additively conserved quantities. Under isospin transformations in particular, from Eq. (3) the charge behaves as the sum of an isoscalar and an isovector, so that only $|\Delta I| \leq 1$ transitions can be induced by the current if it has the same transformation properties as the charge. Since the G parity of such a neutral, non-strange current is given by $C(-1)^I$ and the conventional current has charge conjugation properties corresponding to C = -1, the isoscalar and isovector components of the electromagnetic current have G parity -1 and +1, respectively.

Although the simplest possibility certainly is to have the electromagnetic current possess the same transformation properties under internal symmetries

as the charge, this is not forced on us by general principles. In recent years two possibilities for components of the electromagnetic current have been discussed a great deal which do not reflect the simple intuitive idea of currents as moving charges:

1. First is the possiblity that there is a component of the current with isospin I=2. The lack of experimental evidence against this possibility was first pointed out by Grishin et al.[9] and by Dombey and Kabir[10], and has recently been stressed again by Sanda and Shaw[11] who make the further claim that in fact experimental evidence for an I=2 component now exists from comparison of π^+ and π^- photoproduction in the region of the first resonance.

Their claim is based on the observation that the total cross section difference,

$$\Delta = \frac{k}{q}\left[\sigma_T(\gamma n \to \pi^- p) - \sigma_T(\gamma p \to \pi^+ n)\right], \qquad (4)$$

where k and q are the photon and pion center of mass momenta respectively, should be slowly varying with energy in the first resonance region if $|\Delta I| \leq 1$, since an isospin $\frac{3}{2}$ resonance then gives a contribution which would cancel in the cross section difference of Eq. (4). Since the available data[12] indicate that Δ varies rapidly as the energy is varied through the first resonance region, Sanda and Shaw took this as indicative of an I=2 component of the current.

However, as pointed out by others[13, 14], this test for an I=2 component of the current is not unambiguous and relies on some additional knowledge of the non-resonant amplitudes, which Sanda and Shaw take from dispersion theory predictions. At present, in addition to the introduction of an isotensor term,

one still has the possibilities that:

(a) The data for $\sigma_T(\gamma n \rightarrow \pi^- p)$, which come from photoproduction of π^- mesons from deuterium and have rather large errors, should be systematically renormalized to higher values (by $\sim$ 20%).

(b) The electric and magnetic dipole transitions of the neutron to the $J = \frac{1}{2}$ pion-nucleon final state do not agree with the simple dispersion theory predictions, with the electric dipole amplitude in particular being strongly energy dependent[13].

The question of the existence of an isotensor term should then still be regarded as unsettled. Further experiments, particularly[14] measurements of $\gamma n \rightarrow \pi^0 n$, are needed before the definite presence or absence of an I=2 component of the electromagnetic current is established on the basis of pion photoproduction experiments.

2. Second, it was noted by Bernstein, Feinberg, and Lee[15] following the discovery[16] of CP non-invariance in the decay of K_L^0 mesons that although invariance of electromagnetic interactions under parity (space reflections) was well established from nuclear physics experiments, the experimental evidence for C (charge conjugation) invariance was almost totally lacking at that time. Assuming CPT invariance, which follows from sacred principles of local field theory, then C non-invariance, together with parity invariance, implies CP and therefore T violation in electromagnetic interactions. The presence of such a violation may be invoked to explain the existence of CP violation in K_L^0 decay as well as its approximate magnitude. Such a failure of C invariance may be looked upon as due to a mismatch[17] between the charge conjugation and time reversal operators of the strong and electromagnetic interactions, so that if C is the charge conjugation

operator of strong interactions,

$$CJ_\mu(x)C^{-1} \neq -J_\mu(x). \tag{5}$$

Thus charge conjugation violation in electromagnetic interactions corresponds to the current

$$K_\mu(x) = \frac{1}{2}\left[J_\mu(x) + CJ_\mu(x)C^{-1} \right] \tag{6}$$

with the property

$$CK_\mu(x)C^{-1} = +K_\mu(x) \tag{7}$$

not being identically zero. However the corresponding charge,

$$Q_K = -i\int d^3x\, K_4(\vec{x}, t), \tag{8}$$

is still conserved, and all known hadrons must have $Q_K=0$ since they are known to have total charges which change sign under the operator C. Even given the restriction that $Q_K=0$, it is still possible to exhibit explicit Lagrangian models[18] utilizing higher spin fields which have $Q_K=0$ but $K_\mu(x) \neq 0$.

Since the proposal of Bernstein et al.[15], a rather large number of experiments have been performed looking for C and T invariance violation in electromagnetic processes. The results of these experiments can be very briefly summarized by the statement that there is presently no conclusive evidence for C or T violation. Particular examples of photoproduction and electroproduction experiments searching for such a violation include:

(a) Measurement of the up-down asymmetry in inelastic electron scattering with a polarized target, as suggested by Christ and Lee[19], The data[20] are consistent with zero asymmetry (i.e., no T violation) within errors of a few percent, particularly in the region of the second and third pion-nucleon resonanaces where T violation due to an I=0 current $K_\mu^{(0)}$ should manifest itself.

(b) A search for a failure of reciprocity (T violation) between $\gamma d \rightarrow np$ and $np \rightarrow \gamma d$. Experiment[21] indicates no failure to within errors of a few percent at energies where the first resonance is an important (virtual) intermediate state and T violation due to an I=1 current $K_\mu^{(1)}$ should be present.

(c) A search for a failure of reciprocity (T violation) between $\gamma n \rightarrow \pi^- p$ and $\pi^- p \rightarrow \gamma n$. Recent radiative capture experiments[22] indicate a discrepancy of about two standard deviations with the π^- photoproduction measurements on deuterium near the first resonance, but not at higher energy. This has led Sanda and Shaw[23] to suggest a model where C violation is produced only by a component of an isotensor current, $K_\mu^{(2)}$. Resolution of the question of whether this failure of T invariance is only apparent, however, rests on the $\gamma n \rightarrow \pi^- p$ experiments and the related question of a possible isotensor current. Much better experiments on both photoproduction off deuterium and radiative capture are needed before any T violation is established in this particular process.

Thus, although the evidence for the proposition that the electromagnetic current as well as the charge behave under internal symmetry transformations according to Eq. (3) is not compelling, there are no experiments conclusively showing the opposite. In the following we will assume this proposition to be true, keeping in mind the need for better experimental verification.

C Vector Meson Dominance

The amplitude for the electromagnetic transition $\gamma + A \rightarrow B$ between hadron states A and B is proportional to $\epsilon_\mu \langle B | J_\mu | A \rangle$ if ϵ_μ is the polarization vector of the photon. The matrix element $\langle B | J_\mu | A \rangle$ may in general be decomposed into a sum of products of tensors which depend on the momenta and spins of the hadrons A and B times Lorentz invariant scalar amplitudes. If we consider dispersion relations in the photon's four-momentum squared for such amplitudes, they may be dominated by low mass vector meson poles[24], very much as dispersion relations for matrix elements of the divergence of the axial-vector current are dominated by the pion pole[25]. In other words, if $F_{AB}(q^2)$ is an invariant amplitude or form factor for the process $\gamma + A \rightarrow B$, with photon four-momentum $q_\mu = (p_B - p_A)_\mu$, then a dispersion relation for $F_{AB}(q^2)$,

$$F_{AB}(q^2) = \frac{1}{\pi} \int_{M_0^2}^{\infty} dM^2 \; \frac{\mathrm{Im} F_{AB}(M^2)}{q^2 + M^2} \; , \qquad (9)$$

may be dominated, at least for small values of q^2, by the vector meson poles which are closest to $q^2 = 0$. To be specific, let us consider the isovector part of the electromagnetic current only, so that the rho meson is the lowest mass pole in the dispersion relation. Then, ignoring the width of the rho meson

$$F_{AB}(q^2) = \frac{\left(\frac{em_\rho^2}{f_\rho}\right) g_{\rho AB}}{q^2 + m_\rho^2} + \frac{1}{\pi} \int_{>m_\rho^2}^{\infty} dM^2 \; \frac{\mathrm{Im} F_{AB}(M^2)}{q^2 + M^2} \; , \qquad (10)$$

where (em_ρ^2/f_ρ) and $g_{\rho AB}$ are coupling constants defining the strength of the photon-rho and A-B-rho transitions at the rho pole. Rho meson dominance is

then just the statement that the integral in Eq. (10) is negligible, so that we obtain the basic result,

$$F_{AB}(q^2) \simeq \left(\frac{em_\rho^2}{f_\rho}\right) g_{\rho AB} \Big/ \left(q^2 + m_\rho^2\right). \tag{11}$$

In the particular case where A and B are the same single hadron, the quantities $F_{AA}(q^2)$ are usually called form factors, and one of them, say $F^Q_{AA}(q^2)$ is the isovector charge form factor which for a hadron A (with non-zero isospin) may be chosen with a normalization such that

$$F^Q_{AA}(0) = e. \tag{12}$$

Combining this with Eq. (11) we obtain

$$\frac{g^Q_{\rho AA}}{f_\rho} \simeq 1 , \tag{13}$$

so that the rho meson is coupled to an arbitrary hadron A (with non-zero isospin) with an approximately universal strength, f_ρ, as long as we can neglect the integral in Eq. (10) for $q^2 = 0$.

Up to this point we have closely followed the discussion of vector meson dominance by Gell-Mann and Zachariasen[24], An alternate path with the same basic final results was taken by Sakurai[26] in the context of a specific field theory with elementary vector mesons. This field theoretical path is clearly formulated in terms of a current-field identity[27]

$$J_\mu^{(3)}(x) = \left(\frac{em_\rho^2}{f_\rho}\right) \rho_\mu(x) \ , \qquad (14)$$

where $J_\mu^{(3)}(x)$ is the isovector electromagnetic current and $\rho_\mu(x)$ is the field of the rho meson. Taking matrix elements of Eq. (14) between hadron states A and B yields

$$\langle B \left| J_\mu^{(3)} \right| A \rangle = \left(\frac{em_\rho^2}{f_\rho}\right) \left(\frac{1}{q^2 + m_\rho^2}\right) \langle B \left| J_\mu^{(\rho)} \right| A \rangle \ , \qquad (15)$$

where $J_\mu^{(\rho)}$ is the rho meson source current, $(\Box + m_\rho^2)\rho_\mu(x) = J_\mu^{(\rho)}(x)$. If we now assume that $\langle B \left| J_\mu^{(\rho)} \right| A \rangle$ is slowly varying in q^2, so that it has the value it takes on at the rho meson pole ($q^2 = -m_\rho^2$), then we recover the basic Eq. (11) and the discussion immediately following it.

Both approaches to vector meson dominanace clearly require making assumptions. In the dispersion theory derivation, we must neglect the integral in Eq. (10), while in the field theoretical derivation we must make a smoothness (or slow variation) assumption. The dispersion theoretic derivation makes it clear though that independent of whether special field theories with elementary fields are applicable (or even exist), approximate vector dominance, Eq. (11) , and universality, Eq. (13), simply follow from the dynamical assumption of the neglect of the continuum integral in Eq. (10).

Conventionally, vector meson dominance has usually come to mean dominance by the rho meson for the isovector electromagnetic current, and by the omega and phi mesons for the isoscalar current. Since if we take matrix

elements of Eq. (14) between the vacuum and one rho meson state we obtain

$$\langle 0 \left| J_\mu(x) \right| \rho \rangle = \left(\frac{em_\rho^2}{f_\rho} \right) \phi_\rho(x) \ , \tag{16}$$

where $\phi_\rho(x)$ is the rho meson wave function, the coupling strength (em_ρ^2 / f_ρ) is directly measurable from rho meson decay into lepton pairs or electron-positron colliding beam experiments where the relevant Feynman amplitude is proportional to $j_\mu^{\text{leptons}} (\delta_{\mu\nu} / q^2) \langle 0 \left| J_\nu(0) \right| \rho \rangle$ with a resultant rho width for decay into lepton pairs $\Gamma(\rho \to e^+ e^-) = \left(\frac{4\pi\alpha^2}{3} \right) \left(m_\rho / f_\rho^{\,2} \right)$. Defining f_ω and f_ϕ analogously to f_ρ in Eq. (14), the Orsay experiments[28] give

$$\begin{aligned} f_\rho^{\,2}/4\pi &= 1.99 \pm 0.11 \\ f_\omega^{\,2}/4\pi &= 14.0 \pm 2.8 \\ f_\phi^{\,2}/4\pi &= 11.0 \pm 0.9 \end{aligned} \tag{17}$$

which, within the vector dominance model, fix once and for all the ratio of strengths between hadron transitions involving photons and those involving the vector mesons ρ, ω, and ϕ.

Within this framework of ρ, ω, and ϕ dominance a number of experimentally testable relations between electromagnetic and hadronic processes have been derived. These have been reviewed in many places (see, in particular, the review of Sakurai[29]) and we shall mention some of the specific tests in these lectures in discussing particular photoproduction reactions. In general, while the quantitive tests of vector meson dominance have sometimes

revealed discrepancies between the theoretical predictions and experimental results, at least qualitatively the model must be regarded as successful. Particularly for real photon ($q^2 = 0$) processes, the corresponding vector meson processes show very much the same behavior as functions of energy and momentum transfer, and vector meson dominance has had a very useful role to play in making dynamical connections between photoproduction and purely hadronic reactions.

III General Features of the Photoproduction Cross Sections

While the cross sections for specific photon intitiated processes like rho meson or pion photoproduction have been measured some time ago over a wide energy range, the first measurements of the total cross section for $\gamma + p \rightarrow$ hadrons over a large energy range came quite recently. In large part this is because the cross section for hadron production by photons on protons is more than a hundred times smaller then that for electron-positron pair production (the Bethe-Heitler process), so that the quantity which one ordinarily determines in a transmission-type total cross section measurement is very largely made up of unwanted electromagnetic background. Fortunately the electron-positron pairs all appear in a very restricted kinematical region (a narrow forward cone) and can be appropriately eliminated from inclusion in the measurement. As a result, there now exist measurements of the total photoabsorption cross section on protons, $\sigma_T^{\gamma p}(\nu)$, extending from threshold to photon energies, ν, of almost 20 GeV from a combination of counter[30], bubble chamber[31], and inelastic electron scattering[32] (extrapolated from the scattering region of space-like exchanged photons to the case of real light-like photons) experiments.

Figure 1 shows a smoothed version of these measurements of $\sigma_T^{\gamma p}(\nu)$ together with the total cross section for pi-zero meson-proton scattering (equal to the average of the pi-plus and pi-minus proton total cross sections by isotopic spin conservation) divided by a convenient scale factor of 250. At low energies both total cross sections show the clear excitation of the same prominent states of the nucleon --- the first, second, third and fourth N* resonances. Except for the second resonance, the excitation of the main resonances in the photon and

pion cases are even roughly in proportion. As the energy of the photon increases into the multi-GeV region, the total cross section slowly decreases, much as the pion-nucleon total cross section does, and seems to be going toward a non-zero value at infinite energy of order 100 μb. The photon-neutron total cross section, extracted from measurements of the photon-deuteron total cross section[30], is generally smaller then the photon-proton cross section at the same energy, but also appears to slowly decrease wtih increasing energy, and is consistent with approaching the same limit at infinite energy[30].

When one examines how specific hadron multiplicities make up the total cross section, there again emerges a picture remarkably similar to that for the purely hadronic case. Table 1 shows the composition of the photon-proton total cross section in terms of the individual topological cross sections[31] for various numbers of final charged hadrons at photon energies of 1.4, 2.8, 4.7 and 9.3 GeV. The charged hadron prongs enumerated in the table are those due to pions and nucleons, the strange particle production cross section being listed separately. With increasing photon energy, higher charged multiplicities become more important, with any particular charged multiplicity seeming to rise with increasing energy at first, to reach a maximum, and then slowly to fall-off (see σ (3 prong) in Table 1). The mean charged multiplicity, $\langle n_{charged} \rangle$ shown in Table 1, is slowly rising as a result, being quite consistent[33] with a logarithmic increase with the photon energy, ν. Strange particle production, on the other hand, is small and shows no increase at the higher energies. All these features, as well as others[33] of the final state, are very much as in the purely hadronic case, e.g. proton-proton collisions[34], where they also known to persist to much higher energies. Whether these features of photon-nucleon collisions also extend to higher energies, and more importantly, whether they are the same for the space-like virtual photons involved in electron scattering, are among the very important questions to be answered experimentally in the near future.

TABLE 1 Topological cross sections

Photon Energy ν (GeV)	1.4	2.8	4.7	9.3
σ(1 prong) (μb)	54.9 ± 3.2	22.7 ± 1.5	15.6 ± 1.2	8.6 ± 1.4
σ(3 prong) (μb)	85.6 ± 3.7	91.7 ± 2.5	81.4 ± 2.2	63.8 ± 3.3
σ(5 prong) (μb)	0.2 ± 0.2	8.4 ± 0.4	19.6 ± 0.6	33.6 ± 2.5
σ(7 prong) (μb)	----	0.05 ± 0.03	0.84 ± 0.08	7.3 ± 0.8
σ(9 prong) (μb)	----	----	----	0.6 ± 0.1
σ(strange particles) (μb)	4.4 ± 0.9	8.1 ± 0.5	8.5 ± 0.5	8.2 ± 0.8
$\sigma_T^{\gamma p}$ (μb)	145 ± 6	131 ± 3	126 ± 3	122 ± 5
$\langle n_{charged} \rangle = \frac{\sum n\sigma(n)}{\sum \sigma(n)}$	2.2	2.8	3.1	3.7

IV Photoproduction of Pions at Low Energy - Partial Wave Analysis

At low energies photoproduction strongly reflects the formation of direct channel nucleon resonances, as can be seen from the total cross section in Figure 1. Single pion photoproduction in particular is dominated by the presence of direct channel resonances. With the accumulation of extensive and accurate data, particularly on photoproduction off protons, pion photoproduction is becoming amenable to the same kinds of phase shift analysis which have been applied to pion-nucleon scattering, where a wealth of structure has been discovered.

Such phase shift analyses are the only means available which allow one to obtain detailed information on the photon induced transitions between the nucleon and its excited states. This information is of interest in examining the consequences of various higher symmetry schemes which relate one such transition to another, in testing the validity of certain sum rules, and as a proving ground for various dynamical models of the nucleon and the nucleon resonances. Unfortunately, because of the spin of the photon, a detailed partial wave analysis of photoproduction is more complicated in general than the corresponding analysis for pion-nucleon elastic scattering. However, with the advent of good polarized photon beams this may not actually be such a disadvantage in the future, since, if available, the dependence of the cross section on the photon's polarization gives one very useful additional information. Moreover, one has the advantage that pion-nucleon phase shift analyses already have established the quantum numbers of all the low mass nucleon resonances, so that one knows which partial waves are resonant and can consequently greatly constrain the possible solutions for

photoproduction to a quite limited domain.

The process of pion photoproduction is shown schematically in Figure 2 where the four-momenta (in the center-of-mass) of the photon, initial nucleon, pion, and final nucleon are $k = (\vec{k}, ik)$, $p_1 = (\vec{p_1}, iE_1)$, $q = (\vec{q}, i\omega)$, and $p_2 = (\vec{p_2}, iE_2)$ respectively. The corresponding S-matrix element for $\gamma + N_1 \longrightarrow \pi + N_2$ is:

$$S_{fi} = (2\pi)^4 i\,\delta^{(4)}(p_2+q-p_1-k)\sqrt{\frac{M_N^2}{4kE_1\omega E_2}}\; T_{fi}\,, \tag{18}$$

with the center of mass scattering amplitude

$$f_{fi} = \left(\frac{M_N}{4\pi W}\right) T_{fi}\,, \tag{19}$$

where $W = k + E_1 = \omega + E_2$ is the total center of mass energy.

While it is convenient for some dynamical purposes such as writing dispersion relations to decompose T_{fi} (and hence f_{fi}) into the invariant amplitudes given by Chew, Goldberger, Low and Nambu[35], for the purpose of partial wave analysis it is useful to use helicity amplitudes. Quantizing the particles' spins along their direction of motion, we can define helicity amplitudes[36] $f_{\mu\lambda}(W, \theta, \phi) = f_{\mu\lambda}(W, \theta)$ where we have chosen the xz plane as the scattering plane ($\phi=0$), z axis in the direction of the incident photon, θ the scattering angle from the photon direction to that of the pion, and $\lambda = \lambda_\gamma - \lambda_1$, and $\mu = \lambda_\pi - \lambda_2 = -\lambda_2$ are the net initial and final state helicities. Since $\lambda_\gamma = \pm 1, \lambda_1 = \pm\frac{1}{2}$, and $\lambda_2 = \pm\frac{1}{2}$, there are eight possible helicity amplitudes, but actually only four are independent because of parity conservation[36]:

$$f_{-\mu,-\lambda}(W, \theta) = -(-1)^{\lambda-\mu} f_{\mu,\lambda}(W, \theta)\,. \tag{20}$$

We choose these four to be (following Walker[37]):

$$H_1 = f_{1/2,\,3/2}(W,\theta) = +f_{-1/2,\,-3/2}(W,\theta)$$

$$H_2 = f_{1/2,\,1/2}(W,\theta) = -f_{-1/2,\,-1/2}(W,\theta) \tag{21}$$

$$H_3 = f_{-1/2,\,3/2}(W,\theta) = -f_{1/2,\,-3/2}(W,\theta)$$

$$H_4 = f_{-1/2,\,1/2}(W,\theta) = +f_{1/2,\,-1/2}(W,\theta) \quad .$$

In terms of these amplitudes the differential cross section (unpolarized) is simply,

$$\frac{d\sigma}{d\Omega} = \left(\frac{q}{k}\right) \frac{1}{2} \sum_{i=1}^{4} \left| H_i \right|^2 \tag{22}$$

The recoil nucleon polarization (along the $\hat{k} \times \hat{q}$ or $\hat{y}$ direction with our choice of axes),

$$P = \frac{-\frac{q}{k}\ \mathrm{Im}(H_1 H_3^* + H_2 H_4^*)}{\left(\frac{d\sigma}{d\Omega}\right)} \quad , \tag{23}$$

the polarized target asymmetry (also with respect to the $\hat{k} \times \hat{q}$ or $\hat{y}$ direction),

$$A = \frac{\sigma_{up} - \sigma_{down}}{\sigma_{up} + \sigma_{down}} = \frac{\frac{q}{k}\,\mathrm{Im}(H_1 H_2^* + H_3 H_4^*)}{\left(\frac{d\sigma}{d\Omega}\right)} \quad , \tag{24}$$

and the asymmetry for photons polarized perpendicular and parallel to the production (x-z) plane,

$$\sum = \frac{\sigma_\perp - \sigma_{11}}{\sigma_\perp - \sigma_{11}} = \frac{\frac{q}{k}\,\mathrm{Re}\,(H_1 H_4^* + H_2 H_3^*)}{\left(\frac{d\sigma}{d\Omega}\right)} \quad , \tag{25}$$

also all take very simple forms in terms of helicity amplitudes, $H_1 \ldots H_4$.

Each of the helicity amplitudes $f_{\mu\lambda}(W, \theta, \phi)$ has a standard expansion[36],

$$f_{\mu,\lambda}(W,\theta,\phi) = \sum_{j=\frac{1}{2}}^{\infty} (2j+1)\; f^j_{\mu\lambda}(W)\; d^j_{\lambda\mu}(\theta) e^{i(\lambda-\mu)\phi} \tag{26}$$

in terms of partial wave amplitudes, $f^j_{\mu\lambda}(W)$, of total angular momentum j, and the corresponding Wigner rotation functions, $d^j_{\lambda\mu}(\theta)$.

Although the amplitudes $f^j_{\mu\lambda}(W)$ correspond to definite total angular momentum j, they contain both parities. Since we want to consider the contributions of single resonances of definite j and parity, it is useful to define combinations[37] of the amplitudes of given total j:

$$A_{(j-1/2)^+}(W) = -\frac{1}{\sqrt{2}}\left(f_{1/2,1/2}(W) + f^j_{-1/2,1/2}(W)\right)$$

$$A_{(j+1/2)^-}(W) = \frac{1}{\sqrt{2}}\left(f^j_{1/2,1/2}(W) - f^j_{-1/2,1/2}(W)\right)$$

$$B_{(j-1/2)^+}(W) = \sqrt{\frac{2}{(j-1/2)\ (j+3/2)}}\left(f^j_{1/2,\,3/2}(W) + f^j_{-1/2,\,3/2}(W)\right) \quad (27)$$

$$B_{(j+1/2)^-}(W) = -\sqrt{\frac{2}{(j-1/2)\ (j+3/2)}}\left(f^j_{1/2,\,3/2}(W) - f^j_{-1/2,\,3/2}(W)\right)$$

The A (B) amplitudes involve net helicity 1/2(3/2) in the initial state, while the subscript notation on the A and B amplitudes in Eq. (27) is that of Chew et al.[35]: $A_{\ell^\pm}$ and $B_{\ell^\pm}$ correspond to a state with final pion orbital angular momentum ℓ, definite parity $P=(-1)^{\ell+1}$, and total angular momentum $j=\ell\pm\frac{1}{2}$. They are directly related to the conventional electric and magnetic multiple transition amplitudes[35], $E_{\ell^\pm}$ and $M_{\ell^\pm}$ by[37]

$$E_{0^+} = A_{0^+}\ ,\quad M_{1^-} = A_{1^-}$$

and for $\ell \geq 1$

$$E_{\ell^+} = \left(A_{\ell^+} + \left(\frac{\ell}{2}\right) B_{\ell^+}\right)\Big/\left(\ell+1\right) \quad (28)$$

$$M_{\ell^+} = \left(A_{\ell^+} - \left(\frac{\ell+2}{2}\right) B_{\ell^+}\right)\Big/\left(\ell+1\right)$$

$$E_{(\ell+1)^-} = -\left(A_{(\ell+1)^-} - \left(\frac{\ell+2}{2}\right) B_{(\ell+1)^-}\right)\Big/\left(\ell+1\right)$$

$$M_{(\ell+1)^-} = \left(A_{(\ell+1)^-} - \left(\frac{\ell}{2}\right) B_{(\ell+1)^-}\right)\Big/\left(\ell+1\right).$$

The complications due to the photon spin are reflected here in that there are two

amplitudes (A and B or alternately E and M) for each total angular momentum and parity rather than just one as in pion-nucleon scattering. Putting the definition of the partial wave amplitudes of definite parity, Eq. (27), in the general expansion of Jacob and Wick, Eq. (26), we finally obtain (ϕ=0)

$$H_1 = f_{1/2,\,3/2}(W,\theta) = \sum_j (2j+1)\sqrt{\frac{(j-1/2)(j+3/2)}{8}}\left[B_{(j-1/2)^+}(W) - B_{(j+1/2)^-}(W)\right] d^j_{3/2,\,1/2}(\theta)$$

$$H_2 = f_{1/2,\,1/2}(W,\theta) = \sum_j (2j+1)\sqrt{1/2}\left[A_{(j+1/2)^-}(W) - A_{(j-1/2)^+}(W)\right] d^j_{1/2,\,1/2}(\theta) \qquad (29)$$

$$H_3 = f_{-1/2,\,3/2}(W,\theta) = \sum_j (2j+1)\sqrt{\frac{(j-1/2)(j+3/2)}{8}}\left[B_{(j-1/2)^+}(W) + B_{(j+1/2)^-}(W)\right] d^j_{3/2,\,-1/2}(\theta)$$

$$H_4 = f_{-1/2,\,1/2}(W,\theta) = \sum_j (2j+1)\sqrt{1/2}\left[-A_{(j+1/2)^-}(W) - A_{(j-1/2)^+}(W)\right] d^j_{1/2,\,-1/2}(\theta) \ .$$

Since all physical quantities, such as those in Eqs. (22) - (25), are related to products of the amplitudes $H_1 \ldots H_4$ and Eq. (29) expresses these in terms of partial waves of given angular momentum and parity, this establishes the formalism necessary in order to perform a partial wave analysis of pion photoproduction.

There is one more slight complication to be dealt with: Since the photon couples to a current which has both an isoscalar and an isovector part, there are three independent isospin amplitudes for single pion photoproduction. Any amplitude A can be decomposed into amplitudes for an isoscalar transition to an $I=\frac{1}{2}$ final state, A^0; for an isovector transition to an $I=\frac{1}{2}$ final state, $A^{1/2}$, and for an isovector transitions to an $I=\frac{3}{2}$ state $A^{3/2}$. In terms of these, the amplitudes for the (four) possible single pion photoproduction reactions can be decomposed as:

$$A(\gamma p \to \pi^+ n) = \sqrt{\frac{2}{3}} A^0 + \frac{\sqrt{2}}{3} A^{\frac{1}{2}} - \frac{\sqrt{2}}{3} A^{\frac{3}{2}}$$

$$A(\gamma p \to \pi^0 p) = \sqrt{\frac{1}{3}} A^0 + \frac{1}{3} A^{\frac{1}{2}} + \frac{2}{3} A^{\frac{3}{2}}$$

$$A(\gamma n \to \pi^- p) = \sqrt{\frac{2}{3}} A^0 - \frac{\sqrt{2}}{3} A^{\frac{1}{2}} + \frac{\sqrt{2}}{3} A^{\frac{3}{2}} \qquad (30)$$

$$A(\gamma n \to \pi^0 n) = -\sqrt{\frac{1}{3}} A^0 + \frac{1}{3} A^{\frac{1}{2}} + \frac{2}{3} A^{\frac{3}{2}} .$$

Using the above equations, a number of analyses of pion photoproduction have been made in recent years. Since the photoproduction data are generally not complete enough, all such analyses employ additional information taken from pion-nucleon scattering to restrict the solution(s). In particular, dispersion relations (often in the resonance dominance approximation) plus a knowledge of the elastic pion-nucleon phase shifts have been very usefully employed at low energies[38]. At higher energies, where there is considerable inelasticity and

many more partial waves are important, it has been assumed that the only rapidly varying multipole amplitudes are those which contain the resonances discovered in pion-nucleon analyses. These partial waves are parametrized by Breit-Wigner forms with adjustable parameters, while the remaining amplitudes are assumed to be smooth, outside of contributions to them from the Born approximation terms[37]. Using such a "generalized isobar" model[37,39], considerable progress in untangling the multipole amplitudes in photoproduction has been made.

The results of these analyses have been reviewed at some length by Walker[40]. Some of the more interesting results on the electromagnetic coupling of the nucleon to the resonances are that[37,40]: (1) The first resonance[41], P_{33} (1236), is excited almost entirely through the magnetic dipole amplitude, M_1+, the electric quadrapole amplitude, E_1+, being very small ($A_1+ \simeq -\frac{1}{2} B_1+$ at resonance). (2) The second resonance, D_{13} (1518), is excited mostly through B_2-, initial net helicity $\frac{3}{2}$, and not through the helicity $\frac{1}{2}$ amplitude, A_2- ($E_2-/M_2- \simeq 3$). In addition, from a comparison of data from both neutron and photon targets, the excitation is found to be mainly through the isovector component of the current and not the isoscalar. (3) There is some evidence for excitation of the S_{11} (1550) resonance, which must proceed through the $A_0+ = E_0+$ amplitude (clearer evidence for excitation of this resonance comes from eta meson photoproduction, $\gamma p \rightarrow \eta p$). (4) The third resonance, F_{15} (1688), like the second, also is dominantly excited through the helicity $\frac{3}{2}$ amplitude B_3-. However, it doesn't seem to be excited in photoproduction off neutrons. This requires equal isoscalar and isovector contributions to B_3-, so that they add in the proton case, while cancelling for the neutron. (5) The D_{15} (1680) resonance is photoproduced very weakly. The amount of photoproduction

of P_{11} (1470) is not well determined, although probably not very large.

Some of these experimental observations are very much in accord with theoretical expectations, or at least are in agreement with certain models, while others have not yet been explained in any simple manner. The size and magnetic dipole character of the transition to the P_{33} (1236), for example, was predicted quite accurately in the earliest applications of dispersion theory to photoproduction[35]. The magnetic dipole nature and the approximate magnitude of the P_{33} transition, the vanishing of F_{15} (1688) formation with a neutron target, as well as the signs and rough magnitudes of many other transition amplitudes are predicted in a very simple quark model[37, 42]. The smallness of the net helicity $\frac{1}{2}$ amplitudes, however, seems to be a numerical accident due to particular coupling strengths[42] in the quark model, and was not predicted in advance by any theory. As we will see later, some of these features of the low energy resonance excitation are correlated through sum rules with the high energy behavior of pion photoproduction, and vice versa. This, while very interesting, does not "explain" the behavior of the resonance transition amplitudes, but only makes the mystery of the particular pattern of electromagnetic couplings chosen by nature that much greater.

V Compton Scattering

A The Forward Compton Amplitudes

In addition to obviously being a basic process involving the interaction of photons and hadrons, Compton scattering off nucleons has the distinction of also having served theoretically as the process for which dispersion relations were first proposed within the context of quantum field theory. While first written down and proved only for the amplitudes of forward Compton scattering by Gell-Mann, Goldberger, and Thirring[43], dispersion relations were soon applied to forward pion-nucleon scattering, other forward amplitudes, various off-shell amplitudes, and to non-forward amplitudes[44], all with great theoretical as well as experimental[45] success up to the present day. In the intervening fifteen years, the dispersion relations for forward Compton scattering were mostly neglected, perhaps because both the imaginary part of the forward Compton amplitudes, in the form of the total photoabsorption cross sections, and the real part of these amplitudes were almost totally unknown experimentally, so that there was no possibility of testing the dispersion relations or investigating their further experimental or theoretical consequences. This situation has now been remedied in large part with recent measurements of both the total photoabsorption cross section and Compton scattering at high energy.

In this section, we shall use the process of nucleon Compton scattering to illustrate the use of dispersion relations and the behavior of the real part of a forward amplitude when it is calculated from the imaginary part by means of a dispersion relation. This will hopefully both provide us with some insight into the behavior of forward amplitudes at low and high energies and allow us to

investigate some questions of theoretical interest concerning the asymptotic behavior of the real part of the amplitude at high energy.

The process of interest is then $\gamma+N \rightarrow \gamma+N$, and if we specialize to the case of forward scattering, there is just one continuous variable on which the scattering depends. We may take this to be the total center-of-mass energy, W, or, since we will mostly work in the laboratory frame where the nucleon is at rest, we will use the photon laboratory energy ν which is related to W by

$$\nu = \frac{W^2 - M_N^2}{2M_N} \quad . \tag{31}$$

Written out between the Pauli spinors of the intital and final nucleons, the scattering amplitude in the laboratory frame must be of the form[43]

$$f(\nu) = \chi_f^* \left[f_1(\nu)\, \vec{\epsilon}_2^{\,*} \cdot \vec{\epsilon}_1 + i\vec{\sigma} \cdot \left(\vec{\epsilon}_2^{\,*} \times \vec{\epsilon}_1 \right) f_2(\nu) \right] \chi_i, \tag{32}$$

where ϵ_1 and ϵ_2 are the polarization vectors of the initial and final photons respectively. Averaging over nucleon spins, we are left with only $f_1(\nu)$, the spin-averaged forward amplitude. While f_1 and f_2 correspond respectively to parallel and perpendicular linear polarizations for the initial and final photons, they can also be related to the two independent circular polarization, i.e. helicity, amplitudes for forward Compton scattering. If the photon and nucleon spins are parallel (photon helicity = +1, nucleon helicity = $-\frac{1}{2}$, and net helicity in the photon direction = $+\frac{3}{2}$) then the amplitude is

$$f_p(\nu) = f_1(\nu) - f_2(\nu) \ , \tag{33}$$

while if the spins are anti-parallel)photon helicity = +1, nucleon helicity = $+\frac{1}{2}$, and net helicity along the photon direction = $+\frac{1}{2}$) the amplitude is

$$f_a(\nu) = f_1(\nu)+f_2(\nu) \quad . \tag{34}$$

The amplitudes f_p and f_a are simply related by the optical theorem to the total cross sections σ_p and σ_a for photon + nucleon⟶hadrons (we work only to order e^2 in the amplitude) when the photon spin is parallel or anti-parallel to the nucleon spin:

$$\begin{aligned} \mathrm{Im}f_p(\nu) &= \frac{\nu}{4\pi}\,\sigma_p(\nu) \\ \mathrm{Im}f_a(\nu) &= \frac{\nu}{4\pi}\,\sigma_a(\nu) \quad . \end{aligned} \tag{35}$$

Therefore,

$$\mathrm{Im}f_1(\nu) = \frac{\nu}{4\pi}\,\frac{\sigma_a(\nu)+\sigma_p(\nu)}{2} = \frac{\nu}{4\pi}\,\sigma_T(\nu)\ , \tag{36a}$$

where $\sigma_T(\nu)$ is the spin averaged total cross section, and

$$\mathrm{Im}f_2(\nu) = \frac{\nu}{4\pi}\,\frac{\sigma_a(\nu)-\sigma_p(\nu)}{2} \quad . \tag{36b}$$

The component of the total cross sections due to single pion production is given in terms of the multipoles introduced in Section IV by

$$\begin{aligned} \sigma_a &= \left(\frac{8\pi q}{k}\right)\sum_{j=\frac{1}{2}}^{\infty}\left(j+\frac{1}{2}\right)\left(\left|A_{\left(j-\frac{1}{2}\right)^+}\right|^2+\left|A_{\left(j+\frac{1}{2}\right)^-}\right|^2\right) \\ \sigma_p &= \left(\frac{8\pi q}{k}\right)\sum_{j=\frac{1}{2}}^{\infty}\frac{\left(j-\frac{1}{2}\right)\left(j+\frac{1}{2}\right)\left(j+\frac{3}{2}\right)}{4}\left(\left|B_{\left(j-\frac{1}{2}\right)^+}\right|^2+\left|B_{\left(j+\frac{1}{2}\right)^-}\right|^2\right) \end{aligned} \tag{37}$$

so that

$$\sigma_T = \left(\frac{4\pi q}{k}\right)\sum_{j=\frac{1}{2}}^{\infty}\left[\left(j+\frac{1}{2}\right)\left(\left|A_{\left(j-\frac{1}{2}\right)+}\right|^2 + \left|A_{\left(j+\frac{1}{2}\right)-}\right|^2\right)\right.$$

$$\left. + \frac{\left(j-\frac{1}{2}\right)\left(j+\frac{1}{2}\right)\left(j+\frac{3}{2}\right)}{4}\left(\left|B_{\left(j+\frac{1}{2}\right)+}\right| + \left|B_{\left(j+\frac{1}{2}\right)-}\right|^2\right)\right] \quad (38)$$

$$= \frac{2\pi q}{k}\sum_{\ell=0}^{\infty}\left[\ell(\ell+1)^2\left|M_{\ell+}\right|^2 + (\ell+1)^2(\ell+2)\left|E_{\ell+}\right|^2\right.$$

$$\left. + (\ell+1)^2(\ell+2)\left|M_{(\ell+1)-}\right|^2 + \ell(\ell+2)^2\left|E_{(\ell+1)-}\right|^2\right],$$

where q and k are again the pion and photon center of mass momenta ($\nu = Wk/M_N$).

In the absence of both a circularly polarized beam and polarized nucleon target it is only $\sigma_T(\nu) = [\sigma_a(\nu)+\sigma_p(\nu)]/2$ which is accessible to experimental measurement, although the single pion production component of σ_a and σ_p separately is constructable through Eq. (37). Similarly, in the absence of polarized targets and beams, it is only the spin averaged Compton scattering differential cross sections

$$\left(\frac{d\sigma}{d\Omega}\right)_{\theta=0^o} = \left|f(\nu)\right|^2 = \left|f_1(\nu)\right|^2 + \left|f_2(\nu)\right|^2 \quad (39)$$

which is measured experimentally.

However, if we knew only the imaginary parts of $f_1(\nu)$ and $f_2(\nu)$, we could calculate the corresponding real parts by means of dispersion relations. For, using the fact that $f_1(\nu)$ is even and $f_2(\nu)$ odd under crossing ($\nu \rightarrow -\nu$), we

have the dispersion relations[43]

$$\text{Re } f_1(\nu) = f_1(0) + \frac{\nu^2}{\pi} \int_{\nu_0}^{\infty} \frac{d\nu'^2}{\nu'^2 - \nu^2} \frac{\text{Im} f_1(\nu')}{\nu'^2} \tag{40}$$

and

$$\text{Re } f_2(\nu) = \frac{2\nu}{\pi} \int_{\nu_0}^{\infty} \frac{d\nu'}{\nu'^2 - \nu^2} \text{Im} f_2(\nu') \quad , \tag{41}$$

where both principal value integrals start at $\nu_0 = \mu + \mu^2/(2M_N) \simeq 150$ MeV, the threshold for single pion photoproduction (μ is the pion mass). The dispersion relation for $f_1(\nu)$ in Eq. (40) was written with a subtraction, since both the high energy behavior of $\text{Im} f_1(\nu)$ and the Thomson limit for Compton scattering off protons, $f_1(0) = -\alpha/M_N$, indicate the impossibility of an unsubtracted dispersion relation holding. In fact, we have the quite general low energy theorems[46] that state that as $\nu \to 0$

$$f_1(\nu) \to -\frac{\alpha}{M_N} \tag{42a}$$

and

$$f_2(\nu)/\nu \to f_2'(0) = \frac{-\alpha(\mu_{\text{anom}})^2}{2M_N^2} \quad , \tag{42b}$$

where μ_{anom} is the anomalous magnetic moment of the nucleon. Eq. (42b), together with the unsubtracted dispersion relation in Eq. (41), give rise to the

Drell-Hearn-Gerasimov sum rule[47] for the anomalous magnetic moment squared:

$$(\mu_{anom})^2 = -\frac{4M_N^2}{\pi\alpha}\int_{\nu_0}^{\infty}\frac{d\nu'}{\nu'^2}\,\mathrm{Im}f_2(\nu') = \frac{M_N^2}{2\pi^2\alpha}\int_{\nu_0}^{\infty}\frac{d\nu'}{\nu'}\left[\sigma_p(\nu')-\sigma_a(\nu')\right] . \tag{43}$$

The sum rule appears to be satisfied for a proton target when saturated with low mass resonances[48]. This is completely non-trivial since there is no requirement that the integral on the right hand side even have the correct sign. The fact that it does reflects the strong dominance of the net helicity $\frac{3}{2}$ (σ_p) over helicity $\frac{1}{2}$ (σ_a) couplings of the nucleon resonances to the photon plus nucleon as noted in Section IV from the analysis of single pion photoproduction.

While saturation of the Drell-Hearn-Gerasimov sum rule by a few low lying resonances contributions indicates that such an approximation is adequate for calculating $f_2(\nu)$ near $\nu = 0$ from the dispersion relation, the lack of real data for $\mathrm{Im}f_2(\nu) = \frac{\nu}{4\pi}\left[\sigma_a(\nu)-\sigma_p(\nu)\right]/2$ prevents one from making any more extensive calculations of $f_2(\nu)$ at the present time. In the case of $f_1(\nu)$, however, there is knowledge of $\mathrm{Im}f_1(\nu) = \frac{\nu}{4\pi}\sigma_T(\nu)$ up to almost 20 GeV (see Figure 1) so we shall concentrate our attention on this amplitude for the proton. With the low energy theorem value for $f_1(0)$, the dispersion relation for $f_1(\nu)$ reads:

$$\mathrm{Re}f_1(\nu) = -\frac{\alpha}{M_N} + \frac{\nu^2}{\pi}\int_{\nu_0}^{\infty}\frac{d\nu'^2}{\nu'^2-\nu^2}\,\frac{\mathrm{Im}f_1(\nu')}{\nu'^2} \tag{44}$$

$$= -\frac{\alpha}{M_N} + \frac{\nu^2}{2\pi^2}\int_{\nu_0}^{\infty}\frac{d\nu'^2}{\nu'^2-\nu^2}\,\sigma_T(\nu') .$$

In order to carry out the integral in Eq. (44) we need in principle to know the total cross section to infinite energy. Obviously we must make some assumptions about the general behavior of total cross sections at high energy in order to extrapolate $\sigma_T(\nu)$ for use in Eq. (44). The conventional assumption is that the high energy behavior of total cross sections is smooth, say a sum of powers of ν. In particular this is the case in Regge pole theory where at high energies the imaginary part of the forward amplitude behaves as

$$\mathrm{Im} f_1(\nu) = \sum_i \left(\frac{c_i}{4\pi}\right) \nu^{\alpha_i(0)} , \tag{45}$$

so that

$$\sigma_T(\nu) = \sum_i c_i \nu^{\alpha_i(0)-1} , \tag{46}$$

where the c_i are constants and the $\alpha_i(0)$ are the t=0 intercepts of the Regge trajectories, $\alpha_i(t)$, which can be exchanged in the t- channel of elastic scattering (in this case Compton scattering). One can also take it as an empirical fact that parametrizations such as those in Eq. (46), with only a few terms in the sum, give very good fits to the energy dependence of purely hadronic total cross sections[49]. There it is found that the leading isospin 0 and 1 trajectories (those with $\alpha_i(0) > 0$) are the Pomeron (corresponding to diffraction scattering and constant total cross sections) which has $\alpha_p(0)=1$ and the P', A_2, ρ and ω trajectories, all of which have $\alpha(0) \simeq 0.5$ as determined either from the usual linear Regge trajectories (with slope $\approx 1/\mathrm{GeV}^2$) passing through the physical

particle positions or from fits to the hadron-hadron total cross sections at high energies[49]. For Compton scattering only t-channel trajectories with C = +1 are allowed, so we can restrict our attention to only the P' and A_2 trajectories in addition to the Pomeron.

We then assume[50] that the total cross section behaves at high energy (say $\nu > 2$ GeV) as

$$\sigma_T(\nu) = c_1 \nu^{\alpha_p(0)-1} + c_2 \nu^{\alpha_1(0)-1} \tag{47}$$

with $\alpha_p(0)=1$ and $\alpha_1(0) \simeq 0.5$, up to terms which vanish faster than $\frac{1}{\nu}$. This particular analytic form is clearly an assumption, based on Regge pole theory plus the empirically observed behavior of hadronic total cross sections. Given this assumption, one can determine the constants c_1 and c_2 from the photon-proton total cross section experiments (to which a form such as that in Eq. (47) provides an excellent fit[50]), and use the resulting expression for performing the high energy part of the dispersion integral in Eq. (44).

The Argand diagram of f_1 at low energies computed[50] using the dispersion relation with the above assumptions is shown in Figure 3. Clear circles due to the first, second, third, and fourth resonances are seen. At high energies both $\mathrm{Re}f_1(\nu)$ and $\mathrm{Im}f_1(\nu)$ are smooth functions, with $\mathrm{Re}f_1(\nu)/\mathrm{Im}f_1(\nu)$ being negative and decreasing with increasing energy. The exact magnitude of the real part depends slightly on what kind of fit[50] to the high energy $\sigma_T(\nu)$ data is used, as shown in Figure 4, but in magnitude the real part of $f_1(\nu)$ is always less than 20% of the imaginary part for energies above about 10 GeV, and generally behaves much as in hadronic processes[49].

B Constant Terms in the Asymptotic Behavior of Forward Amplitudes

Suppose that the forward scattering amplitude $f(\nu)$ has the Regge

high energy behavior

$$f(\nu) = \sum_{i,\, \alpha_i(0) > 0} \frac{-1 - e^{-i\pi\alpha_i(0)}}{\sin \pi\alpha_i(0)} \left(\frac{c_i}{4\pi}\right) \nu^{\alpha_i(0)} \tag{48}$$

$$+ C + (\text{terms which go to zero as } \nu \to \infty)$$

where we have explicitely separated the term C (which is a real constant) corresponding to a term in the sum with $\alpha_i(0)=0$. Note that the particular high energy behavior exhibited in Eq. (48) is an assumption motivated by Regge theory. Other forms are possible in general, e.g. logarithms of ν. Given Eq. (48) the behavior of the real and imaginary parts of $f(\nu)$ is

$$\text{Re } f(\nu) = \sum_{i,\, \alpha_i(0) > 0} \left(\frac{c_i}{4\pi}\right) \left(-\cot\left(\frac{\pi\alpha_i(0)}{2}\right)\right) \nu^{\alpha_i(0)} \tag{49a}$$

$$+ C + (\text{terms which go to zero at } \gamma \to \infty)$$

$$\text{Im } f(\nu) = \sum_{i,\, \alpha_i(0) > 0} \left(\frac{c_i}{4\pi}\right) \nu^{\alpha_i(0)} \tag{49b}$$

$$+ (\text{terms which go to zero as } \nu \to \infty)$$

Thus all the terms in Re $f(\nu)$ except C which don't vanish at infinite energy could be obtained from Im $f(\nu)$. To calculate C let us define $f^{(R)}(\nu)$ for all ν as:

$$f^{(R)}(\nu) \equiv \sum_{i,\, \alpha_i(0) > 0} \frac{-1 - e^{-i\pi\alpha_i(0)}}{\sin \pi\alpha_i(0)} \left(\frac{c_i}{4\pi}\right) \nu^{\alpha_i(0)} + C. \tag{50}$$

Clearly, $f^{(R)}(\nu)$ differs from $f(\nu)$ only in terms which to to zero as $\nu \to \infty$. This new function obeys the dispersion relation

$$f^{(R)}(\nu) = C + \frac{\nu^2}{\pi} \int_0^\infty \frac{d\nu'^2}{\nu'^2 - \nu^2 - i\epsilon} \frac{\text{Im } f^{(R)}(\nu')}{\nu'^2}, \tag{51}$$

as is easily verified by explicit calculation, while we assume that the original amplitude $f(\nu)$ obeys a dispersion relation of the form:

$$f(\nu) = f(0) + \frac{\nu^2}{\pi} \int_{\nu_0}^\infty \frac{d\nu'^2}{\nu'^2 - \nu^2 - i\epsilon} \frac{\text{Im } f(\nu')}{\nu'^2} . \tag{52}$$

From the definition of $f^{(R)}(\nu)$ we have that $f(\nu) - f^{(R)}(\nu) \to 0$ as $\nu \to \infty$. Subtracting the two dispersion relations, Eqs. (51) and (52), we obtain on letting $\nu \to \infty$:

$$C = f(0) + \frac{1}{\pi} \int_0^{\nu_0} \frac{d\nu'^2}{\nu'^2} \text{Im } f^{(R)}(\nu') + \frac{1}{\pi} \int_{\nu_0}^\infty \frac{d\nu'^2}{\nu'^2} \text{Im } \left[f^{(R)}(\nu') - f(\nu') \right]. \tag{53}$$

The last integral in Eq. (53) is convergent because $f^{(R)}(\nu) - f(\nu)$ goes to zero as $\nu \to \infty$. In fact, one usually assumes, as was done[50] in the calculation of Re $f_1(\nu)$ discussed above, that for large values of ν, say $\nu \geq N$, one has Im $f(\nu)$ = Im $f^{(R)}(\nu)$ to arbitrarily high accuracy. In that case Eq. (53) becomes

$$C = f(0) + \frac{2}{\pi} \int_0^N \frac{d\nu'}{\nu'} \text{Im } f^{(R)}(\nu) - \frac{2}{\pi} \int_{\nu_0}^N \frac{d\nu'}{\nu'} \text{Im } f(\nu') \tag{54a}$$

or

$$\frac{1}{2\pi^2} \int_{\nu_0}^N d\nu' \, \sigma_T(\nu') = f(0) - C + \sum_i \left(\frac{c_i}{2\pi^2} \right) \frac{N^{\alpha_i(0)}}{\alpha_i(0)} . \tag{54b}$$

Thus, assuming that the forward amplitude $f(\nu)$ has the Regge high energy behavior of Eq. (48), then Eq. (53) or Eq. (54) allows us to determine C purely from a knowledge of the behavior of imaginary part of $f(\nu)$ (i.e. the total cross section) and $f(0)$. In the particular case of Compton scattering off protons, the low energy theorem tells us that $f_1(0) = -\alpha/M_N \simeq -3.0\ \mu b\text{-GeV}$. Evaluation the integral in Eq. (54) up to N=1.68 GeV (corresponding to W=2.0 GeV), and assuming that Im $f_1(\nu)$ has Regge high energy behavior of the form $(c_1/4\pi)\nu + (c_2/4\pi)\nu^{\alpha(0)}$, with $\alpha(0) \simeq 0.5$, then it seems that the constant C is non-zero for the forward Compton amplitude[50]. In fact, it appears that[50,51,52] $C \simeq -3\ \mu b\text{-GeV}$, i.e., it has the magnitude and sign of the Thomson limit, $f_1(0)$, a possibility first suggested by Creutz, Drell, and Paschos[51]. In Regge language, such a real constant term in the high energy forward amplitude corresponds to a J-plane singularity with $\alpha(0) = 0$. Whether $\alpha(t) \equiv 0$, so that we are dealing with a fixed pole at J=0, is impossible to tell from the present considerations. However, since such fixed poles are not forbidden by unitarity for amplitudes involving two currents, as they are for purely hadronic amplitudes, and since there is no known Regge pole trajectory with the correct quantum numbers and with $\alpha(0) \simeq 0$, it is quite possible that within the framework of Eq. (48) $C \neq 0$ for Compton scattering represents a fixed pole in Regge terminology.

C Non-Forward Compton Scattering

When we go from forward to non-forward Compton scattering, the number of independent amplitudes goes from two to six. The decomposition into invariant amplitudes and their relation to helicity amplitudes can be found in the paper of Bardeen and Tung[53]. In spite of the complicated spin structure, one expects a rather simple differential cross section for Compton

scattering at high energy. This is because it is an elastic process, and in analogy to all elastic hadron-hadron scattering at high energy, should be dominantly diffractive (dominated by Pomeron exchange in Regge language).

This is just what is observed[54]. The measured differential cross sections are strongly forward peaked and near the forward direction are almost energy independent from 5 to 17 GeV. If t is minus the square of the momentum transfer, then the measured differential cross sections $\frac{d\sigma}{dt}$ for $|t| \lesssim 1$ GeV^2 are well fit by the form Ae^{Bt} where B is in the range 6 to 8 GeV^{-2}. This is similar to the slope of the differential cross section observed in meson-nucleon elastic scattering in the same energy region.

If the data are extrapolated to the forward direction, t=0, they can be compared with what is expected from Eq. (39):

$$\frac{\nu^2}{\pi}\left(\frac{d\sigma}{dt}\right)_{t=0} = \left(\frac{d\sigma}{d\Omega}\right)_{\theta=0^\circ} = \left(\frac{\nu\sigma_T}{4\pi}\right)^2 + \left|\mathrm{Re}\, f_1(\nu)\right|^2 + \left|f_2\right|^2,$$

where Im $f_1(\nu)$ has been replaced by its optical theorem value. The values obtained for the forward cross section[54], particularly those extrapolated from the very small t measurements of Boyarski et al., are in excellent agreement with the values predicted from the real and imaginary parts of $f_1(\nu)$ alone, and imply that the $|f_2(\nu)|^2$ term is less than about 10% of the dominant term at high energies, $|\mathrm{Im}\, f_1(\nu)|^2 = (\nu\sigma_T/4\pi)^2$. Since $|\mathrm{Re}\, f_1(\nu)|^2$ is also only a few percent of $|\mathrm{Im}\, f_1(\nu)|^2$ at high energy, these measurements unfortunately do not put very strong constants on Re $f_1(\nu)$ for comparison with the dispersion relation predictions, although they do imply that $|\mathrm{Re}\, f_1(\nu_1)|$ can not be much larger than these predictions. The measurements can then be used to set strong limits on extra subtraction constants[55] in the dispersion relation of the form

$\lambda\nu^2$. A more stringent test of the dispersion relation for the spin-averaged forward amplitude must await measurement of the interference between the known Bethe-Heither amplitude for producting low invariant mass electron-positron pairs and the Compton contribution to pair production, which will allow a determination of both the sign and magnitude of the real part of the Compton amplitude[56].

VI Vector Meson Photoproduction

A Photoproduction of Rho, Omega, and Phi Mesons

Aside from Compton scattering, the photoproduction of rho, omega, and phi mesons are the prime examples of diffractive processes in photon initiated reactions. The diffractive nature of these processes was to be expected since the vector mesons have the same quantum numbers as the photon, allowing exchange of the quantum numbers of the vacuum. In fact, in the vector dominance model one would view vector meson photoproduction as taking place (see Figures 5a and b) through the photon becoming a virtual vector meson, with the vector meson then scattering elastically on the nucleon to produce the vector meson-nucleon final state. From such a viewpoint one expects vector meson photoproduction to look very much like meson-nucleon elastic scattering, which we will see is indeed the case.

Compared to ordinary elastic scattering of hadrons, however, photoproduction of vector mesons is presently unique experimentally in that it permits direct and relatively easy study of the spin dependence of diffraction scattering. This possibility arises both because of the use of polarized high energy photon beams and because the decay of the vector meson can be employed as a polarisation analyzer of the final meson. This unique access to the spin dependence has been utilized in rho meson photoproduction to give us some very interesting information on diffraction scattering.

Rho meson photoproduction, starting at photon energies of a few GeV, acts like a diffractive process [57,58]. The differential cross section in the forward direction has almost a constant value--it is in fact falling very slowly with energy, just like pion-nucleon forward scattering[57,58]. The exact magnitude of $d\sigma/dt$ in

the forward direction depends somewhat on what model is taken to explain the skewed rho line shape[57], but is roughly $100\mu b/GeV^2$ for photon energies in the 5 to 10 GeV range. The differential cross section is strongly forward peaked, and very similar to pion-nucleon elastic scattering with an exponential dependence of $d\sigma/dt$ on the momentum transfer squared $|t|$, for small t. Fits to the slope, B, (assuming $d\sigma/dt = Ae^{Bt}$) give values in the range 6 to 8 GeV^{-2}, again depending on the model taken for the rho lineshape, with smaller slopes corresponding to models which also give smaller values of $d\sigma/dt$ in the forward direction[57]. Measurements[59] of the real part of the rho photoproduction amplitude by studying asymmetric pair production show that at photon energies of 4 to 5 GeV the real part is negative and is 20 to 30% of the imaginary part in magnitude. Thus the imaginary part of the amplitude dominates as it should for a diffractive process.

Using polarized photon beams it has been established that rho photoproduction proceeds almost entirely through natural spin-parity ($J^p = 0^+, 1^-, 2^+, 3^-, \ldots$) exchanges, with the contribution of unnatural spin-parity ($J^p = 0^-, 1^+, 2^-, 3^+, \ldots$) exchanges being very small[57,58]. Even at energies of a few GeV, one has over 90% natural spin parity exchange[57]. This is quite remarkable at such low energies and sets rather strong limits on any possible unnatural spin-parity exchange component of diffraction. In this regard rho photoproduction is a unique process for setting such a limit, because there can be no unnatural spin-parity exchange in elastic meson-nucleon scattering, and because the spin dependence is unmeasured for processes like elastic proton-proton scattering where such an exchange is possible.

Of even more interest is the spin orientation of the rho meson relative to that of the incident photon. If diffraction scattering proceeded through exchange of some object (the Pomeron), then the spin orientation of the final rho would depend directly on the coupling of the Pomeron at the photon-rho-Pomeron vertex.

Two particular possibilities for this coupling are: (a) The Pomeron acts like a $J^P = 0^+$ object in its couplings. In this case there should be no helicity flip (from the photon to the rho) in the t- channel. As a result the rho meson should have only spin components equal to ±1 (like the photon) along the z-axis in the Gottfried-Jackson frame[60] (beam direction as z-axis in the rho meson rest frame), which acts as a measure of t-channel helicity components. (b) The Pomeron acts in such a way as to conserve s-channel helicity, so that the rho should have only spin components (helicity) equal to ±1 along the z-axis in the helicity frame (rho direction of motion in the center of mass as z-axis).

Experiment[57] unambiguously favors the second possibility in the case of rho photoproduction, at least for $|t| \leq 0.4$ GeV^2. This has led to the hypothesis[61] that s-channel helicity conservation is a general property of diffraction scattering (or Pomeron exchange). While the present rho photoproduction experiments only test this hypothesis at the photon-rho-Pomeron vertex, experiment and theoretical analysis indicate that the nucleon's helicity is conserved in high energy pion-nucleon scattering[62,63]. Furthermore, it is possible to have the exchange of a t-channel object with natural spin-parity and factorizable couplings produce s-channel helicity conservation[61,64]. What seems like an obvious s-channel phenomenon then has a possible t-channel interpretation. While the extent of the validity of s-channel helicity conservation in diffraction scattering remains to be established experimentally, the hypothesis has stimulated much theoretical activity attempting to understand its origins and consequences. The spin dependence of diffraction scattering has gone from being an "inessential" complication to being of prime interest. While we understand rather little about the exact nature of diffraction scattering or Pomeron exchange, if the hypothesis of s-chanel helicity conservation is generally valid it is a remarkable simplicity, presumably calling for an equally simple explanation.

While rho meson photoproduction remains as the best piece of evidence for helicity conservation in diffraction scattering, one naturally looks at the photoproduction of the other vector mesons, omega and phi, for confirming evidence. However the omega photoproduction cross section, in contrast to the rho, falls rather dramatically with increasing energy[57]. The explanation of this energy dependence is rather simple. From the coupling constants of the photon to the vector mesons given in Eq. (17), isospin one exchanges (like π and A_2) are 50 to 100 times more important relative to diffraction scattering in omega photoproduction than in rho photoproduction. The importance of pion exchange is verified experimentally using polarized photons to separate the natural and unnatural spin-parity exchanges. An appreciable cross section due to unnatural spin-parity exchange is found[57] (about one-half the cross section at $\nu = 2.8$ GeV). The energy dependence ($\sigma \propto 1/\nu^2$) and magnitude of the unnatural spin-parity exchange part of the cross section agree with predictions from one pion exchange and explain most of the energy dependence found in the total cross section for omega photoproduction. The cross section due to natural spin-parity exchange is mostly diffractive, but still appears to have some energy dependence, presumably due to relatively important contributions from A_2 (and P') exchange[65].

Phi photoproduction, on the other hand, should be the most favorable photoproduction reaction in which study Pomeron exchange. This is because with the usual mixing of the SU(3) singlet vector meson with the eighth member of the octet to form the physical omega and phi, the phi is just the mixture of singlet and octet, composed of only strange quarks, such that all the non-Pomeron exchanges decouple in phi photoproduction[66]. Very accurate data are unfortunately lacking for phi photoproduction, although it is known that the total cross section is approximatly energy independent and about 0.5 μb[57]. Good measurements of

phi photoproduction at high energy to determine if the forward scattering is energy independent, if the shape of the differential cross section changes with energy, and if s-channel helicity is conserved are clearly needed to complete the picture of vector meson photoproduction.

B Tests of the Vector Dominance Model

The amplitudes for vector meson photoproduction are related by the vector dominance model both to those for Compton scattering and those for elastic vector meson-nucleon scattering. Applying vector meson dominance first to one photon leg of the Compton amplitude gives

$$A(\gamma p \rightarrow \gamma p) = \sum_V \left(\frac{e}{f_V}\right) A(\gamma p \rightarrow V p) \ , \qquad (55)$$

where the sum is to be taken over the known vector mesons: rho,omega and phi. Squaring the imaginary part of this relation, (neglecting the spin dependence) yields[67]

$$\left(\frac{1}{1+\eta_\gamma^2}\right) \frac{d\sigma}{dt} \left(\gamma p \rightarrow \gamma p\right) = \left[\sum_V \left(\frac{\alpha}{(1+\eta_V^2)\left(f_V^2/4_\pi\right)} \frac{d\sigma}{dt} (\gamma p \rightarrow V p)\right)^{1/2}\right]^2 , \qquad (56)$$

where η_V is the ratio of real to imaginary parts for $\gamma p \rightarrow V p$. Eq. (56) provides a direct test of the vector dominance model in terms of measurable cross sections. In the forward direction Eq. (56) reduces to a relation between the total photon-proton cross section and the forward vector meson photoproduction cross sections[67].

By far the largest cross section on the right hand side is that due to rho meson photoproduction. Although there is still not complete agreement on the rho cross sections, the right hand side of Eq. (56) is smaller than the left hand

side if we use the Orsay colliding beam values[28] for $f_V^2/4\pi$. Models of the rho line shape that give larger forward rho photoproduction cross sections improve the situation at $t=0$, but then the t dependence of the two sides of Eq. (56) is different, resulting in factor of two disagreement[54] by $t \simeq 1$ GeV^2. With smaller values of the forward rho cross section, both sides of Eq. (56) have compatable t dependences[54]. Then a value of $f_\rho^2/4\pi = 1.2$ to 1.4 instead of the Orsay value of $f_\rho^2/4\pi = 1.99 \pm 0.11$ would put the two sides in agreement[54,58]. It seems quite generally to be the case that <u>smaller</u> values of $f_V^2/4\pi$ than the colliding beam values are required to make the vector dominance relations between Compton scattering and vector meson photoproduction agree with experiment.

This is not the case for the vector meson dominance relations between vector meson photoproduction and elastic vector meson-nucleon scattering. Applying vector meson dominance to the photon leg in the amplitude (Figure 5) for photoproduction of a vector meson, V, yields on squaring,

$$\frac{d\sigma}{dt}\ (\gamma p \to Vp) = \left(\frac{e}{f_V}\right)^2 \frac{d\sigma}{dt}\ (Vp \to Vp)\ , \tag{57}$$

where we have neglected spin dependence and transitions of the kind $V_1 p \to V_2 p\ (V_1 \neq V_2)$. In the forward direction, Eq. (57) reduces, using the optical theorem, to[67]

$$\left.\frac{d\sigma}{dt}\ (\gamma p \to Vp)\right|_{\theta=0^o} = \frac{\alpha}{\left(f_V^2/4_\pi\right)} \frac{\left[\sigma_T(Vp)\right]^2}{16\pi}\ . \tag{58}$$

While $\sigma_T(Vp)$, the total vector meson-proton cross section, can not be directly measured because of the vector meson lifetimes, it can be deduced from the A dependence of vector meson photoproduction experiments on complex nuclei[69].

These experiments (for photon energies of 5 to 10 GeV) give[69] rho-nucleon and omega-nucleon total cross sections in the range 27 to 30 mb. This also agrees with the quark model prediction that these cross sections should be the same and equal to the average of the pi plus-and pi minus-proton total cross sections (equal to about 28 mb at 5 GeV).

With values of 27 to 30 mb for the rho-nucleon and omega-nucleon total cross sections, the right hand side of Eq. (58) is too large compared to the left hand side if the colliding beam values for $f_V^2/4\pi$ are used. In other words, the two sides of Eq. (50) would be brought into agreement if $f_V^2/4\pi$ were increased relative to the colliding beam results. In the case of the rho, one needs values of $f_\rho^2/4\pi$ of 2.8 to 3.2 (rather than 1.99 ± 0.11) in order to obtain agreement of the two sides of Eq. (58). These larger values of $f_V^2/4\pi$ are also in accord with the results of the vector meson photoproduction experiments on complex nuclei which find values[69] of $f_\rho^2/4\pi$, for example, of 2.4 to 3.2. Thus it generally seems to be the case that <u>larger</u> values of $f_V^2/4\pi$ than the colliding beam values are required to make the vector dominance relations between vector meson photoproduction and vector meson elastic scattering agree with experiment.

Overall we thus find qualitative agreement of vector meson photoproduction with vector dominance, but quantitative disagreement when we try to do better than about a factor of two. This quantitative disagreement can be blamed on a dependence of the coupling constants on the photon's invariant mass squared in the field theoretic approach to vector meson dominance or, alternately, on contributions to the dispersion relation in the photon's mass squared from higher mass states with the quantum numbers of the photon, such as higher mass vector mesons[69]. With the sizable colliding beam cross sections beyond the rho, omega, and phi region found at Frascati[70], such additional contributions to the dispersion relation in the mass squared are presumably present.

VII Photoproduction of Charged Pions at High Energy

A Photoproduction of Charged Pions-Kinematics

Pion photoproduction at high energy presents many of the features of inelastic two body or quasi-two body (nondiffractive) reactions found in both hadronic and photoproduction processes in general. It has the advantage that the use of polarized photon beams allows us to analyze the spin dependence, at least partially, and to decompose the differential cross section into components due to different types of exchanges. The resulting experimental information provides an excellent example of both our difficulties and successes in understanding phenomena like pion exchange, peaks and dips in differential cross sections, energy dependence of reactions, etc.

The process of pion photoproduction is shown schematically in Figure 2. We will be interested particularly in large values of the total center of mass energy squared, $s = -(p_1+k)^2$, and small (negative) values of minus the invariant momentum transfer squared, $t = -(k-q)^2$. The Feynman amplitude, T_{fi} of Eq. (18) can be decomposed into four invariant amplitudes[35] as follows

$$\begin{aligned} T = \bar{u}(p_2) \Big[& A_1(s,t) i \gamma_5 \gamma \cdot \epsilon \gamma \cdot k \\ & + A_2(s,t)\, 2i\gamma_5 (P \cdot \epsilon q \cdot k - P \cdot k q \cdot \epsilon) \\ & + A_3(s,t)\, \gamma_5 (\gamma \cdot \epsilon q \cdot k - \gamma \cdot k q \cdot \epsilon) \\ & + A_4(s,t)\, 2\gamma_5 (\gamma \cdot \epsilon P \cdot k - \gamma \cdot k P \cdot \epsilon - i M_N \gamma \cdot \epsilon \gamma \cdot k \Big] u(p_1) \quad , \end{aligned} \tag{59}$$

where $P = (p_1+p_2)/2$ and ϵ_μ is the polarization vector of the incident photon. The invariant amplitudes $A_i(s,t)$ are Lorentz scalars, free of kinematic

singularities, and by a somewhat lengthy but straightforward calculation can be related to linear combinations of the s-channel helicity amplitudes discussed in Section IV. However, for high energy processes it is more convenient to think in terms of t-channel exchanges and to employ t-channel helicity amplitudes divided by certain factors to eliminate kinematic singularities. The four parity conserving t-channel amplitudes[71] used are related to the invariant amplitudes by

$$F_1 = -A_1 + 2M_N A_4$$

$$F_2 = (t-\mu^2)\,(A_1 + tA_2)$$

$$F_3 = 2M_N A_1 - tA_4$$

$$F_4 = -A_3 \quad , \tag{60}$$

where μ is the pion mass. The amplitudes F_1 and F_3 involve natural spin-parity exchanges in the t-channel, while F_2 and F_4 are the result of unnatural spin-parity exchanges. This statement is exact for F_1 and F_2, which involve no spin flip (in the t-channel) and true to leading order in s for F_3 and F_4 which correspond to spin flip. In terms of these amplitudes, the differential cross section can be written to leading order in s as

$$\frac{d\sigma}{dt} = \frac{1}{32\pi}\left[\frac{(-t)\,|F_1|^2 + |F_3|^2}{4M_N^2}\left(1 - \frac{t}{4M_N^2}\right) + \frac{|F_2|^2}{(t-\mu^2)^2} - t\,|F_4|^2\right] . \tag{61}$$

Neglecting terms of order $t/4M_N^2$ Eq. (61), can be rewritten in terms of the invariant amplitudes as

$$\frac{d\sigma}{dt} = \frac{1}{32\pi}\left[|A_1|^2 - t|A_4|^2 + |A_1+tA_2|^2 - t|A_3|^2\right]. \tag{62}$$

The first two terms on the right hand side of Eq. (62) arise from the amplitudes F_1 and F_3 due to natural spin-parity exchange, while the last two arise from F_2 and F_4 due to unnatural spin-parity exchange. These two sets of terms can be separated experimentally by using linearly polarized photon beams, since the cross section for photons polarized perpendicular to the production plane is (to leading order in s)

$$\frac{d\sigma_\perp}{dt} = \frac{1}{16\pi}\left\{|A_1|^2 - t|A_4|^2\right\}, \tag{63}$$

while that for photons polarized parallel to the production plane is

$$\frac{d\sigma_\parallel}{dt} = \frac{1}{16\pi}\left\{|A_1+tA_2|^2 - t|A_3|^2\right\}, \tag{64}$$

i.e. just the natural and unnatural spin-parity parts of the differential cross section[72].

As a final piece of kinematics, we note that in terms of t-channel amplitudes the asymmetry in the scattering from a polarized target (recall Eq. (24)) is[73]

$$A = \frac{\frac{\sqrt{-t}}{16\pi}\ \mathrm{Im}\left[\frac{F_1^* F_3}{4M_N^2}\left(1-\frac{t}{4M_N^2}\right) + \frac{F_2^* F_4}{\mu^2 - t}\right]}{\left(\frac{d\sigma}{dt}\right)} \tag{65}$$

which, again dropping terms of order $t/4M^2$, is expressible in terms of the invariant amplitudes as

$$A = \frac{-\frac{\sqrt{-t}}{16\pi}\ \mathrm{Im}\left[A_1^* A_4 + A_3^*(A_1+tA_2)\right]}{\left(\frac{d\sigma}{dt}\right)}. \tag{66}$$

The first term in the numerator of Eq. (65) or Eq. (66) arises from interference of natural spin-parity exchanges, while the second corresponds to interference of unnatural spin-parity exchanges.

B Charged Pion Photoproduction at Small t

The most conspicuous feature of charged pion photoproduction is the sharp forward peak. The differential cross section[74] for $\gamma p \to \pi^+ n$ jumps about a factor of two between $t = -0.02$ GeV^2 and $t=0$ (see Figure 6a). This is such a small t range for such a rapid variation that it could only be due to the very nearby (to $t=0$) t-channel singularity coming from the exchange of the pion. The s dependence of the near forward cross section, $\left(s-M_N^2\right)^2 \frac{d\sigma}{dt} \simeq$ constant in s, also agrees with what is is expected from pion exchange. However, if we look at the t-channel parity conserving amplitudes, the pion can only contribute to F_2, and at $t=0$ we have from Eq. (60) that

$$F_3(t=0) = -\frac{2M_N}{\mu^2} F_2(t=0) = 2M_N A_1(t=0), \tag{67}$$

since the invariant amplitudes can have no kinematic singularities. Thus if the pion contribution leads to F_2 being non-zero at $t=0$, so is the amplitude F_3 (due to a natural spin parity contribution), and the $t=0$ differential cross section becomes

$$\left.\frac{d\sigma}{dt}\right|_{t=0} = \frac{1}{16\pi}\left|\frac{F_3(t=0)}{2M_N}\right|^2 = \frac{1}{16\pi}\left|\frac{F_2(t=0)}{-\mu^2}\right|^2 = \frac{1}{16\pi}|A_1(t=0)|^2 . \tag{68}$$

The kinematic relation at $t=0$ in Eq. (67) is often referred to as a "conspiracy relation." If only a single particle or Regge trajectory is exchanged

then it is satisfied trivially by $F_2(t=0) = F_3(t=0) = 0$, a possibility sometimes called "evasion" and in obvious contradiction to experiment. If $F_2(t=0)$ and $F_3(t=0) \neq 0$ (called a "conspiracy"), then there is a natural spin-parity exchange (a conspirator trajectory in Regge pole theory) contribution to F_3 with just the correct magnitude at t=0 to match the pion contribution to F_2.

Although it is possible to make adequate fits to the pion photoproduction data alone with a theory using Regge poles (including, of course, a conspirator trajectory) such theories have difficulties because of the predictions they make through factorization of pole residues[75]. It has been increasingly realized that the most natural explanation for the forward peak in $\gamma p \rightarrow \pi^+ n$ and $\gamma n \rightarrow \pi^- p$ is to be found in pion exchange plus absorptive corrections, or equivalently, poles and associated cuts in the angular momentum plane. The manner[76] in which the forward peak comes about in such a model is seen in Figure 7. The slowly varying cut contribution to F_2 interferes destructively with the rapidly varying pion contribution (which would vanish by itself at t=0) to produce a total amplitude for F_2 with a sharp forward peak. The amplitude F_3, which contains no pion contribution, is expected to be slowly varying in the region near t=0, and hence to have roughly the value it has at t=0 where the conspiracy relation, Eq. (67), must be satisfied. As a result, all the rapid t variation in $\frac{d\sigma}{dt}$ is due to the pion contribtuion to the amplitude F_2. Since the overall differential cross section drops by about a factor of two between t=0 and $-0.02\ GeV^2$ and the natural and unnatural spin-parity parts of $\frac{d\sigma}{dt}$ are equal at t=0, the unnatural spin-parity part of the cross section must change from one-half the total at t=0, to near zero at $t = -0.02\ GeV^2$. As a result, the polarized photon asymmetry, Σ, would appear as in Figure 6b, as is indeed observed experimentally[74].

Independent of a specific t-channel model for the forward peak, its existence and magnitude can be predicted from s-channel considerations involving finite energy sum rules[77]. Let us consider in particular the amplitude $F_2^{(-)}$ in charged pion photoproduction due to the isovector component of the electromagnetic current. Then if $F_2^{(-)}$ has the (Regge) high energy behavior,

$$F_2^{(-)}(\nu, t) \xrightarrow[\nu \to \infty]{} \beta(t)\alpha(t) \frac{-1-e^{-i\pi\alpha(t)}}{\sin \pi\alpha(t)} \nu^{\alpha(t)-1}, \tag{69}$$

where

$$\nu = -k \cdot P/M_N = \frac{s-M_N^2}{2M_N} + \frac{t-\mu^2}{4M_N}, \tag{70}$$

it obeys the finite energy sum rule ($F_2^{(-)}$ is odd under crossing, $\nu \to -\nu$) for sufficiently large N,

$$\int_0^N d\nu \ \mathrm{Im}\ F_2^{(-)}(\nu, t) = \beta(t)\ N^{\alpha(t)} \tag{71}$$

Explicitly separating the Born term[35], we can rewrite Eq. (71) as

$$\frac{eg}{4M_N}(\mu^2+t) + \frac{1}{\pi}\int_{\nu_0}^N \mathrm{Im}\ F_2^{(-)}(\nu, t)\, d\nu = \frac{\beta(t)\ N^{\alpha(t)}}{\pi} \tag{72}$$

where $\nu_0 = \mu + \mu^2/2M_N + (t-\mu^2)/4M_N$ is the threshold for pion photoproduction and g is the pion-nucleon coupling constant ($g^2/4\pi \simeq 14.8$). An evaluation[78] of the contributions to the integral in Eq. (72) at t=0 shows that they are small compared to the Born term. This is again connected to the dominantly helicity $\frac{3}{2}$ transitions to the second and third resonances discussed in Section IV, since only the helicity $\frac{1}{2}$ state of a resonance contributes to Eq. (72) at t=0.

From the dominance of the Born term at t=0 we immediately predict that $\beta(t=0)$ and hence $F_2(\nu, t=0)$ does not vanish, so the conspiracy relation, Eq. (67) is nontrivially satisfied, and furthermore, that the magnitude of the differential cross section is given approximately by the nucleon Born term contribution, which is in fact the case experimentally. As t is decreased from zero, the Born term in Eq. (72) decreases, vanishes at $t = -\mu^2 = -0.02\ \text{GeV}^2$, and then becomes negative. Hence, since the integrand is relatively small in magnitude, from the behavior of the Born term we also expect a zero in $\beta(t)$ near $t = -0.02$, as is again found experimentally. A sum rule for $F_3(\nu, t)$ shows it to be slowly varying with t. Thus all the main features of charged pion photoproduction near the forward direction can be deduced from the finite energy sum rules together with the knowledge that the Born term dominates the sum rule for $F_2^{(-)}$. In fact, if we note from experiment that the effective value of $\alpha(t)$ in Eq. (69) is approximately zero, then a "pseudomodel" of pion photoproduction can be developed[79] where one simply integrates over the low energy data and through finite energy sum rules obtains the t dependence at high energy. Such an approach[79] is very successful, at least for $|t| \leq 0.1\ \text{GeV}^2$. One might then say that we do understand the behavior of charged pion photoproduction in some detail at small t, both from an s-channel and t-channel point of view.

C Charged Pion Photoproduction at Intermediate t Values

The same cannot be said about the behavior at larger values of t, where the situation is definitely rather complicated from any point of view. In Table II, are listed the quantum numbers of possible t-channel exchanges together with possible candidates for such exchanges from among the known mesons and the parity conserving t-channel amplitudes to which they contribute.

TABLE 2 Exchanges in Charged Pion Photoproduction

$P(-1)^J$	G	Possible Exchanged Particle	Parity Conserving t-channel Amplitude(s)
+1	-1	A_2	F_1^V, F_3^V
+1	+1	ρ	F_1^S, F_3^S
-1	-1	π	F_2^V
-1	+1	B	F_2^S
-1	-1	A_1	F_4^V

We have labelled the parity-conserving t-channel amplitudes by an S or V superscript depending on whether they are due to the isoscalar or isovector component of the elctromagnetic current, respectively. The ratio of $d\sigma/dt(\gamma n \to \pi^- p)/d\sigma/dt(\gamma p \to \pi^+ n)$ measures the interference of the amplitudes due to the isoscalar and isovector components of the current since any particular helicity amplitude, A, has the decomposition A^S+A^V for $\gamma p \to \pi^+ n$ and A^S-A^V for $\gamma n \to \pi^- p$ (see Eq. (30)). Then using the connection of perpendicular and parallel (to the production plane) photon polarization to natural and unnatural spin-parity exchange, we write the various possible cross sections as

$$
\begin{aligned}
\frac{d\sigma_\perp}{dt}(\gamma p \to \pi^+ n) &= |\text{"}A_2\text{"}+\text{"}\rho\text{"}|^2 \\
\frac{d\sigma_\parallel}{dt}(\gamma p \to \pi^+ n) &= |\text{"}\pi\text{"} + \text{"B"}|^2 + |\text{"}A_1\text{"}|^2 \\
\frac{d\sigma_\perp}{dt}(\gamma n \to \pi^- p) &= |-\text{"}A_2\text{"}+\text{"}\rho\text{"}|^2 \\
\frac{d\sigma_\parallel}{dt}(\gamma n \to \pi^- p) &= |-\text{"}\pi\text{"}+\text{"B"}|^2 + |\text{"}A_1\text{"}|^2 ,
\end{aligned}
\tag{73}
$$

where $|\text{"}A_2\text{"} + \text{"}\rho\text{"}|^2$ represents the contribution of $|F_1^V + F_1^S|^2$ and $|F_3^V + F_3^S|^2$ to $d\sigma_\perp/dt(\gamma p \to \pi^+ n)$, etc. An analysis of the present experimental data[74] then indicates that:

(1) Although $d\sigma_\perp/dt(\gamma p \to \pi^+ n)$ is by far the dominant part of π^+ photoproduction for $|t| \geq 0.02$ GeV^2 ($\Sigma = 0.5$ to 1.0 at least out to $|t| \simeq 1$ GeV^2), the energy dependence of $\gamma p \to \pi^+ n$ corresponds to an

effective value of the Regge trajectory, $\alpha(t)$, of zero or less for $0 \leq |t| \leq 1\ \mathrm{GeV}^2$. Thus, although ρ and A_2 exchange might be expected to dominate $d\sigma_\perp/dt$, there is no sign of the corresponding energy dependence (which would yield $\alpha(t) \simeq 0.5 + t/\mathrm{GeV}^2$).

(2) While $d\sigma_\perp/dt(\gamma n \to \pi^- p)$ and $d\sigma_\perp/dt(\gamma p \to \pi^+ n)$ are equal at very small t where presumably only absorptive cuts due to pion exchange dominate, their ratio (of π^-/π^+) decreases to a minimum value of ~ 0.2 at $t = -0.4\ \mathrm{GeV}^2$. This requires that the "ρ" and "A_2" contributions are of comparable magnitude and interfere strongly in the F_1 and F_3 amplitudes. If the "ρ" and "A_2" contributions had the phase of the Regge signature factor $\mp 1 - e^{-i\pi\alpha(t)}$, they could not interfere since they would be 90° out of phase assuming $\alpha_\rho(t) = \alpha_{A_2}(t)$. Also, any "nonsense zero" (due to a factor of $\alpha(t)$ in the ρ exchange contribution) would result in an absence of interference where $\alpha(t) = 0 (t \simeq -0.6\ \mathrm{GeV}^2)$, while experiment shows almost maximal interference there.

(3) The values of $d\sigma_\parallel/dt(\gamma p \to \pi^+ n)$ and $d\sigma_\parallel/dt(\gamma n \to \pi^- p)$ are equal within rather large errors. There is then no need for the "B" term in Eq. (73), although it may be present and out of phase with the "π" term.

(4) The large values[79] of the asymmetry for $\gamma p \to \pi^+ n$ using a polarized target at photon energies of 5 and 16 GeV require both the (out of phase) F_1 and F_3 amplitudes to be present in π^+ photoproduction.

In short, we have a rather complicated situation in charged pion photoproduction at intermediate t values. Both natural and unnatrual spin-parity exchanges are present for $|t| \leq 1\ \mathrm{GeV}^2$, and both the isovector and isoscalar components of the electromagnetic current make important contributions to $d\sigma/dt$ in this t range. Simple Regge pole models fail, presumably again due to the importance of absorptive corrections or cuts in the angular momentum

plane. This failure is a general feature of other inelastic photoproduction processes such as $\gamma p \rightarrow \eta^0 p$, $\gamma p \rightarrow p$, $\gamma p \rightarrow K^+ \Lambda$, etc., which we do not have the time to discuss here, but which are well treated elsewhere (see particularly reference 65). We have concentrated on only charged pion photoproduction, where there is much experimental information and where both our successes and difficulties are most apparent. While we understand many of the phenomena at least qualitatively, we clearly do not have a well founded theory on the basis of which we can make detailed quantitative predictions.

D Tests of the Vector Dominance Model

Whatever the specifics of the dynamics of charged pion photoproduction, one expects the same dynamics in pion production of vector mesons if the vector dominance model is to be true. Specifically, one has the relation[80]

$$\frac{1}{2}\left[\frac{d\sigma_{\perp,\parallel}}{dt}(\gamma p \rightarrow \pi^+ n) + \frac{d\sigma_{\perp,\parallel}}{dt}(\gamma n \rightarrow \pi^- p)\right]$$

$$= \left(\frac{e}{f_\rho}\right)^2 \left(\frac{q_\pi}{k_\gamma}\right)^2 (\rho_{11} \pm \rho_{1-1}) \frac{d\sigma}{dt}(\pi^- p \rightarrow \rho^0 n) \quad , \qquad (74)$$

where the π^+ and π^- differential cross sections have been added to cancel the isovector-isoscalar interference term on the left hand side and the ω and ϕ production terms have been dropped from the right hand side as numerically negligible. The combination of density matrix elements $\rho_{11} \pm \rho_{1-1}$ for the rho meson corresponds to linear polarization perpendicular or parallel to the production plane, and is presumably to be evaluated in the helicity frame[29]. Averaging over the two polarizations yields

$$\frac{1}{2}\left[\frac{d\sigma}{dt}(\gamma p \to \pi^+ n) + \frac{d\sigma}{dt}(\gamma n \to \pi^- p)\right]$$

$$= \left(\frac{e}{f_\rho}\right)^2 \left(\frac{q_\pi}{k_\gamma}\right)^2 \rho_{11} \frac{d\sigma}{dt}(\pi^- p \to \rho^0 n) \quad . \tag{75}$$

Qualitatively, the most striking prediction of photoproduction and Eqs. (74) and (75) is the existence of a forward peak in $\pi^- p \to \rho^0 n$ due to a rapid variation of $(\rho_{11} - \rho_{1-1}) \frac{d\sigma}{dt}(\pi^- p \to \rho^0 n)$. This has recently been observed[81] in an investigation of the reaction $\pi^- p \to \pi^+ \pi^- p$ for small t values at 15 GeV. Moreover subject to some assumption on the behavior of the s-wave pion pairs, it appears that Eq. (74) is quantitatively verified for small t in the case of polarization parallel to the production plane and the colliding beam value for $f_\rho^2/4\pi$. There are quantitative difficulties in the case of perpendicular polarization, however, as both near the forward peak and at intermediate t values the left hand side of Eq. (74) is too large[74,81]. This would require a smaller value of $f_\rho^2/4\pi$ than given by the colliding beam experiments if Eq. (74) were to be in agreement with experiment for perpendicular polarization. But such a change in $f_\rho^2/4\pi$ would ruin the agreement in the case of parallel polarization. Thus again, we find qualitative agreement with the vector dominance model, but quantitative troubles if we consider the predicted relations in detail.

VIII Inelastic Electron Scattering: Introduction

Since the electron is apparently an elementary, structureless particle with a known electromagnetic interaction with matter, inelastic electron scattering is an ideal probe of the structure of other composite objects such as atoms and nuclei. By bombarding a target with a beam of known energy and detecting only the outgoing electrons, one can determine the charge distribution within an object, and hence gain information on the constituents inside.

An example is shown in Figure 8 where a "typical" result of scattering electrons of given incident energy through a fixed angle on a nucleus is shown. For final energies near the incident one, one sees the peaks due to elastic scattering and the excitation of discrete nuclear levels. At lower final energies (greater energy loss) there is a broad quasi-elastic peak due to electrons scattering off the constituent nucleons and ejecting them from the nucleus.

In the case of hadrons like the nucleon, we believe we are dealing with a composite object in some sense or another, but we do not know what the basic constituents are, if any, nor do we know the nature of the forces which bind them together. Furthermore, there is a very important difference between hadrons and atoms or nuclei in that the binding energy of the system is not small compared to the overall mass in the former case, as it is in the latter. Quark constituents of the nucleon, for example, must be very strongly bound or we would have seen them long ago. This lack of weak binding in the case of a constituent of a hadron makes it unclear that one can carry over the simple version of the idea of electron scattering as a direct probe of substructure from atomic or nuclear systems to hadrons. Nevertheless this way of thinking, particularly in terms of point quark constituents, has been very useful both in predicting and interpreting the results of inelastic scattering of electrons off nucleons and in relating and predicting the

behavior of other processes[82]. We shall discuss this approach to inelastic electron scattering in more detail in Section XI.

Another way of approaching the subject of inelastic electron scattering is through the use of ideas borrowed from strong interactions. We have already discussed some of these ideas in connection with specific photoproduction processes. In particular, if we consider electron-nucleon scattering as in fact a collision of a virtual photon (emitted by the electron) with the target nucleon, we can apply theoretical ideas on hadronic two-body collisions, the difference with hadron-hardon processes being that the "mass" of one of the incident particles (the photon) can be varied. This turns out to be an important advantage, and leads to very interesting applications of strong interaction theoretical ideas, particularly those of duality which equate the description of a scattering amplitude in terms of direct channel resonances and background to that in terms of exchanges in the crossed channel. We shall spend some time developing this approach to inelastic electron scattering in Section XIII.

A third method of approach is in terms of light-cone commutators. As we shall see in the next section, measurements of inelastic electron-nucleon scattering can be related to the Fourier transform of the matrix element of the commutator of two electromagnetic currents taken between nucleon states,

$$\int d^4x\, e^{-iq\cdot x} \langle p \left| \left[J_\mu(x),\, J_\nu(0) \right] \right| p \rangle \quad .$$

where q_μ is the four-momentum of the exchanged photon. If we consider scattering at high energies and momentum transfer, and in particular the limit where the energy loss of the electron and the momentum transfer squared both become infinite in a fixed ratio, then the scattering is governed[83] by the behavior of the commutator $\left[J_\mu(x),\, J_\nu(0) \right]$ as x_μ approaches the light cone, $x^2 = 0$. This suggests

making a light cone expansion[84] of the commutator of two electromagnetic currents, with the coefficients in the expansion being operators (e.g., another current) in general. One hopes that some or all of the operators appearing in the expansion can be abstracted from simple free field theories (e.g., a free quark field theory), very much in analogy to the algebra of currents at equal times which holds at the tip of the light cone[85]. The light cone expansion of the commutator of two currents may then be applied to various processes[83,84], electron scattering in the limit of infinite energy losses and momentum transfers being one particular case when the commutator is sandwiched between nucleon states. Especially when additional assumptions are made about the matrix elements of the light cone commutator, many (but not all) of the results of the approach in terms of quark constituents of the nucleon can be reproduced[85]. While we shall not discuss this subject in any detail, considerable progress has been made in unifying the ideas of scale invariance, the algebra of current commutators on the light cone, and some of the results of the quark constituent approach (see reference 85), and it is an important area of present research.

IX Kinematics of Inelastic Electron-Nucleon Scattering

We are interested in the process shown in Figure 9, where k and k' are the initial and final electron four-momenta, q is the four-momentum transfer carried by the virtual photon, and p is the target nucleon's four-momentum. The final hadronic state n then has four-momentum $p_n = p + q$ and invariant mass squared $W^2 = -(p+q)^2$. In the laboratory frame (initial nucleon at rest) with E and E' the energies of the initial and final electrons, the Lorentz scalar variable

$$\nu = -p \cdot q/M_N = E - E' \tag{76}$$

is the virtual photon's energy, and the invariant momentum transfer squared is

$$q^2 = 4\,E\,E'\,\sin^2\theta/2\ , \tag{77}$$

where θ is the scattering angle and the electron mass has been neglected compared to its energy. Knowing ν and q^2 from measuring the incident and scattered electron, the invariant mass W of the final hadrons is fixed by

$$s = W^2 = 2\,M_N\nu + M_N^2 - q^2\ . \tag{78}$$

The S-matrix element for the process in Figure 9 may be written using the rules of quantum electrodynamics at the photon-electron vertex as

$$S_{fi} = \delta_{fi} + (2\pi)^4 i\delta^{(4)}(p_n + k' - p - k)\sqrt{\frac{m_e^2}{E\,E'}}\ \left(-e\,\bar{u}(k) i\gamma_\mu\, u(k)\right)$$
$$\times \left(\delta_{\mu\nu}/q^2\right) \langle p_n | J_\nu\,(0) | p\rangle\ , \tag{79}$$

where J_ν is the (hadronic) electromagnetic current operator. Averaging over initial and summing over final electron and nucleon spins, we are led to an expression for the double differential cross section in the laboratory for detection

of only the final electron of the form

$$\frac{d^2\sigma}{d\Omega' dE'} = \frac{1}{(2\pi)^2} \frac{E'}{E} \left(\frac{e^2}{q^2}\right)^2 L_{\mu\nu} W_{\mu\nu} \quad , \tag{80}$$

where the factor $L_{\mu\nu}$ arises from the trace of the gamma matrices due to the electron (neglecting the electron mass),

$$L_{\mu\nu} = \frac{1}{2}\left[k_\mu k'_\nu + k'_\mu k_\nu + \left(\frac{q^2}{2}\right) \delta_{\mu\nu}\right] \quad , \tag{81}$$

and the structure of the nucleon is summarized in

$$W_{\mu\nu} = \frac{1}{2} \sum_{\substack{\text{nucleon} \\ \text{spin}}} \sum_{n} \left(\frac{1}{e^2}\right) \langle p|J_\mu(0)|n\rangle$$

$$\langle n|J_\nu(0)|p\rangle (2\pi)^3 \delta^{(4)}(p_n - p - q) \tag{82}$$

$$= \frac{1}{2} \sum_{\substack{\text{nucleon} \\ \text{spin}}} \left(\frac{1}{2\pi e^2}\right) \int d^4x e^{-iq\cdot x} \langle p|\left[J_\mu(x), J_\nu(0)\right]|p\rangle \quad ,$$

where the second term in the commutator is zero by energy conservation for $\nu > 0$.

By Lorentz and gauge invariance the tensor $W_{\mu\nu}$ may be written as[86]

$$W_{\mu\nu} = W_1(\nu, q^2)\left(\delta_{\mu\nu} - \frac{q_\mu q_\nu}{q^2}\right) + W_2(\nu, q^2)$$

$$\left(p_\mu - \frac{p\cdot q q_\mu}{q^2}\right)\left(p_\nu - \frac{p\cdot q q_\nu}{q^2}\right) \Big/ M_N^2 \quad . \tag{83}$$

The quantity $W_{\mu\nu}$ is just $(1/4\pi^2\alpha)$ times the imaginary part of the Feynman amplitude for forward Compton scattering of virtual photons of mass$^2 = -q^2$. In terms of W_1 and W_2 the experimentally measured double differential cross

section resulting from combining Eqs.(80), (81), and (83) is

$$\frac{d^2\sigma}{d\Omega' dE'} = \frac{4\alpha^2 E'^2}{q^4}\left[2W_1(\nu, q^2)\sin^2\theta/2 + W_2(\nu, q^2)\cos^2\theta/2\right], \quad (84)$$

so that the structure functions W_1 and W_2, as they depend on ν and q^2, summarize the results of inelastic electron-nucleon scattering.

As noted above, $W_{\mu\nu}$ is proportional to the imaginary part of the amplitude for forward (virtual) photon-nucleon scattering. By the optical theorem, the imaginary part of the forward Compton amplitude is proportional to the total cross section for photons on nucleons. In fact, we could consider inelastic electron scattering as being a collision between the exchanged (virtual) photon and the target nucleon. One is then simply studying the total cross section for the process "γ" + N $\longrightarrow$ hadrons, where the hadrons have an invariant mass W and we are able to vary the energy, mass, and polarization of the incident photon beam. This leads one to define virtual photon-nucleon total cross sections for transversely and longitudinally polarized photons[87] $\sigma_T(\nu, q^2)$ and $\sigma_S(\nu, q^2)$. In terms of these total cross sections

$$\frac{d^2\sigma}{d\Omega' dE'} = \frac{\alpha}{4\pi^2}\frac{K}{q^2}\frac{E'}{E}\left(\frac{2}{1-\epsilon}\right)(\sigma_T + \epsilon\,\sigma_S) \quad (85)$$

where

$$K = \nu - q^2/2M_N$$

and

$$\epsilon = \frac{1}{1 + 2(1+\nu^2/q^2)\tan^2\theta/2},$$

so that $0 \leq \epsilon \leq 1$.

On comparison with Eq. (84), we have the relations

$$W_1(\nu, q^2) = \frac{K}{4\pi^2\alpha}\ \sigma_T(\nu, q^2)$$

$$W_2(\nu, q^2) = \frac{K}{4\pi^2\alpha}\ \frac{q^2}{q^2+\nu^2}\left[\sigma_T(\nu, q^2) + \sigma_S(\nu, q^2)\right]. \qquad (86)$$

At $q^2 = 0$, $\sigma_T(\nu, q^2=0)$ is just the total photoabsorption cross section of real photons on nucleons (shown for the proton in Figure 1). The quantity $\sigma_S(\nu, q^2)$ must vanish at $q^2 = 0$ because of the constraints of gauge invariance. The contribution of the single pion plus nucleon channel to σ_T and σ_S may be expressed in terms of sums of squares of multipole amplitudes, very much as was done for real photons in Section V, with the electric and magnetic multipoles contributing to $\sigma_T(\nu, q^2)$, and the longitudinal multipoles to $\sigma_S(\nu, q^2)$[88].

The results of experiment are then to be expressed in terms of W_1 and W_2 (or σ_T and σ_S, which are related through Eq. 86) as they depend on ν and q^2. A kinematic map of the $\nu - q^2$ plane is shown in Figure 10. The lines at fixed W correspond to given values of the hadronic missing mass. Measurements along the line W = 0.94 GeV = M_N correspond in particular to elastic scattering where W_1 and W_2 have delta functions due to the nucleon pole:

$$W_1^{\text{elastic}}(\nu, q^2) = \frac{G_M^2(q^2)}{4M_N^2}\ \delta\left(\nu - q^2/2M_N\right)$$

$$W_2^{\text{elastic}}(\nu, q^2) = \frac{G_E^2(q^2) + \frac{q^2}{4M_N^2}\,G_M^2(q^2)}{1 + \frac{q^2}{4M_N^2}}\ \delta\left(\nu - q^2/2M\right) \quad , \qquad (87)$$

$G_E(q^2)$ and $G_M(q^2)$ being the usual electric and magnetic form factors of the nucleon. Measurements of inelastic scattering are usually made at fixed angle and incident energy, with varying final energy as shown in Figure 10. As the energy loss increases (final energy decreases) one first encounters the elastic peak, then the region of prominent resonance excitation, and finally, for $W \gtrsim 2$ GeV, the inelastic continuum. Measurement of the scattering along two (or more) fixed θ lines in the $\nu - q^2$ plane allows separation of W_1 and W_2 (or σ_T and σ_S) at the crossover point, which then has the same values of ν and q^2 but a different value of θ and ϵ for the different lines.

All the above discussion may obviously be applied as well to inelastic muon-nucleon scattering. There are also two other closely related processes. First, in the above we averaged over the electron and nucleon spins, as is done in all present experiments. In the future it should be possible to employ a polarized electron beam and a polarized target to determine the spin dependent structure functions $d(\nu, q^2)$ and $g(\nu, q^2)$ defined by[89]

$$\frac{1}{2}\left\{\sum_n \langle p,s|J_\mu(0)|n\rangle \langle n|J_\nu(0)|p,s\rangle (2\pi)^3\delta^{(4)}(p_n - p - q)\right.$$

$$\left. - \sum_n \langle p,-s|J_\mu(0)|n\rangle \langle n|J_\nu(0)|p,-s\rangle (2\pi)^3\delta^{(4)}(p_n - p - q)\right\} \qquad (88)$$

$$= \frac{1}{4\pi M_N}\left\{-\epsilon_{\mu\nu\lambda\sigma} q_\lambda s_\sigma d(\nu,q^2) + (s\cdot q)\,\epsilon_{\mu\nu\lambda\sigma} q_\lambda p_\sigma g(\nu,q^2)\right\},$$

where the antisymmetric tensor $\epsilon_{\mu\nu\lambda\sigma}$ is +1 in the case ϵ_{1234} and s_σ is a covariant spin four-vector for the nucleon ($s^2 = 1$, $s \cdot p = 0$).

Using the lepton trace,

$$L_{\mu\nu} = \frac{1}{2}\left(k_\mu k'_\nu + k'_\mu k_\nu + (q^2/2)\delta_{\mu\nu} \mp i\epsilon_{\mu\nu\lambda\sigma} k_\lambda k'_\sigma\right)$$

for helicity $\pm \frac{1}{2}$ electrons, one calculates that the spin dependent structure functions lead to the measurable difference,

$$\frac{d^2\sigma^{\uparrow\downarrow}}{d\Omega' dE'} - \frac{d^2\sigma^{\uparrow\uparrow}}{d\Omega' dE'} = \frac{4\alpha^2 E'}{q^2 E}\left(\frac{1}{4\pi M_N}\right) \times \left\{(E + E'\cos\theta)\, d(\nu, q^2) + (E - E'\cos\theta)(E + E')\, M_N g(\nu, q^2)\right\}, \tag{89}$$

where $d^2\sigma^{\uparrow\downarrow}/d\Omega' dE'$ $\left(d^2\sigma^{\uparrow\uparrow}/d\Omega' dE'\right)$ is the double differential cross section when the spins of the electron and nucleon are antiparallel (parallel) and along the direction of the incident beam. Note that both a polarized beam and target are required as otherwise the antisymmetric (in $\mu \longleftrightarrow \nu$) tensor in Eq. (88) gives zero when contracted with the symmetric lepton trace in Eq. (81). Just as one can define total photon-nucleon cross sections, σ_T and σ_S, which are linearly related to W_1 and W_2, it is possible to define[90] total cross sections σ_P and σ_A $\left(\sigma_T = \frac{1}{2}(\sigma_P + \sigma_A)\right)$ for (virtual) photon spin parallel and antiparallel to the nucleon spin, respectively. These are then linearly related to $d(\nu, q^2)$ and $g(\nu, q^2)$ and, neglecting a possible cross term between longitudinal and transverse polarizations, the difference of double differential cross sections appearing in Eq. (89) can be alternatively rewritten in terms of σ_P and σ_A[90].

Second, through the conserved vector current hypothesis[91] the weak vector current (strangeness non-changing) is related by an isospin rotation to the isovector part of the electromagnetic current. Thus neutrino and antineutrino-nucleon inelastic scattering would be expected to exhibit similar properties to inelastic electron scattering. For such processes, not only do we have the structure functions W_1 and W_2, which now get contributions from both the vector and axial-

vector currents, but also a structure function W_3 which arises from the interference between the vector and axial-vector currents. The double differential cross section for neutrino (antineutrino)-nucleon inelastic scattering is[92] (neglecting lepton masses)

$$\frac{d^2\sigma}{d\Omega' dE'} = \frac{G^2 (E')^2}{2\pi^2} \left[2 \sin^2\left(\frac{\theta}{2}\right) W_1^{(\pm)}\left(\nu, q^2\right) + \cos^2\left(\frac{\theta}{2}\right) W_2^{(\pm)}\left(\nu, q^2\right) \right.$$

$$\left. \mp \frac{E+E'}{M_N} \sin^2\left(\frac{\theta}{2}\right) W_3^{(\pm)}\left(\nu, q^2\right) \right] , \qquad (90)$$

where the weak coupling constant $G \simeq 1.0 \times 10^{-5}/M_N^2$, and the +(-) superscript corresponds to neutrinos (antineutrinos). The close similarity to Eq. (84) for inelastic electron scattering is evident.

X Inelastic Electron Scattering Experiments and Scaling

The first measurements of inelastic electron scattering at high energies and momentum transfers[93] showed that besides the excitation of the prominent nucleon resonances there is a large cross section for "deep" inelastic scattering with excitation of the continuum. The size of the cross sections may be simply summarized as being roughly point-like: When the cross section at fixed q^2 is integrated over ν one obtains a result which is the same order of magnitude as the Mott cross section for scattering from a point proton.

What are the other properties of this large cross section? Measurements of the scattering at different angles but the same value of ν and q^2, as we saw in the previous section, permit a separation of the contributions of W_1 and W_2 to the double differential cross section. Such a separation of W_1 and W_2 is equivalent to a knowledge of $R = \sigma_S/\sigma_T$ by Eq. (86). The value of R obtained by averaging over the present data[94] in the deep inelastic region is $R = 0.18 \pm 0.10$. This is certainly small, and given possible systematic errors it is possible, although unlikely, that $R = 0$. The individual values of R do not show any strong dependence on ν or q^2. The scattering is thus dominantly transverse, rather than longitudinal.

The same measurements[93] which showed the point-like size of the scattering also showed a second phenomenon, the scaling behavior proposed by Bjorken[95]. "Scaling" is the statement that as ν and $q^2 \longrightarrow \infty$, νW_2 and W_1 become non-trivial functions of the dimensionless ratio $\omega = 2M_N\nu/q^2$ only, rather than functions of both ν and q^2 as would be the case a priori. We may look for the scaling behavior in the data where ν and q^2 are finite by studying the behavior of νW_2 and W_1 at any fixed value of ω as we vary q^2 (and therefore ν) and see if they tend to (non-zero) limiting values as q^2 becomes large. Since from a theoretical standpoint scaling is a statement of behavior as ν and $q^2 \longrightarrow \infty$, any other

dimensionless variable, ω', such that $\omega' \longrightarrow \omega$ as ν and $q^2 \longrightarrow \infty$, is in principle just as suitable as ω as a scaling variable. Another variable could in fact lead to the scaling behavior sooner in the sense that νW_2 and W_1 could become independent of q^2 (and hence equal to their $q^2 \longrightarrow \infty$ limit) for smaller values of q^2 if they are studied as functions of q^2 at fixed ω' rather than ω.

This is in fact the case for inelastic electron-proton scattering. If we take data with $q^2 \geq 1\ \text{GeV}^2$ and for the moment stay away from the low W region with prominent nucleon resonances, then there is a more rapid approach to scaling behavior if one uses the variable[96]

$$\omega' = 1 + W^2/q^2 = \omega + M_N^2/q^2 \quad . \tag{91}$$

Clearly ω' is dimensionless and is the same as ω in the Bjorken limit of ν and $q^2 \longrightarrow \infty$. Using a fixed value[94] of R = 0.18, Figure 11 shows νW_2 and $2M_N W_1$ as functions of ω' for various q^2 intervals and $W \geq 2.0$ GeV (beyond the prominent resonances). Clearly both νW_2 and W_1 scale non-trivially (i.e., are finite and independent of q^2 at fixed ω') to within the accuracy of the data for ω' in the range $1 < \omega' < 10$, as long as $q^2 \geq 1\ \text{GeV}^2$ and $W \geq 2.0\ \text{GeV}$[94]. The scaling of νW_2 and W_1 is independent of the particular value of R chosen in plotting Figure 11. As long as R is small, as shown by direct measurements, one obtains essentially the same result of scaling for both W_1 and νW_2 starting at incredibly low values of $q^2 \simeq 1\ \text{GeV}^2$.

Another way of looking at the results of the deep inelastic scattering experiments is shown in Figure 12 where the experimentally measured combination of total cross sections, $\sigma_T + \epsilon\sigma_S$, is plotted against q^2/W^2 for various hadron masses W. Also shown is $G_E^2(q^2) + \left(q^2/4M_N^2\right)G_M^2(q^2)$, the analogue of $\sigma_T + \sigma_S$ for W = 0.94 GeV, i.e., elastic scattering. When $1/9 < q^2/W^2 \lesssim 1/3$, corresponding to the relatively flat part of νW_2 between ω' of 4 and 10 in Figure 11, $\sigma_T + \epsilon\sigma_S$

falls slowly (like $1/q^2$). But when q^2/W^2 becomes large, we come below the knee in νW_2 and $\sigma_T + \epsilon\sigma_S$ falls rapidly, roughly like $1/q^6$ for fixed W. From Eq. (86), a $1/q^6$ behavior for $\sigma_T + \sigma_S$ as $q^2 \longrightarrow \infty$ implies that[94]

$$\nu W_2 \propto \left(W^2/q^2\right)^3 = (\omega' - 1)^3 \tag{92}$$

as $q^2/W^2 \longrightarrow \infty$ or $\omega' \longrightarrow 1$. The behavior of $\sigma_T + \sigma_S \propto 1/q^6$ as $q^2 \longrightarrow \infty$ at fixed W is just the behavior of the elastic analogue of $\sigma_T + \sigma_S$, $G_E^2(q^2) + \frac{q^2}{4M_N^2} G_M^2(q^2)$, at large q^2 if we take dipole forms for $G_{Ep}(q^2)$ and $G_{Mp}(q^2)$. As noted many times previously, the deep inelastic ($W \gtrsim 2$ GeV) cross section does fall with increasing q^2 more slowly than elastic scattering at the same value of q^2, particularly for values of q^2 of a few GeV^2 for which ω' is in the range where νW_2 is approximately constant. But for sufficiently large values of q^2 the cross section for any fixed W falls rapidly, very much as elastic scattering does already at much lower values of q^2.

Another very interesting property of the deep inelastic cross section is that it is isospin-dependent, i.e., different for neutron and proton targets. Neglecting corrections for internal motion, final state interactions, and Glauber corrections, the neutron cross sections are given by the difference of the deuterium and hydrogen cross sections[97]. With this assumption, the data[96] indicate that the neutron cross sections are smaller than the proton cross sections over a large kinematic range. Assuming that at each ν and q^2 value the same value of $R = \sigma_S/\sigma_T$ holds for both the neutron and proton, then $\nu W_{2n}/\nu W_{2p}$ is smaller than unity at least for $\omega' \lesssim 6$, and νW_{2n} scales within the accuracy of the data[96]. If one plots $\nu W_{2p} - \nu W_{2n}$, then there appears to be a maximum near $\omega' = 4$, at which point $\nu W_{2p} - \nu W_{2n} \simeq 0.1$ and the ratio $\nu W_{2n}/\nu W_{2p} \simeq 2/3$.

These properties of inelastic electron scattering would be expected to carry over to inelastic neutrino (or antineutrino) scattering. There one would expect the structure functions W_1, νW_2, and νW_3, to scale[92]. Unfortunately the present data[98] do not allow a clean separation of the three form factors. There is, however, evidence for a consequence of scaling, namely, that the total cross section should rise linearly with the incident neutrino energy. The present results[98] are those for neutrinos,

$$\sigma(E) = (0.52 \pm 0.13) \frac{G^2 M_N E}{\pi} \tag{93}$$

per nucleon from a propane-filled bubble chamber experiment. There is also some evidence[98] that use of ω' rather than ω leads to scaling sooner in inelastic neutrino-nucleon scattering, just as it does for inelastic electron-nucleon scattering.

From the above discussion, it is clear that the existing experiments which detect the final electron only are rather extensive and cover the presently available energy and momentum transfer region rather completely. Aside from refinements and filling in some accessible regions between existing measurements, the next step in inelastic electron scattering experiments is to investigate the nature of the hadronic final state. Preliminary results[99] indicate that the rho-plus-nucleon final state forms a decreasing percentage of the total hadrons as q^2 increases from zero to ~ 1 GeV^2. Experiments have also been performed on forward pion and proton electroproduction[100], and many other experiments are planned. This is a very interesting subject which, together with the investigation of the spin dependence of inelastic electron scattering and inelastic neutrino scattering, will clearly occupy much attention at both electron and proton accelerators in the next few years.

XI The Parton Model

The large magnitude of the inelastic electron-nucleon scattering data and the scaling behavior arise naturally in the models where the nucleon is composed of point constituents. In fact such a model was originally used to predict that the cross sections for inelastic electron-proton scattering would be of point-like magnitude[101]. The key means of implementing such a model is to view the nucleon in an infinite momentum frame of reference where the nucleon is Lorentz-contracted into a thin pancake and the motion of the constituents, called partons[102], is slowed to a standstill by time dilatation. If the partons in the nucleon are limited in the magnitude of their momentum in its rest frame, then in the infinite momentum frame they will each have a finite fraction x_i of the infinite momentum, P, with $\sum x_i = 1$. If, following Drell and Yan[103], we choose the center of mass of the incident electron and nucleon as the electron energy goes to infinity as the infinite momentum frame, then the time of interaction of the virtual photon is of order

$$T_{int} \sim \frac{1}{(q_0)_{cm}} \simeq \frac{4P}{2M_N\nu - q^2} \quad ,$$

where P is the momentum of the incident electron in the center of mass. The lifetime of a state made up of partons of momentum fractions x_i is on the other hand of order

$$T_{lifetime} \sim \frac{1}{\sum E_i - E} = \frac{1}{\sum_i \sqrt{x_i^2 P^2 + k_{i\perp}^2 + M_i^2} - \sqrt{P^2 + M^2}}$$

$$\simeq \frac{2P}{\sum_i \left(\frac{k_{i\perp}^2 + M_i^2}{x_i} \right) - M^2} \quad .$$

Thus if

$$2M_N\nu - q^2 \gg \sum_i \left(\frac{k_{i\perp}^2 + M_i^2}{x_i} \right) - M^2 \ ,$$

then $T_{int} \ll T_{lifetime}$ and one may treat the electron as scattering instantaneously off the long-lived, essentially free, partons, i.e., one can use the impulse approximation. The inequality is satisfied if $2M_N\nu$ and q^2 are much greater than any transverse momentum squared or mass squared, with the ratio $\omega = 2M_N\nu/q^2$ fixed. Then the fraction of longitudinal momentum, x, on the parton from which the electron scatters is given by $(1/\omega)$ which is fixed and non-zero (see below and reference 102), so that

$$\sum_i \left(\frac{k_{i\perp}^2 + M_i^2}{x_i} \right) - M^2$$

is bounded, while $2M\nu - q^2 = q^2(\omega - 1)$ is increasing linearly with q^2.

With the imposition of a transverse momentum cutoff, Drell, Levy and Yan[104] have shown that the canonical quantum field theory of interacting pions and nucleons gives rise to such a parton picture in the infinite momentum frame. The partons in this model are the virtual pions and nucleons making up the nucleon, with the interacting partons, i.e., the free point constituents which interact with the electromagnetic current, being the bare nucleons, and not the pions.

In summary, the detailed assumptions made in the parton model of inelastic electron scattering are[102]:

(1) The nucleon consists of a superposition of a number (N) of point constituents (partons) which can be treated as free particles in the infinite momentum frame as $2M_N\nu$ and q^2 become infinitely large with the ratio $\omega = 2M_N\nu/q^2$ fixed.

The exact configuration of the partons and their fractions of the total momentum depend on the strong interactions.

(2) The partons have negligible transverse momenta (compared to $\sqrt{q^2}$) and, as $P \longrightarrow \infty$, the i'th parton has (neglecting masses and transverse momenta) a fraction x_i of the total momentum of the proton

$$P_i \simeq x_i P \ ,$$

with $0 \leq x_i \leq 1$.

(3) In the infinite momentum frame the electron scatters instantaneously off the point parton leaving it with the same mass and charge. A little calculation then shows that the contribution of a single parton (with a fraction x_i of the longitudinal momentum) to $W_2(\nu, q^2)$ is:

$$W_2^{(i)}(\nu, q^2) = Q_i^2 \, \delta\left(\nu - q^2/2 M_N x_i\right)$$

$$= \frac{Q_i^2 \, x_i}{\nu} \, \delta\left(x_i - q^2/2 M_N \nu\right) \ . \tag{94}$$

Let $P(N)$ be the probability of N partons occurring ($\sum P(N) = 1$), $\sum_{i=1}^{N} Q_i^2$ the sum of the squares of their charges and $f_N(x)$ the distribution of longitudinal momentum fraction normalized so that

$$\int_0^1 f_N(x_i)\, dx_i = 1 \ . \tag{95}$$

Then νW_2 for such a distribution of partons is given by[102]

$$\nu W_2(\nu, q^2) = \nu \sum_N P(N) \sum_{i=1}^{N} Q_i^2 \int_0^1 dx_i \, f_N(x_i) \, \delta\left(\nu - q^2/2 M_N x_i\right)$$

$$= \sum_N P(N) \sum_i Q_i^2 \, x f_N(x) \Big|_{x = q^2/2M_N\nu} \tag{96}$$

$$= F_2\left(x = q^2/2M_N\nu = 1/\omega\right) .$$

The quantity $\nu W_2(\nu, q^2) = F_2(x)$ is then predicted to scale[95], i.e., be just a function of $x = 1/\omega$ at infinite q^2 and ν. The point-like magnitude of the data has been put in through the assumption of point constituents. The shape of $F_2(x)/x$ gives a weighted average of $f_N(x)$, the distribution of longitudinal momentum of the partons. A similar calculation indicates that $W_1(\nu, q^2)$ should scale: $W_1(\nu, q^2) = F_1(x)$ as $2M_N\nu$ and $q^2 \longrightarrow \infty$. The exact relation between $F_1(x)$ and $F_2(x)$ depends on the spin of the partons, with $2M_N x F_1(x) = F_2(x)$ (corresponding to $R = \sigma_S/\sigma_T = 0$) in the case of spin $\frac{1}{2}$ constituents.

If one is willing to take the parton model seriously in a quantitative sense, two sum rules emerge immediately from these considerations. From the normalization condition, Eq. (95), and assuming the same distribution of longitudinal momenta for all the partons so that

$$\int_0^1 x_i f_N(x_i)\, dx_i = 1/N , \tag{97}$$

we obtain the sum rules[102]

$$\int_0^\infty d\nu \, W_2(\nu, q^2) = \int_0^1 \frac{dx}{x} F(x) = \sum_N P(N) \left(\sum_{i=1}^N Q_i^2 \right) , \tag{98}$$

and

$$\frac{q^2}{2M_N}\int_0^\infty \frac{d\nu}{\nu}\, W_2(\nu, q^2) = \int_0^1 dx\, F(x) = \sum_N P(N)\left(\sum_{i=1}^{N}\frac{Q_i^2}{N}\right), \qquad (99)$$

relating moments of the data to the sum of the squares of the charges and the average charge squared of the partons, respectively.

Since experiment[94] suggests that $R = \sigma_S/\sigma_T$ is small, one thinks in terms of mostly spin $\frac{1}{2}$ partons. If all the partons carry conventional charges $Q_i = \pm 1$, then $\sum_i Q_i^2/N = 1$. On the other hand, considering the nucleon as made up of three quark partons, one has $\sum_i Q_i^2/N = (4/9 + 4/9 + 1/9)/3 = 1/3$ for the proton and $\sum_i Q_i^2/N = (4/9 + 1/9 + 1/9)/3 = 2/9$ for the neutron. Experimentally[96], the left-hand sides of Eq. (99) for the proton and neutron are

$$\begin{aligned} \int_{0.1}^1 dx\, F_{2p}(x) &\simeq 0.14 \\ \int_{0.1}^1 dx\, F_{2n}(x) &\simeq 0.10\ , \end{aligned} \qquad (100)$$

with errors of ± 15% from the values of F_2 constructed from the small angle (6° and 10°) data[93]. The large angle data[94] (with larger values of q^2) and/or using ω' to construct F_2 from the small angle data yield slightly smaller values for $\int_{0.1}^1 F_{2p}(x)\,dx$. Since $\int_0^{0.1} F_2(x)\,dx$, although unmeasured, is less than about 0.03 with any reasonable extrapolation of F_{2p} or F_{2n} to $x = 0$ ($\omega = \infty$), we see that $\int_0^1 dx\, F_{2p}(x)$ and $\int_0^1 dx\, F_{2n}(x)$ are too small to agree with the simplest models. Even a model with a "quark-antiquark sea" (equal amounts of $p\bar{p}$, $n\bar{n}$, and $\lambda\bar{\lambda}$

quarks) as the partons gives $\int_0^1 dx\, F_2(x) = 2/9 \simeq 0.22$, which is larger than either the experimental proton or neutron integrals. One is forced to either disregard Eq. (99) because an assumption made in its derivation is wrong (e.g., the same momentum distribution for each parton and the resulting Eq. 97), or to invoke the presence of neutral partons in order to lower $\sum_i Q_i^2/N$ below 2/9.

No assumption on the parton momentum distribution enters the sum rule in Eq. (98)—it follows simply from the normalization condition of Eq. (95). This sum rule was originally proposed by Gottfried[105] in the form

$$\int_0^\infty \frac{d\nu}{\nu}\, \nu\, W_{2p}(\nu, q^2) = 1 \tag{101}$$

for the proton (but not the neutron) for all q^2 within the context of the quark model where $\sum_i Q_i^2 = 1$. At $q^2 = 0$ this sum rule is trivially satisfied due to the contribution of the Born term and vanishing of the continuum. At finite values of q^2, however, the integral on the left-hand side diverges (logarithmically) if the limit of $\sigma_T(\nu, q^2)$ is non-zero as $\nu \longrightarrow \infty$ at fixed q^2, for then $\nu W_2(\nu, q^2)$ is non-zero in the same limit. Thus, if we are to make any sense of Eq. (101), the constant part of the total cross section (or νW_2) must not be counted in the sum rule. Rather, the manner in which Eq. (101) is satisfied at $q^2 = 0$ (by the Born term) suggests (see Sections XII and XIII) we should include only the direct channel resonances and non-constant part of the total cross section. The possibility that sense can be made of Eq. (101), as well as its $q^2 \longrightarrow \infty$ limit (using the scaling property of $\nu W_2(\nu, q^2)$),

$$\int_1^\infty \frac{d\omega}{\omega}\, F_{2p}\left(\frac{1}{\omega}\right) = \int_0^1 \frac{dx}{x}\, F_{2p}(x) = 1\,, \tag{102}$$

which similarly diverges if $F_{2p}(0) \neq 0$, is discussed in reference 106.

These divergence difficulties are avoided if we consider the difference

$$\int_0^1 \frac{dx}{x}\left[F_{2p}(x) - F_{2n}(x)\right] = \sum_N P(N)\left(\sum_{i,p}^{N} Q_i^2 - \sum_{i,n}^{N} Q_i^2\right), \qquad (103)$$

since the constant part of $F_2(x)$ as $x \longrightarrow 0$ (or $\omega \longrightarrow \infty$), which corresponds to diffractive virtual photon-nucleon scattering (see Section XII) presumably cancels between the proton and neutron. In a parton model where the nucleon consists of three quarks (plus any number of other partons which are the same for both neutron and proton) the right-hand side of Eq. (103) equals 1/3. Experimentally[96]

$$\int_1^{12} \frac{d\omega}{\omega}\left[F_{2p}\left(\frac{1}{\omega}\right) - F_{2n}\left(\frac{1}{\omega}\right)\right] = \int_{1/12}^{1} \frac{dx}{x}\left[F_{2p}(x) - F_{2n}(x)\right] = 0.13, \qquad (104)$$

with rather large errors (± 40%). With a reasonable form for $F_{2p} - F_{2n}$ for large ω (small x) it is possible that the integral from 0 to 1 in x (1 to ∞ in ω) is equal to 1/3, but this requires pushing the values of $F_{2p} - F_{2n}$ to the upper limits of the errors in the present data.

It thus seems that quantitative comparison of the parton model with the data through the sum rules Eq. (98) and (99) leads to a somewhat complicated picture. The measured mean squared charge $\sum_i Q_i^2/N$ is so small that it requires neutral partons to lower the theoretical value below the minimum value of 2/9 obtained in a quark parton model. While $F_{2p} - F_{2n}$ has a broad peak reminiscent of the quasi-elastic peak seen in electron scattering off nuclei (Figure 8), the magnitude of $\int \frac{dx}{x}\left[F_{2p}(x) - F_{2n}(x)\right]$ is at best marginally consistent with quark partons. Nevertheless, the simplest way to remember the experimental data qualitatively is with a parton model in which the nucleon consists of point quarks. A good quantitative fit to the experimental data has in fact been recently achieved

by Kuti and Weiskopf[107] using three "valence" quarks, neutral "gluons," and a quark-antiquark sea.

The parton approach to deep inelastic electron-nucleon scattering is easily extendable to inelastic neutrino (antineutrino)-nucleon scattering. The parton model predicts the scaling of the structure functions (see Section IX) $W_1^{(\pm)} = F_1^{(\pm)}(x)$, $\nu W_2^{(\pm)} = F_2^{(\pm)}(x)$, and $\nu W_3^{(\pm)} = F_3^{(\pm)}(x)$. The simplest three-quark parton model gives in addition[92]

$$2 M_N x F_1^{(\pm)}(x) = F_2^{(\pm)}(x) = -x F_3^{(\pm)}(x) \tag{105a}$$

and

$$\int_0^1 \frac{dx}{x} F_2^{(+)}(x) = 2$$

$$\int_0^1 \frac{dx}{x} F_2^{(-)}(x) = 4 \tag{105b}$$

From appropriate sums and differences of Eq. (105 a and b) and the corresponding quark-parton results for electron scattering,

$$2 M_N x F_1(x) = F_2(x) \tag{106a}$$

and

$$\int_0^1 \frac{dx}{x} F_{2p}(x) = 1$$

$$\int_0^1 \frac{dx}{x} F_{2n}(x) = 2/3 \quad , \tag{106b}$$

one can derive in a few seconds most of the sum rules that have been discussed for inelastic neutrino scattering as well as those relating the structure functions of inelastic neutrino to inelastic electron scattering (see, for example, reference 108). It is also possible to extend the parton model to treatment of deep inelastic electron-positron colliding beam processes[109] and to production of lepton pairs in high-energy hadron-hadron collisions[110].

Many of the results of the parton model are obtainable in other more elegant ways. For example, besides the scaling behavior itself, some, but not all, of the sum rules connecting inelastic neutrino and electron scattering may be derived from light cone commutators[85]. The sum rules which cannot be derived by the light cone commutator approach involve specific assumptions about the matrix elements of operators, taken from the naive quark model, in addition to algebraic statements about the commutator of two currents on the light cone. In the quark-parton model, we are thus mixing both the algebraic (counting) properties of the quark model for the currents with statements on the (quark) structure of the wave function of the nucleon. It is quite possible that the first of these properties is true (even if real quarks do not exist), while the second is false. However, even if the quark-parton model fails in this last regard, it certainly is a very useful guide and mnemonic, provides intuition in many cases where other approaches are inapplicable or fail[111], and gives a unified way of thinking about deep inelastic phenomena[103, 111].

XII High Energy Behavior of the Forward Virtual Photon-Nucleon Amplitude

Let us again consider inelastic electron-nucleon scattering as a collision between the exchanged virtual photon and the target nucleon, and focus our attention on the total cross sections σ_T and σ_S. By the optical theorem, these total cross sections are related to the imaginary part of the forward virtual photon-nucleon scattering amplitude. In the case of hadron-hadron scattering, we have an extensive experimental knowledge of total cross sections and the associated forward scattering amplitude, as well as much accumulated theoretical insight. Some of these experimental observations and theoretical ideas have already been discussed in Section VI in connection with the behavior of the total cross section for real photons on nucleons. In particular, we recall that diffraction scattering or Pomeron exchange in the forward amplitude corresponds to the constant part of total cross sections as the energy increases, while the nondiffractive part of the forward amplitude, due to other, non-Pomeron exchanges gives rise to a component of the forward amplitude which falls with increasing energy.

At large ν and fixed q^2 we have from Eq. (86) that

$$\begin{aligned} \nu W_2 &\propto q^2 (\sigma_T + \sigma_S) \\ W_1 &\propto \nu \sigma_T \ . \end{aligned} \tag{107}$$

Since the total cross sections behave as $\nu^{\alpha(0)-1}$ as $\nu \longrightarrow \infty$, where $\alpha(0)$ is the position of the relevant leading J-plane singularity ($\alpha(0) = 1$ for the Pomeron and $\alpha(0) < 1$ for other exchanges), $\nu W_2(\nu, q^2)$ behaves as $\nu^{\alpha(0)-1}$ and W_1 as $\nu^{\alpha(0)}$ as $\nu \longrightarrow \infty$ at fixed q^2. We then see that νW_2 and W_1/ω' must both behave as $(\omega')^{\alpha(0)-1}$ as $\omega' \longrightarrow \infty$ if the region where scaling takes place overlaps the Regge region where νW_2 and W_1/ν behave as $\nu^{\alpha(0)-1}$.

Thus νW_2 and W_1/ω' should be constant at large ω' if purely diffraction is present ($\alpha(0) = 1$) in the scaling region, while if there is a non-diffractive component of the forward virtual photon-nucleon amplitude, νW_2 and W_1/ω' should decrease as $\omega' \longrightarrow \infty$. Unfortunately, for large values of ω' (say $\omega' > 10$), there is presently no data over a large range of q^2, nor is there a separation of W_1 and W_2, so we have no strong evidence for scaling beyond $\omega' \simeq 10$. If we use the same (small) value of $R = \sigma_S/\sigma_T$ found[94] for $\omega' < 10$, then the data that are available are consistent with scaling and νW_2 decreasing for large values of ω'. For $R = 0$, and assuming scaling holds for all $q^2 \geq 1$ GeV^2, both νW_2 and W_1/ω' decrease by $\sim$ 20% between their maxima at $\omega' \simeq 5$ and $\omega' \simeq 25$. If we increase the assumed value of R for $\omega' > 10$, the values of νW_2 obtained from the differential cross section measurements go up compared to those obtained assuming $R = 0$, but those of W_1/ω' go down. Since W_1 and νW_2 are now known rather well for $\omega' < 10$, one cannot change W_1 or νW_2 in this region. Thus either or both νW_2 and W_1/ω' decrease at large ω' if we accept $q^2 \gtrsim 1$ GeV^2 as relevant for scaling (as it is for $\omega' < 10$). One may alternatively directly consider values of σ_T at points where a separation of σ_S and σ_T has been made[94]. One then finds that σ_T appears to be a maximum between ω' of 3 and 4 and at $q^2 = 1.5$ GeV^2 falls at least as much with increasing energy as the total photo-absorption cross section does over the same ν (or W^2) range as at $q^2 = 0$. Thus, there is experimental evidence from the energy dependence of the measured cross sections for a non-diffractive component to virtual photon-nucleon scattering at values of q^2 for which there is scaling for $\omega' < 10$.

More direct evidence for the presence of a nondiffractive component of the amplitude comes from the difference between neutron and proton inelastic scattering discussed in Section X, since such a difference requires the exchange

of an isospin one object in the forward virtual photon-nucleon amplitude, while the Pomeron is assumed to have isospin zero. Thus there must be a sizable non-diffractive component to forward virtual photon-nucleon scattering. However, present experiments certainly do not rule out νW_2 and W_1/ω' falling to a non-zero value as $\omega' \longrightarrow \infty$, so that some diffractive component may be present, particularly at large ω'. Nor do present experiments rule out νW_2 and/or W_1/ω' falling to zero as $\omega' \longrightarrow \infty$. The question of the exact magnitude of the diffractive and nondiffractive parts of the cross section in the scaling region is then still open (see the discussion in reference 112), with the resolution presumably to be accomplished experimentally when the range of very large ν and q^2 becomes accessible.

XIII Duality and Scaling in Inelastic Electron Scattering

A nondiffractive component of a forward amplitude and the corresponding decreasing total cross section at high energy are correlated with the presence and behavior of resonances at low energy, at least for purely hadronic processes[113]. In particular, total cross sections for processes like K^+p and pp scattering, which have no obvious s-channel resonances at low energy, have essentially constant total cross sections above laboratory energies of a few GeV, while processes like K^-p and $\bar{p}p$ scattering, which have many strong s-channel resonances at low energy, have total cross sections which decrease substantially as the energy is increased above a few GeV. This correlation of the behavior of total cross sections and the presence of resonances is part of the "two-component" picture of duality for two-body amplitudes. In this picture, "Pomeron exchange" or diffraction at high energies is connected to the low energy non-resonant "background," while "ordinary" exchanges (non-Pomeron Regge trajectories or cuts) are connected to the low energy s-channel resonances[113,114]. The connection of resonances at low energies to "ordinary" exchanges at high energies takes quantitative form in terms of finite energy sum rules[77]. These sum rules relate integrals over the imaginary part of the amplitude at low energies to the properties (residue functions, Regge trajectories) of the t-channel exchanges at high energies[115].

Given the presence of a nondiffractive component of the forward virtual photon-nucleon amplitude in the scaling region (from the experimental observations of energy dependence and neutron-proton differences in inelastic electron-nucleon scattering at values of q^2 where scaling is observed), we expect that for $q^2 \gtrsim 1\,\mathrm{GeV}^2$ nucleon resonance electroproduction will have a behavior which is correlated with other features of deep inelastic scattering. In particular, we would like to compare the behavior of the resonances with the behavior of νW_2 and W_1 in the region where scaling behavior is observed.

The behavior of the resonances in comparison to νW_2 in the scaling region[116,117] can be seen in Figures 13 and 14 where the function $\nu W_2(\nu, q^2)$ is plotted versus ω' at various values of q^2 (assuming $R = \sigma_S/\sigma_T = 0.18$). The solid line, which is the same in all cases, is a fit[118] to the data for $W > 1.8$ GeV and $q^2 \geq 1$ GeV^2 where scaling in ω' is observed. We refer to this curve then as the "scaling-limit-curve," $\nu W_2(\omega')$. The values of νW_2 at fixed q^2 are obtained by interpolating the data[93] up to a hadron mass, W, of 3 GeV. Above $W \simeq 1.8$ GeV, where there are no prominent resonances visible, the interpolated values of νW_2 at fixed q^2 agree with the scaling-limit curve, $\nu W_2(\omega')$, as expected from the existence of scaling in ω'.

We first of all note that we can easily see the prominent N* resonances at values of q^2 where νW_2 scales for $W \gtrsim 2$ GeV. A given resonance (including the elastic peak) occurs at $\omega'_R = 1 + M_R^2/q^2$ and moves toward $\omega' = 1$ as q^2 increases. We also note that the prominent resonances do not disappear with increasing q^2 relative to a "background" under them which has the scaling behavior. (Note that for values of q^2 beyond about 3 GeV^2 the present data are not of sufficiently high statistical quality in the low W region to reveal whether the prominent resonances are still present.) Instead, the prominent resonances (and the background) seem to roughly follow in magnitude the scaling-limit-curve at the corresponding value of ω'.

This can be seen even more clearly if the heights of the prominent resonance bumps in νW_2 are divided by $\nu W_2(\omega')$ evaluated at a value of ω' which corresponds to the given resonance and value of q^2 at which measurements were made. Then one sees that the ratio of the height of the resonance bump to the magnitude of the scaling-limit-curve at the appropriate value of ω' remains roughly constant[112,117] for the prominent N* resonances as q^2 changes from 1 to 3 GeV^2.

Thus at least the prominent nucleon resonances have a behavior which is strongly correlated with the scaling behavior of νW_2. Furthermore, a recent analysis[119] of $R = \sigma_S/\sigma_T$ for $W < 2$ GeV shows the same small value (consistent with zero) that is found in the scaling region. In addition, we know that elastic scattering is less from neutrons than from protons, just as is the deep inelastic scattering. One, of course, cannot determine without a detailed partial wave analysis what the q^2 dependence is of the many broad, low spin N* resonances that we know exist from pion-nucleon phase shifts. But the behavior of the prominent N* resonances that we can see gives the essential clue as to what is happening[116,117]: That a substantial part of the scaling behavior of the virtual photon-nucleon amplitude is due to a nondiffractive component of the amplitude which is directly reflected in the behavior of the resonances. In a duality framework we say that the nucleon and N* resonances at low energy are an intrinsic part of the scaling behavior and correspond to the presence of non-Pomeron exchanges at high energy. The resonances build up, in the sense of finite energy sum rules, the nondiffractive part of the amplitude on the average and yield the non-Pomeron exchanges at high energy, resulting in a falling σ_T or $\nu W_2(\omega')$ curve at high energies and a difference between neutron and proton inelastic scattering.

What is unique to studying duality in electroproduction is, of course, the experimentally observed scaling behavior. This allows one to consider data at fixed values of ω', but different values of q^2 and W^2, both within and outside the region of prominent resonances. Thus we can compare the data where there are prominent narrow resonances directly with data for $\nu W_2(\omega')$ for large q^2 and W^2 where nature has accomplished the appropriate averaging of the many broad resonances and backgrounds or t-channel exchanges present here. Hence, without any extrapolation to low energies using a model or theory valid in the high energy

region, one can directly see the beautiful oscillations of νW_2 in the low W region about the scaling-limit-curve, which represents the average of many resonances and backgrounds at large W.

This comparison of the low W and high W regions using scaling can be given quantitative form in terms of a generalized finite energy sum rule[116,117]. The possibility of making a quantitative connection using finite energy sum rules between the low W region where there is N* resonance excitation and the deep inelastic region where scaling takes place is already suggested by Figures 13 and 14 where the scaling-limit-curve appears to roughly average the resonances in νW_2. The relevant sum rule is found[112,117] to be satisfied to within 10% or better for values of q^2 from 1.0 to 3.0 GeV^2 if the integral is carried up to energies or values of ω' which correspond to hadron masses, W, of 2.0 GeV. Considering the statistical as well as systematic errors present in both the data and the interpolation to fixed q^2, the agreement is extremely good. Furthermore, the prominent resonances make important contributions to the sum rule—their removal would destroy it. Thus the resonances play a significant part in building up νW_2 in the sense of finite energy sum rules.

If the prominent resonances are really "following" $\nu W_2(\omega')$ in magnitude, we are led to ask what must be the large q^2 behavior of the form factor of a given hadronic final state of mass W if it is to participate in the scaling behavior of νW_2? It is rather simple to show[116] that if $G(q^2)$ is the excitation form factor of the hadronic final state of mass W and

$$G(q^2) \longrightarrow c(1/q^2)^{n/2} \tag{108}$$

as $q^2 \longrightarrow \infty$, and if νW_2 can be parameterized as

$$\nu W_2 \longrightarrow c'(\omega' - 1)^p \tag{109}$$

as $\omega' \longrightarrow 1$, then these two behaviors can co-exist only if

$$n = p + 1 \tag{110}$$

Thus each hadronic final state of mass W, if it is to participate in the scaling behavior, must have an excitation form factor with a specific power of falloff in q^2 as $q^2 \longrightarrow \infty$, and this power is the same for all W and is related to the power with which νW_2 rises at threshold. If we apply this in the low-energy region to a given resonance of mass M_R, then all resonances which follow $\nu W_2(\omega')$ in magnitude (as we have seen the prominent N* resonance do) must have the same power of falloff in q^2 as $q^2 \longrightarrow \infty$ (including presumably the zeroth resonance or elastic contribution to νW_2 which has $n \simeq 4$), and again this is related to the behavior of νW_2 at threshold. That the resonance excitation form factors all have a behavior at large q^2 which is similar to the behavior of the elastic form factor (with $n \simeq 4$) has been previously indicated[96,120]. As we have $p \simeq 3$ from Eq. (92), it also follows that Eq. (110) is at least approximately satisfied. For the case of the elastic peak in νW_2, Eq. (110) is just the relation of Drell and Yan[121], first found in the parton model.

Thus we see that both qualitatively and quantitatively the behavior of elastic scattering and N* resonance electroproduction is remarkably correlated with the scaling behavior of deep inelastic scattering. In particular, as q^2 changes, the prominent N* resonance bumps in νW_2 closely follow the magnitude of the scaling-limit-curve, $\nu W_2(\omega')$, at the corresponding value of the scaling variable ω'. This leads to relations between the behavior of the resonance excitation or elastic form factors at large q^2 and the behavior of $\nu W_2(\omega')$ as $\omega' \longrightarrow 1$. A quantitative connection between resonance electroproduction and scaling behavior can be made in terms of finite energy sum rules. When integrated over the region of the prominent N* resonances (up to W = 2.0 GeV), the sum rule is satisfied to within 10% or better,

which is within the statistical and systematic errors inherent in the data and its interpolation to fixed q^2.

The connection to ideas of duality taken from purely strong interaction processes is very close and interesting. Qualitatively, the correlation between the height of the prominent resonance bumps and the scaling-limit-curve's magnitude, the fact that $R = \sigma_S/\sigma_T$ is small both in the deep inelastic region and in the low energy resonance region, the prediction of neutron-proton differences, etc., provide examples of the correlation between low and high energy phenomena which is at the heart of duality ideas. Quantitatively, the agreement of the finite energy sum rule over a large range of q^2 where one can still see that there are resonance bumps present in νW_2 and the averaging of the resonance bumps by the scaling-limit-curve, $\nu W_2(\omega')$, provides a very striking example of the averaging of resonances to a smooth curve even outside the Regge regime.

The averaging of the resonances by the scaling-limit-curve is exactly the behavior one expects in dual resonance models of electroproduction where the hadronic final state is completely expressible as a sum of resonances. There have been many models of this kind proposed[121], mostly within the framework of the Veneziano model[122]. Up to now, all such models have been affected with troubles[123] in that they either have bad asymptotic behavior in ν or q^2, or they lack factorization, which must be a basic property of any model based on resonances. In addition, many of the models which agree with experiment quantitatively have additional ad hoc assumptions or parameters. Nevertheless, such models are important at least as theoretical laboratories, and show the consistency of scaling with a world made purely out of resonances.

The relation of the approach to inelastic scattering through duality to other treatments is not completely understood. For example, in our discussion of duality

we have related various properties, particularly those of resonance electroproduction, to the scaling behavior observed to hold for deep inelastic scattering, but we have not predicted scaling, as the parton model does. It is tempting to assume a common origin for both properties of electroproduction in terms of point-like substructure within the nucleon, e.g., quark partons which are responsible both for the deep inelastic scattering and for forming N* resonances when they are excited to specific levels. However, it is difficult to make this into more than a suggestive picture, particularly since one deals with incoherent scattering (the impulse approximation) in the parton model, while resonance phenomena are certainly coherent properties of the whole nucleon. Establishing connections between the various approaches to deep inelastic scattering, as well as establishing clear limits on their individual domains of validity, is clearly an important activity to pursue. Hopefully both future experimental and theoretical work will help us unravel the physical origin of the incredible regularities observed in inelastic electron scattering.

XIV References

1. The development of quantum electrodynamics can be followed in the original papers collected in J. Schwinger (Ed.), Quantum Electrodynamics, Dover, New York (1958).
2. S. J. Brodsky and S. D. Drell, "The present status of quantum electrodynamics" in Annual Review of Nuclear Science, 20, 147 (1970).
3. J. Aldins et al., Phys. Rev. Letters, 23, 441 (1969).
4. T. Appelquist and S. J. Brodsky, Phys. Rev. Letters, 24, 562 (1970); E. de Rafael, B. Lautrup, and A. Petermann, CERN preprint TH-1140 (1970), unpublished.
5. E. R. Williams et al., Phys. Rev. Letters, 26, 721 (1971).
6. A. S. Goldhaber and M. M. Nieto, Phys. Rev. Letters, 21, 567 (1968).
7. We use the standard practice of employing units where $\hbar = c = 1$. The metric is such that $p^2 = p_\mu p_\mu = p_1^2 + p_2^2 + p_3^2 + p_4^2$ (summation convention) = $p^2 - E^2$, so that space-like four-vectors have $p^2 > 0$. The fine structure constant $\alpha = e^2/4\pi \simeq 1/137$. The Dirac matrices γ_μ are hermitian as is γ_5.
8. M. Gell-Mann, Phys. Rev., 92, 833 (1953); K. Nishijma, Progr. Theoret. Phys., 12, 107, Kyoto, (1954).
9. V. G. Grishin et al., Yad. Fiz., 4, 126 (1966) (Soviet J. Nucl. Phys., 4, 90 (1967).
10. N. Dombey and P. K. Kabir, Phys. Rev. Letters, 17, 730 (1966).
11. A. I. Sanda and G. Shaw, Phys. Rev. Letters, 24, 1310 (1970); A. I. Sanda and G. Shaw, Phys. Rev., D3, 243 (1971).
12. H. G. Hilpert et al., Nucl. Phys., B8, 535 (1968) and H. Butenschon, DESY report R1-70/1, 1970, unpublished; E. Lodi-Rizzini et al., Lett. Nuovo Cimento, 3, 697 (1970).

13. P. Noelle and W. Pfeil, Nucl. Phys. B31, 1 (1971).

14. F. A. Berends and D. L. Weaver, preprint, (1971), unpublished.

15. J. Bernstein, G. Feinberg, and T. D. Lee, Phys. Rev., 139, B1650 (1965).

16. J. H. Christenson et al., Phys. Rev. Letters, 13, 138 (1964).

17. See, for example, the discussion of T. D. Lee, Phys. Rev., 140, B959 (1965).

18. T. D. Lee, Phys. Rev., 140, B969 (1965).

19. N. Christ and T. D. Lee, Phys. Rev., 143, 1310 (1966).

20. J. R. Chen et al., Phys. Rev. Letters, 21, 1279 (1968); S. Rock et al., Phys. Rev. Letters, 21, 748 (1970).

21. B. Schrock et al., Phys. Rev. Letters, 26, 1659 (1971); D. Bartlett et al., Princeton University preprint, (1971), unpublished.

22. P. A. Berardo et al., Phys. Rev. Letters, 26, 201 (1971); J. Favier et al., Phys. Letters, 31B, 609 (1970).

23. A. I. Sanda and G. Shaw, Phys. Rev. Letters, 26, 1057 (1971); A. I. Sanda and G. Shaw, preprint, (1971), unpublished.

24. M. Gell-Mann and F. Zachariasen, Phys. Rev., 124, 953 (1961).

25. M. Goldberger and S. B. Treiman, Phys. Rev., 110, 1478 (1958).

26. J. J. Sakurai, Ann. Phys. (N. Y.), 11, 1 (1960).

27. N. Kroll, T. D. Lee, and B. Zumino, Phys. Rev., 157, 1376 (1967).

28. J. C. Bizot et al., Phys. Letters, 32B, 416 (1970).

29. J. J. Sakurai, invited talk in Proceedings of the Fourth International Symposium on Electron and Photon Interactions at High Energies, Liverpool, 1969, edited by D. W. Braben and R. E. Rand (Daresbury Nuclear Physics Laboratory, Daresbury, Lancashire, England, 1970), p. 91.

30. D. O. Caldwell et al., Phys. Rev. Letters, 25, 609 (1970); H. Meyer et al., Phys. Letters, 33B, 189 (1970); T. A. Armstrong et al., Phys. Letters, 34B, 535 (1971).

31. J. Ballam et al., Phys. Rev. Letters, 21, 1566 (1968); J. Ballam et al., Phys. Rev. Letters, 23, 498 (1969); M. Rabin et al., Bull. Am. Phys. Soc., 15, 1634 (1970).

32. E. D. Bloom et al., Stanford Linear Accelerator Center Report, Report No. SLAC-PUB-653 (1969), unpublished.

33. J. Ballam et al., SLAC-Berkeley-Tufts collaboration preprint submitted to the International Symposium on Electron and Photon Interactions at High Energies, Ithaca, New York, 1971.

34. See, for example, the review by A. Wroblewski in Proceedings of the Colloquium on High Multiplicity Hadronic Reactions (Ecole Polytechnique, Paris, 1970), p. 11.

35. G. F. Chew, M. L. Goldberger, F. E. Low, and Y. Nambu, Phys. Rev., 106, 1345 (1957).

36. M. Jacob and G. C. Wick, Ann. Phys. (N. Y.), 1, 404 (1959).

37. R. L. Walker, Phys. Rev., 182, 1729 (1969).

38. G. Hohler and W. Schmidt, Ann. Phys. (N. Y.), 28, 34 (1964); W. Schmidt, Z. f. Phys., 182, 78 (1964); A. Donnachie and G. Shaw, Ann. Phys. (N. Y.), 37, 333 (1966); F. A. Berends, A. Donnachie and D. L. Weaver, Nucl. Phys., B4, 54 (1967).

39. M. Gourdin and P. Salin, Nuovo Cimento, 27, 193 (1963); Y. C. Chau, N. Dombey, and R. G. Moorhouse, Phys. Rev., 163, 1632 (1967).

40. R. L. Walker in Proceedings of the Fourth International Symposium on Electron and Photon Interactions at High Energies, Liverpool, 1969, edited by D. W. Braben and R. E. Rand (Daresbury Nuclear Physics Laboratory, Daresbury, Lancashire, England, 1970), p. 23.

41. We use the notation $L_{2I,2J}(M)$ for resonances in the pion-nucleon system with L the orbital angular momentum, I the isotopic spin, J the total angular momentum, and M the mass in MeV. The resonance parameters are from the compilation of Matts Roos et al., Phys. Letters, 33B, 1 (1970).

42. L. A. Copley, G. Karl, and E. Obryk, Phys. Letters, 29B, 117 (1969); L. A. Copley, G. Karl, and E. Obryk, Nucl. Phys., B13, 303 (1969); R. P. Feynman, M. Kislinger, and F. Ravndal, Phys. Rev., in press.

43. M. Gell-Mann, M. L. Goldberger, and W. Thirring, Phys. Rev., 95, 1612 (1954).

44. See the rapporteur talks by M. L. Goldberger and S. Mandelstam in The Quantum Theory of Fields, Proceedings of the Twelfth Solvay Conference, Brussels, Belgium, 1961 (Interscience Publishers, New York, 1961), pp. 179-196 and 209-224.

45. K. J. Foley et al., Phys. Rev. Letters, 19, 143 (1967); ibid., 857 (1967).

46. M. Gell-Mann and M. L. Goldberger, Phys. Rev., 96, 1423 (1954); F. Low, Phys. Rev., 96, 1428 (1954).

47. S. D. Drell and A. C. Hearn, Phys. Rev. Letters, 16, 908 (1966); S. B. Gerasimov, Sov. J. Nucl. Phys., 2, 430 (1966).

48. Y. C. Chau, N. Dombey, and R. G. Moorhouse, Proceedings of the 1967 International Symposium on Electron and Photon Interactions at High Energies, SLAC, Stanford, California, p. 617; G. C. Fox and D. Z. Freedman, Phys. Rev., 182, 1628 (1969).

49. See, for example, the review by V. Barger in Proceedings of the CERN Topical Conference on High Energy Collisions of Hadrons, Geneva, 1968, CERN 68-7, Vol. 1, p. 3.

50. M. Damashek and F. J. Gilman, Phys. Rev., D1, 1319 (1970).

51. M. J. Creutz, S. D. Drell, and E. A. Paschos, Phys. Rev., 178, 2300 (1969).

52. C. A. Dominguez, C. Ferro Fontan, and R. Suaya, Phys. Letters, 31B, 365 (1970).

53. W. A. Bardeen and W. K. Tung, Phys. Rev., 173, 1423 (1968).

54. R. L. Anderson et al., Phys. Rev. Letters, 25, 1218 (1970); G. Buschorn et al., Phys. Letters, 33B, 241 (1970); D. F. Jacobs and M. Deutsch, Bull. Am. Phys. Soc., 15, 608 (1970); A. M. Boyarski et al., Phys. Rev. Letters, 26, 1600 (1971).

55. S. D. Drell, Comments in Nucl. and Particle Phys., 1, 196 (1967); J. K. Walker, Phys. Rev. Letters, 21, 1618 (1968).

56. S. J. Brodsky, A. C. Hearn, and R. G. Parsons, Phys. Rev., 187, 1899 (1969).

57. A review of the experimental situation and the references to individual experiments are to be found in G. Wolf, "Photoproduction of vector mesons," DESY 70/64, (1970), unpublished, and reference 58.

58. A. Silverman, invited talk in Proceedings of the Fourth International Symposium on Electron and Photon Interactions at High Energies, Liverpool, 1969, edited by D. W. Braben and R. E. Rand (Daresbury Nuclear Physics Laboratory, Daresbury, Lancashire, England, 1970), p. 71.

59. The measurements of the real part of the rho photoproduction amplitude were actually carried out on Beryllium and Carbon by H. Alvensleben et al., Phys. Rev. Letters, 25, 1377 (1970) and P. J. Biggs et al., Daresbury Nuclear Physics Laboratory preprint, (1971), unpublished.

60. K. Gottfried and J. D. Jackson, Nuovo Cimento, 33, 309 (1964).

61. F. J. Gilman, J. Pumplin, A. Schwimmer, and L. Stodolsky, Phys. Letters, 31B, 387 (1970).

62. G. Cozzika et al., paper contributed to the XVth International Conference on High Energy Physics, Kiev, 1970 (unpublished); B. Amblard et al., Proceedings of the Lund Conference on Elementary Particles, p. 152 and 430.

63. G. Hohler and R. Strauss, Z. f. Phys., 232, 205 (1970); V. Barger and R. J. N. Phillips, Phys. Letters, 26B, 730 (1968); H. Harari and Y. Zarmi, Phys. Letters, 32B, 291 (1970); R. Odorico, R. Garcia, and G. A. Garcia-Canal, Phys. Letters, 32B, 375 (1970).

64. L. Jones and D. G. Ravenhall, Phys. Rev., D3, 696 (1971); R. L. Thews, Phys. Rev., D3, 250 (1971). M. L. Blackmon, M. J. King, and K. C. Wali, Syracuse University preprint, (1971), unpublished.

65. H. Harari, invited talk in Proceedings of the Fourth International Symposium on Electron and Photon Interactions at High Energies, Liverpool, 1969, edited by D. W. Braben and R. E. Rand (Daresbury Nuclear Physics Laboratory, Daresbury, Lancashire, England, 1970), p. 107.

66. P. G. O. Freund, Nuovo Cimento, 48, 541 (1967).

67. M. Ross and L. Stodolsky, Phys. Rev., 149, 1172 (1966); P. G. O. Freund, Nuovo Cimento, 44A, 411 (1966).

68. J. Ballam et al., SLAC-Weizmann collaboration preprint submitted to the International Symposium on Electron and Photon Interactions at High Energy, Ithaca, New York, 1971.

69. See the review of these experiments by D. W. G. S. Leith, "Photoproduction and vector dominance," lectures presented at the Scottish Universities Summer School in Physics, 1970 (unpublished).

70. B. Bartoli et al., Nuovo Cimento, 70A, 615 (1970).

71. J. S. Ball, W. R. Frazer, and M. Jacob, Phys. Rev. Letters, 20, 518 (1968).

72. P. Stichel, Z. f. Physik, 180, 170 (1964).

73. J. D. Jackson and C. Quigg, Nucl. Phys., B22, 301 (1970).

74. A review of the experimental situation and references to the individual experiments up to the end of 1969 are found in the invited talk of K. Lubelsmeyer on Pseudoscalar Meson Photoproduction, Proceedings of the Fourth International Symposium on Electron and Photon Interactions at High Energies, Liverpool, 1969, edited by D. W. Braben and R. E. Rand (Daresbury Nuclear Physics Laboratory, Daresbury, Lancashire, England, 1970), p. 45.

75. M. LeBellac, Phys. Letters, 25B, 524 (1967); M. Aderholz et al., Phys. Letters, 27B, 174 (1968).

76. F. Henyey, G. Kane, J. Pumplin and M. Ross, Phys. Rev., 182, 1579 (1969).

77. R. Dolen, D. Horn, and C. Schmid, Phys. Rev., 166, 1768 (1968).

78. A. Bietti et al., Phys. Letters, 26B, 457 (1968); D. P. Roy and S. Y. Chu, Phys. Rev., 171, 1762 (1968); P. Di Vecchia et al., Phys. Letters, 27B, 296 (1968); K. Raman and K. Vasavada, Phys. Rev., 175, 2191 (1968).

79. J. D. Jackson and C. Quigg, Phys. Letters, 29B, 236 (1969).

80. D. S. Beder, Phys. Rev., 149, 1203 (1966); C. Iso and H. Yoshii, Ann. Phys. (N. Y.), 47, 424 (1968).

81. F. Bulos et al., Phys. Rev. Letters, 26, 1453 and 1457 (1971).

82. For a recent review, see S. D. Drell, invited talk on Electromagnetic Interactions presented at the Amsterdam International Conference on Elementary Particles, Amsterdam, 1971, unpublished.

83. R. Brandt, Phys. Rev. Letters, 23, 1149 (1969); ibid., 1260 (1969); B. L. Ioffe, JETP Letters, 9, 97 (1969); R. Jackiw, R. Van Royen, and G. West, Phys. Rev., D2, 2473 (1970); H. Leutwyler and J. Stern, Nucl. Phys., B20, 77 (1970).

84. K. G. Wilson, Phys. Rev., 179, 1499 (1969); R. Brandt and G. Preparata, Nucl. Phys., B27, 541 (1971); Y. Frishman, Phys. Rev. Letters, 25, 966 (1970).

85. H. Fritzsch and M. Gell-Mann, talk presented at the Coral Gables Conference on Fundamental Interactions at High Energy, University of Miami, Coral Gables, Florida, January 1971, and Caltech preprint CALT-68-247, unpublished.

86. S. D. Drell and J. D. Walecka, Ann. Phys. (N. Y.), 28, 18 (1964).

87. L. N. Hand, Phys. Rev., 129, 1834 (1963).

88. F. J. Gilman, Phys. Rev., 167, 1365 (1968).

89. L. Galfi, J. Kuti, and A. Patkos, Phys. Letters, 31B, 465 (1970).

90. J. D. Bjorken, Phys. Rev., D1, 1376 (1970).

91. R. P. Feynman and M. Gell-Mann, Phys. Rev., 109, 193 (1958).

92. J. D. Bjorken and E. A. Paschos, Phys. Rev. D1, 3151 (1970); D. J. Gross and C. H. Llewellyn Smith, Nucl. Phys., B14, 337 (1969).

93. M. Breidenbach et al., Phys. Rev. Letters, 23, 935 (1960); E. D. Bloom et al., Phys. Rev. Letters, 23, 930 (1969); M. Breidenbach, MIT thesis (1970), unpublished.

94. G. Miller et al., SLAC-PUB-815, (1971), unpublished; J. I. Friedman et al., SLAC-PUB-907, (1971), unpublished.

95. J. D. Bjorken, Phys. Rev., 179, 1547 (1969).

96. E. D. Bloom et al., SLAC-PUB-796, report presented to the XVth International Conference on High Energy Physics, Kiev, USSR, 1970, unpublished.

97. G. West, Stanford University preprint, (1971), unpublished.

98. I. Budagov et al., Phys. Letters, 30B, 364 (1969); G. Myatt and D. H. Perkins, Phys. Letters, 34B, 542 (1971).

99. D. E. Andrews et al., Phys. Rev. Letters, 26, 864 (1971).

100. C. Driver et al., Phys Letters, 35B, 77 (1971); C. N. Brown et al., Phys. Rev. Letters, 26, 987 (1971); F. W. Brasse et al., DESY preprint (1971), unpublished; P. D. Kummer et al., Daresbury Nuclear Physics Laboratory preprint, (1971), unpublished.

101. J. D. Bjorken, "Current algebra at small distances," Varenna School Lectures, Course XLI, Varenna, Italy, 1967.

102. R. P. Feynman, Phys. Rev. Letters, 23, 1415 (1969); J. D. Bjorken and E. A. Paschos, Phys. Rev., 185, 1975 (1969).

103. S. D. Drell and T. M. Yan, Ann. Phys. (N. Y.), to be published.

104. S. D. Drell, D. J. Levy, and T. M. Yan, Phys. Rev. Letters, 22, 744 (1969); S. D. Drell, D. J. Levy, and T. M. Yan, Phys. Rev., 187, 2159 (1969); ibid D1, 1035 (1970).

105. K. Gottfried, Phys. Rev. Letters, 18, 1174 (1967).

106. F. J. Gilman, invited talk presented at the Symposium on Hadron Spectroscopy, Balatonfured, Hungary, September 1970, and SLAC-PUB-842, unpublished.

107. J. Kuti and V. F. Weisskopf, MIT preprint,(1971), unpublished.

108. C. H. Llewellyn Smith, Nucl. Phys., B17, 277 (1970).

109. S. D. Drell, D. J. Levy, and T. M. Yan, Phys. Rev., D1, 1617 (1970).

110. S. D. Drell and T. M. Yan, Phys. Rev. Letters, 25, 316 (1970); ibid.,902 (1970).

111. J. D. Bjorken, invited talk presented at the International Conference on Duality and Symmetry in Hadron Physics, Tel Aviv, Israel, April 1971, unpublished.

112. F. J. Gilman, invited talk presented at the International Conference on Duality and Symmetry in Hadron Physics, Tel Aviv, Israel, April 1971, unpublished.

113. H. Harari, Phys. Rev. Letters, 20, 1395 (1968).

114. P. Freund, Phys. Rev. Letters, 20, 235 (1968).

115. For application to the amplitude odd under crossing in pion-nucleon scattering, see reference 77; for the even amplitude, see F. J. Gillman, H. Harari, and Y. Zarmi, Phys. Rev. Letters, 21, 323 (1968).

116. E. D. Bloom and F. J. Gilman, Phys. Rev. Letters, 25, 1120 (1970).

117. E. D. Bloom and F. J. Gilman, SLAC preprint, (1971), unpublished.

118. G. Miller, Stanford thesis and SLAC Report 129 (1970), unpublished.

119. F. W. Brass et al., DESY preprint (1970), unpublished.

120. W. K. H. Panofsky, rapporteur's talk in Proceedings of the Fourteenth International Conference on High Energy Physics, Vienna, Austria, 1969 (CERN Scientific Information Service, Geneva, Switzerland, 1969), p. 23.

121. See, for example, M. Pavkovic, Ann. Phys. (N. Y.), 62, 1 (1971); G. Domokos, S. Kovesi-Domokos, and E. Shonberg, Phys. Rev., D3, 1184 (1971).

122. M. Bander, Nucl. Phys., B13, 587 (1969); R. Brower and J. H. Weis, Phys. Rev., 188, 2486 (1969); ibid., 188, 2495 (1969); ibid., D3, 451 (1971); P. V. Landshoff and J. C. Polkinghorne, Nucl. Phys., B19, 432 (1970); S. Matsuda and J. T. Manassah, Institute for Advanced Study preprint (1971), unpublished.

123. See the review of M. Ademollo, talk presented at the Symposium on Meson Photo- and Electroproduction at Low and Intermediate Energies, Bonn, September 1970, unpublished.

Figure Captions

FIGURE 1 The photon-proton total cross section and the pi-zero -proton total cross section divided by 250

FIGURE 2 Kinematics of single pion photoproduction

FIGURE 3 Argand diagram of the forward Compton amplitude, $f_1(W)$, in the low energy region[50]

FIGURE 4 Ratio of the real to imaginary parts of the forward Compton amplitude, f_1, at high energy for different fits to the total cross section[50]

FIGURE 5 (a) Kinematics of vector meson photoproduction

(b) Vector dominance model view of vector meson photoproduction

FIGURE 6 (a) Differential cross section for $\gamma p \rightarrow \pi^+ n$ at high energy

(b) Polarized photon asymmetry, Σ, for $\gamma p \rightarrow \pi^+ n$

FIGURE 7 Production of a forward peak in pion photoproduction from destructive interference of the pion exchange and absorptive cut amplitudes

FIGURE 8 Inelastic electron scattering from a nucleus

FIGURE 9 Kinematics of inelastic electron-nucleon scattering

FIGURE 10 The ν -q^2 plane with lines of fixed hadron mass, W, and fixed electron scattering angle, θ

FIGURE 11 The structure functions $2M_N W_1$ and νW_2 versus ω' for various q^2 ranges

FIGURE 12 The measured total cross section combination, $\sigma_T + \epsilon \sigma_S$, for various fixed hadron masses, W

FIGURE 13 $\nu W_2(\nu, q^2)$ at valves of q^2=0.75, 1.00, 1.25, 1.50 and 1.75 GeV^2 (data points interpolated from experiment) and $\nu W_2(\omega')$, the scaling-limit-curve (solid line), plotted versus ω'

FIGURE 14 $\nu W_2(\nu, q^2)$ at values of q^2=2.00, 2.25, 2.50, 2.75, and 3.00 GeV^2 (data points, interpolated from experiment) and $\nu W_2(\omega')$, the scaling-limit-curve (solid line), plotted versus ω'

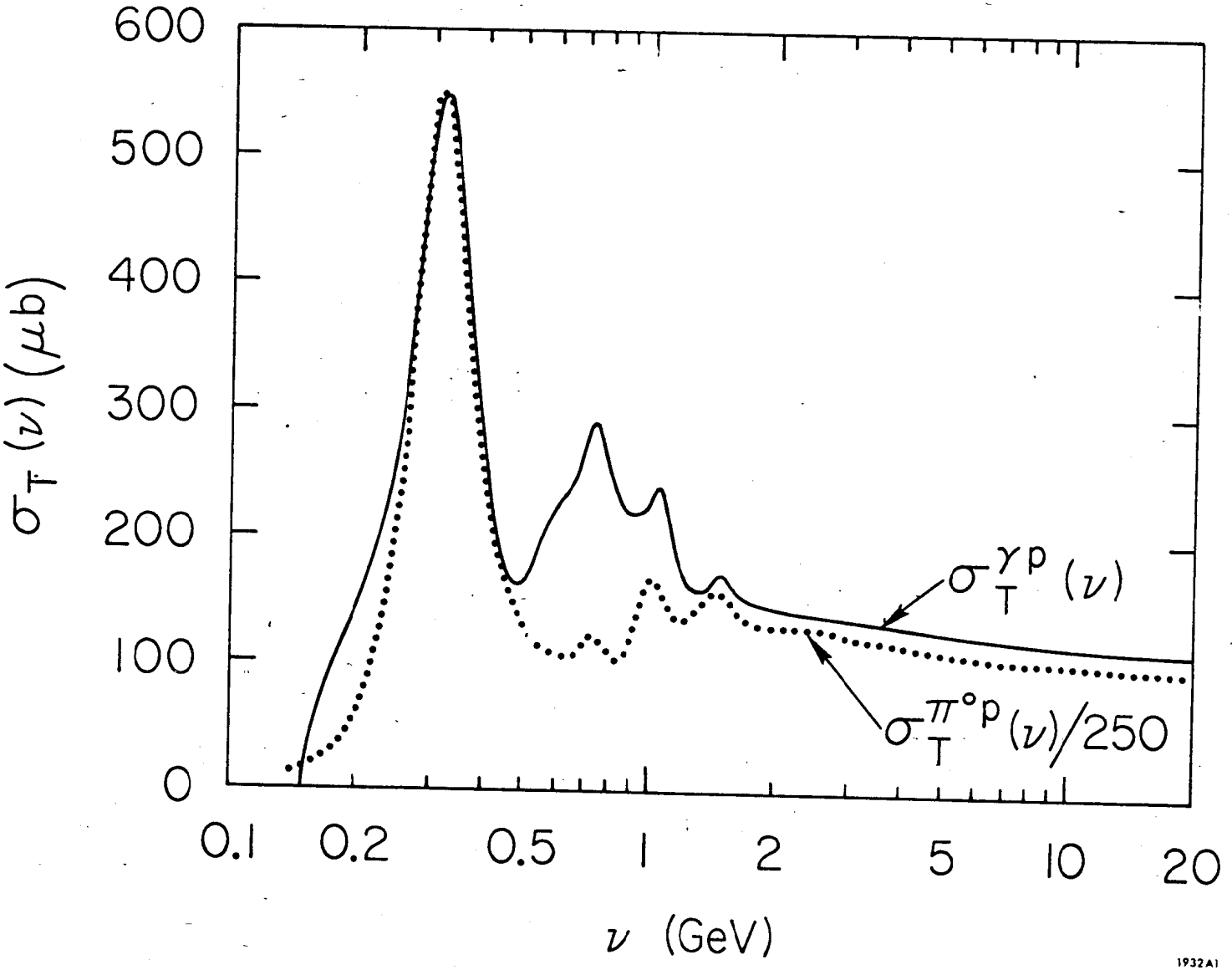
600
500
400
300
200
100
0
$\sigma_T(\nu)$ (μb)
$\sigma_T^{\gamma p}(\nu)$
$\sigma_T^{\pi^\circ p}(\nu)/250$
0.1
0.2
0.5
1
2
5
10
20
ν (GeV)
1932A1

Fig 1

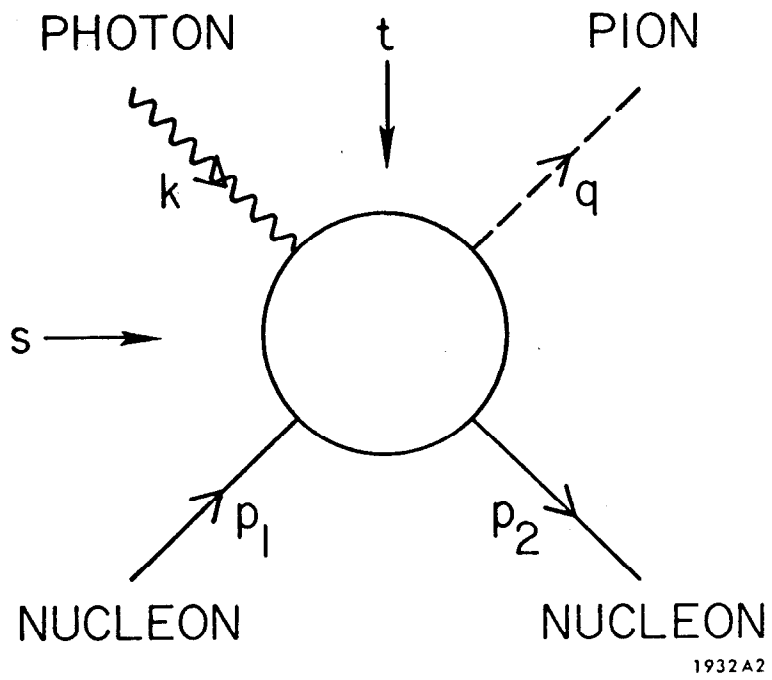

Fig. 2

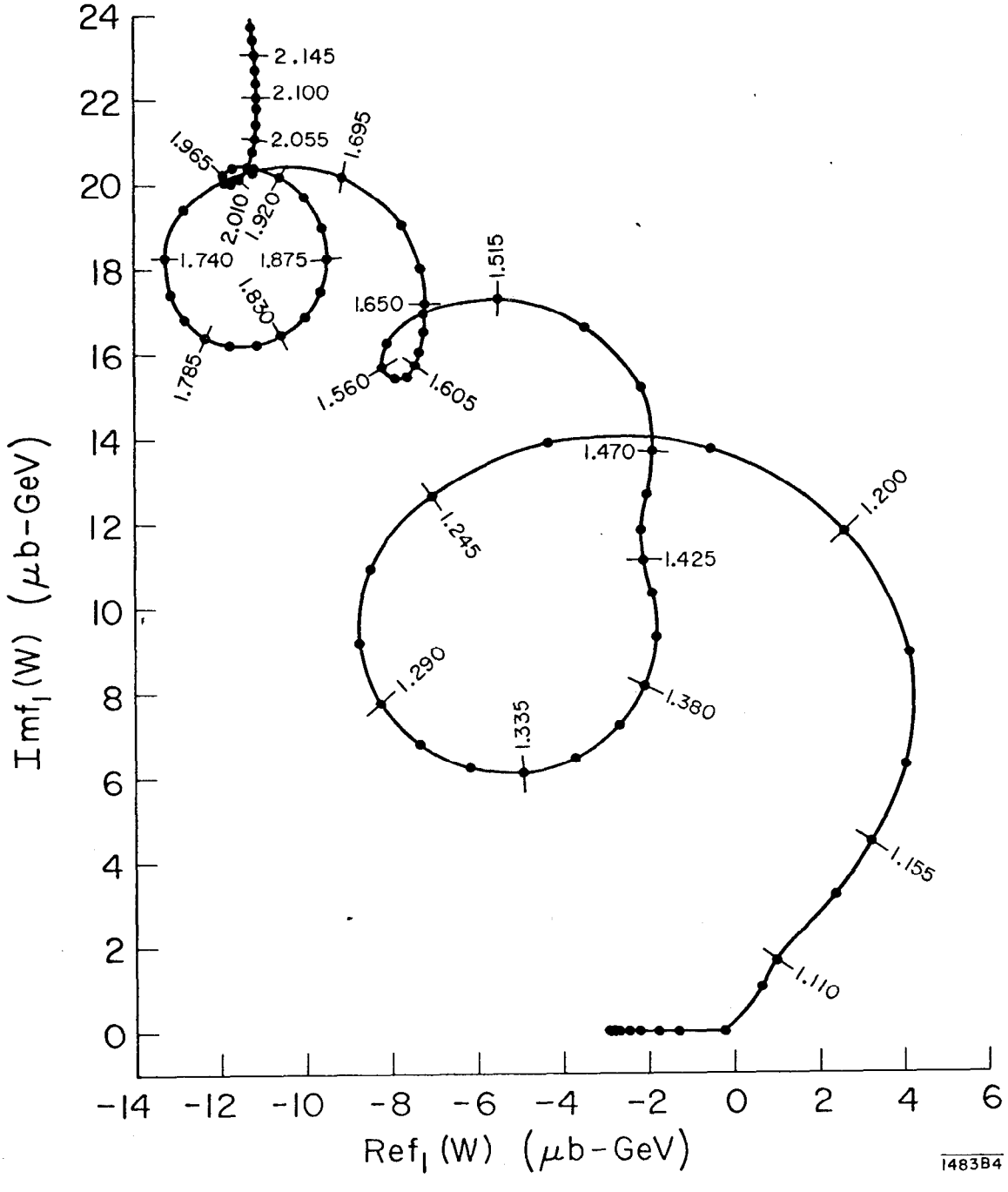
24
22
20
18
16
14
12
10
8
6
4
2
0
-14
-12
-10
-8
-6
-4
-2
0
2
4
6
Imf$_1$(W) (μb-GeV)
Ref$_1$(W) (μb-GeV)
2.145
2.100
2.055
1.965
1.695
2.010
1.920
1.740
1.875
1.830
1.785
1.650
1.515
1.560
1.605
1.470
1.200
1.245
1.425
1.290
1.380
1.335
1.155
1.110
1483B4

Fig. 3

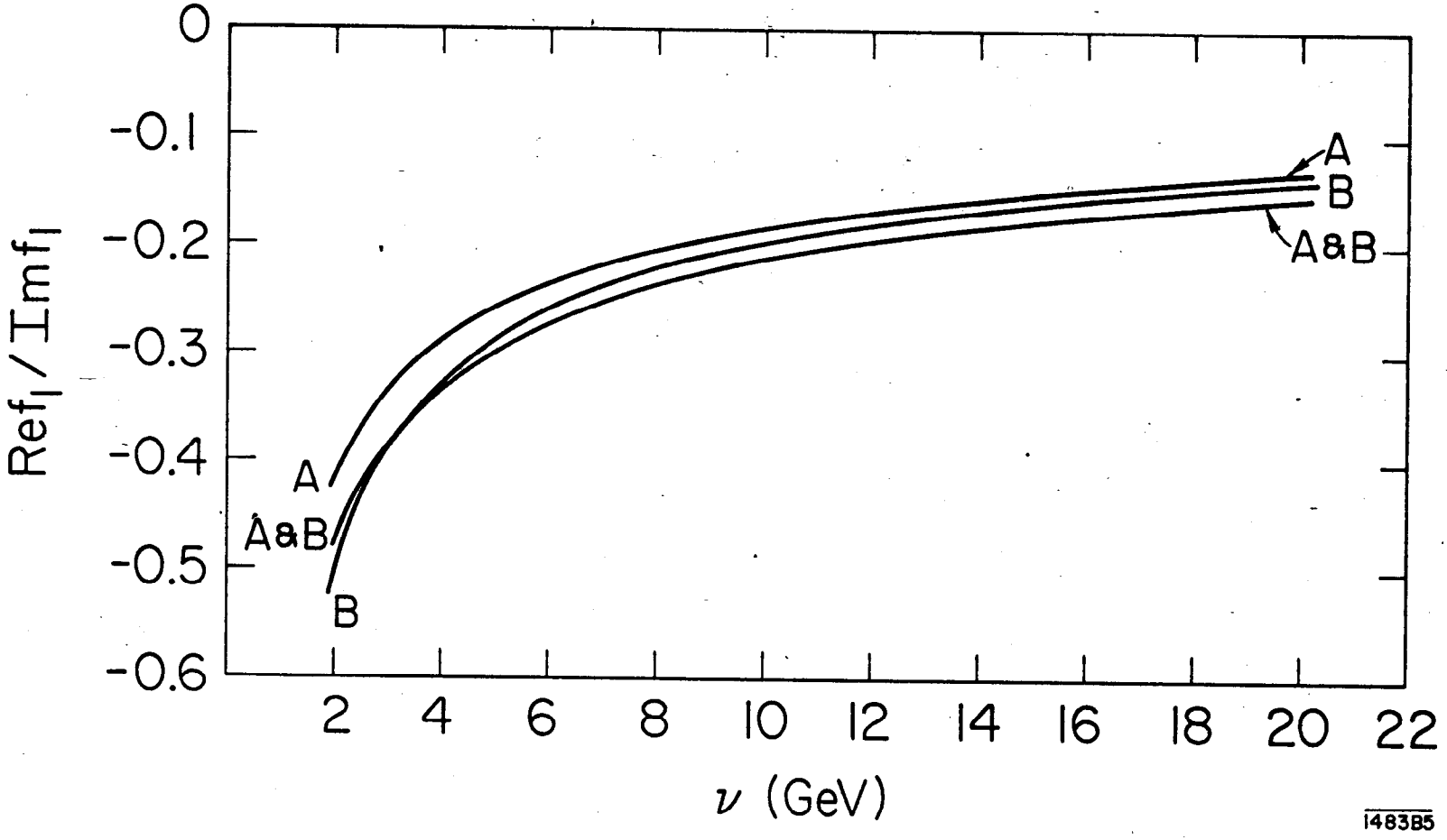
0
-0.1
-0.2
-0.3
-0.4
-0.5
-0.6
Ref$_1$ / Imf$_1$
2
4
6
8
10
12
14
16
18
20
22
ν (GeV)
A
B
A&B
A
A&B
B
1483B5

Fig. 4

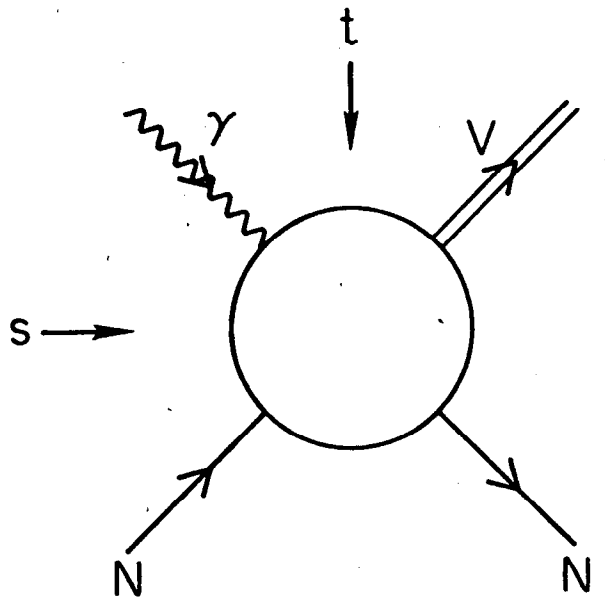

(a)

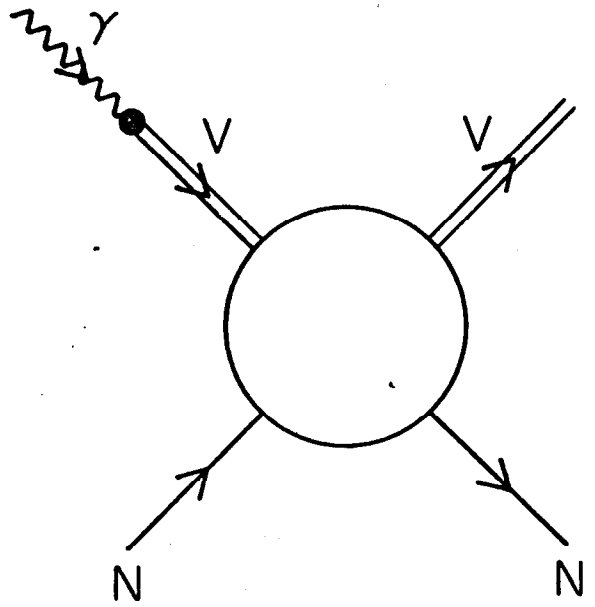

(b)

1932A3

Fig. 5

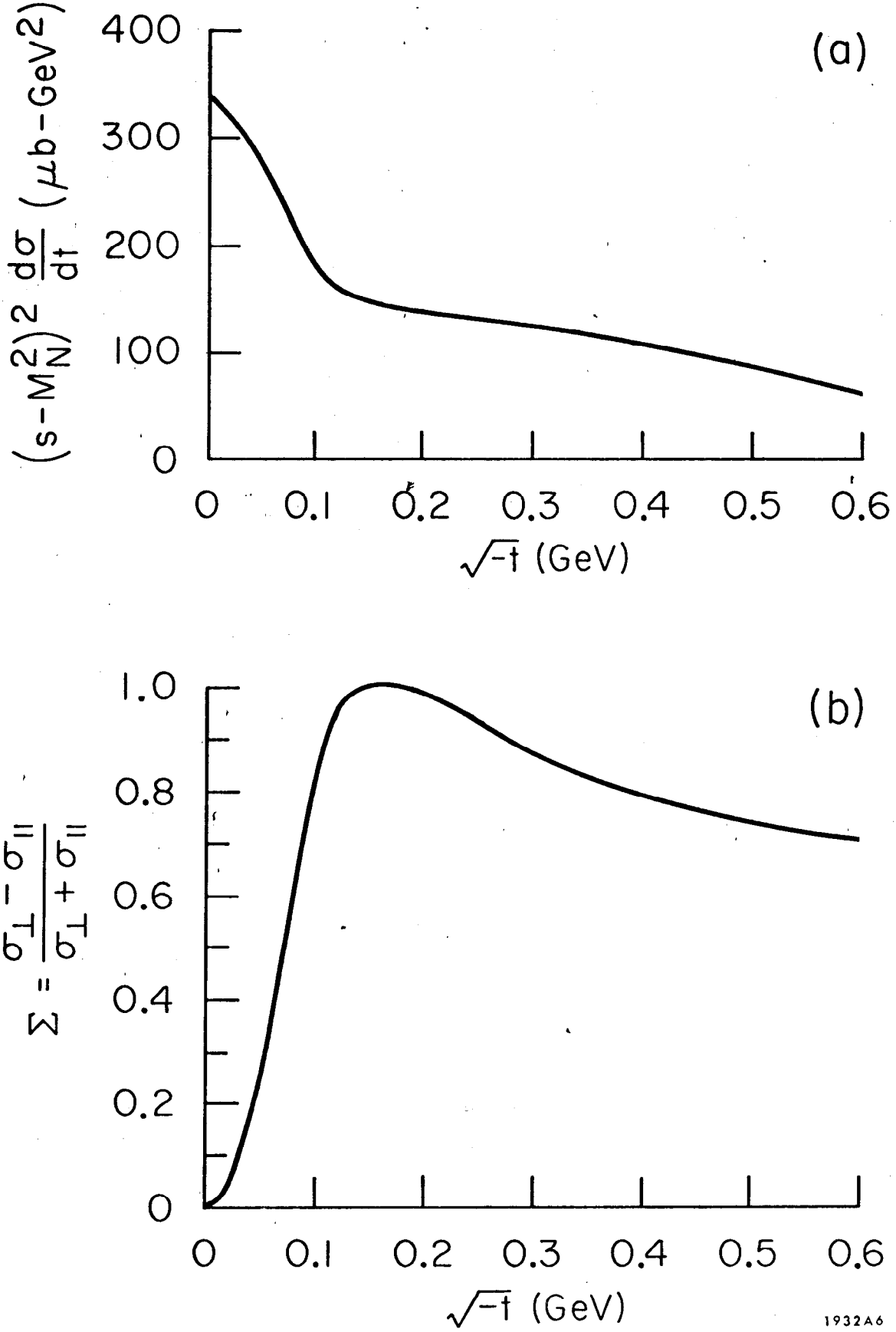
(a)
$(s-M_N^2)^2 \frac{d\sigma}{dt}$ (μb-GeV^2)
400
300
200
100
0
0
0.1
0.2
0.3
0.4
0.5
0.6
$\sqrt{-t}$ (GeV)
(b)
$\Sigma = \frac{\sigma_\perp - \sigma_\parallel}{\sigma_\perp + \sigma_\parallel}$
1.0
0.8
0.6
0.4
0.2
0
0
0.1
0.2
0.3
0.4
0.5
0.6
$\sqrt{-t}$ (GeV)
1932A6

Fig. 6

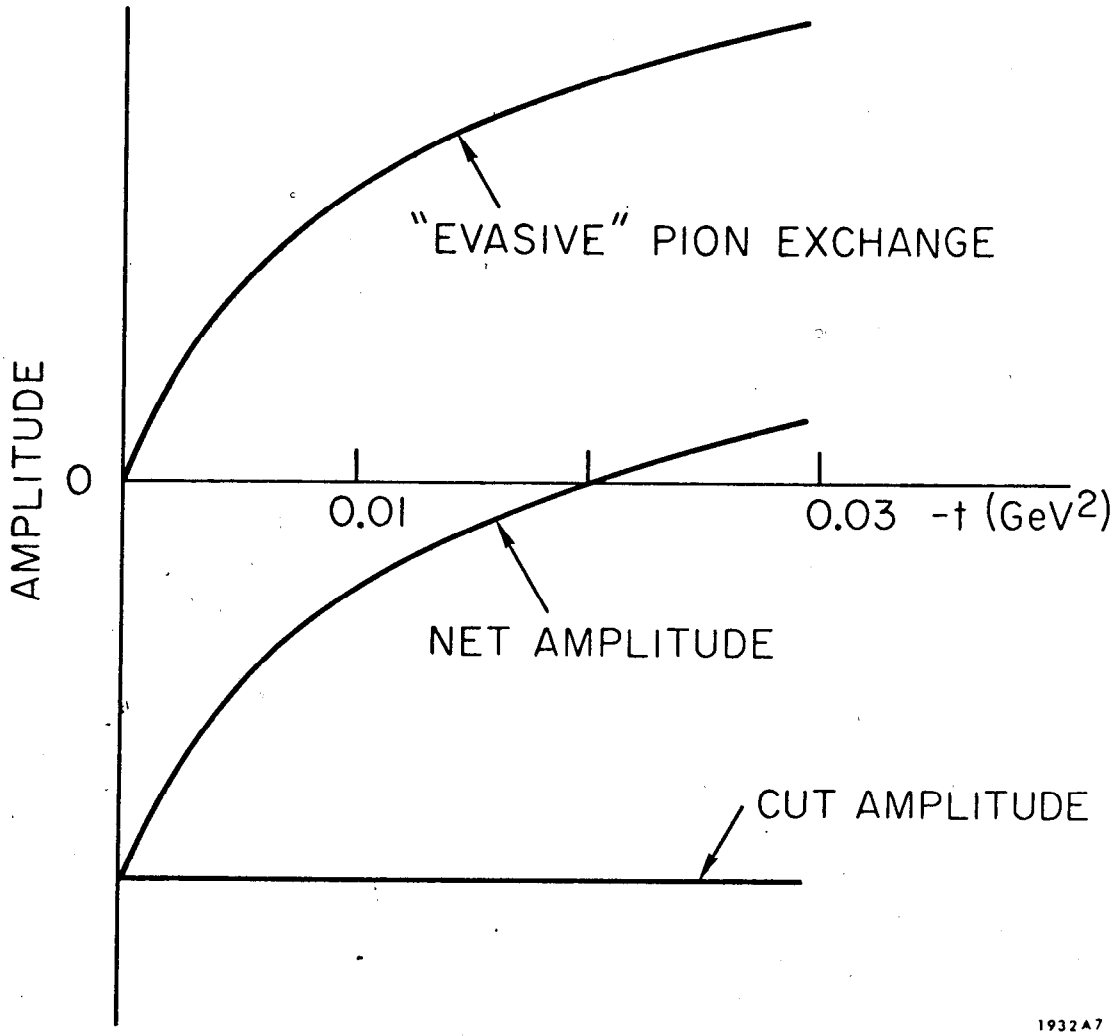
"EVASIVE" PION EXCHANGE
AMPLITUDE
0
0.01
0.03
-t (GeV2)
NET AMPLITUDE
CUT AMPLITUDE
1932A7

Fig. 7

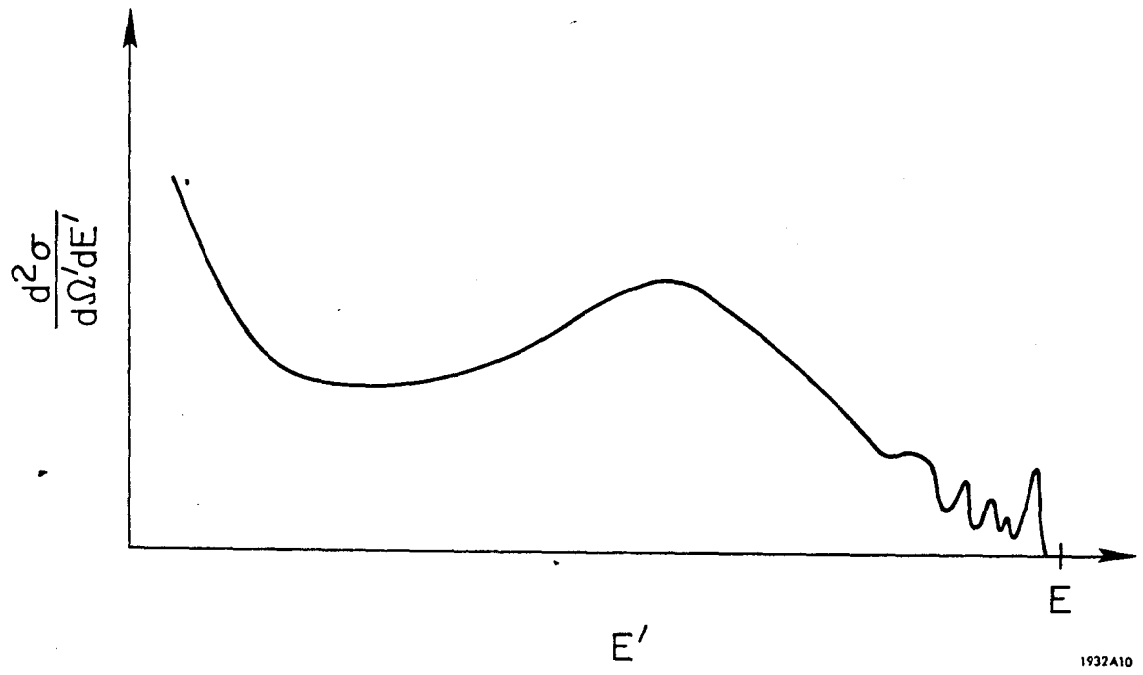

Fig. 8

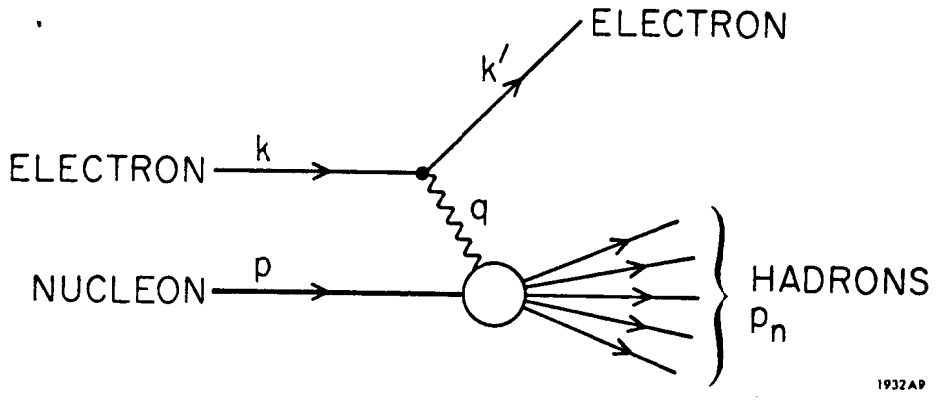

Fig. 9

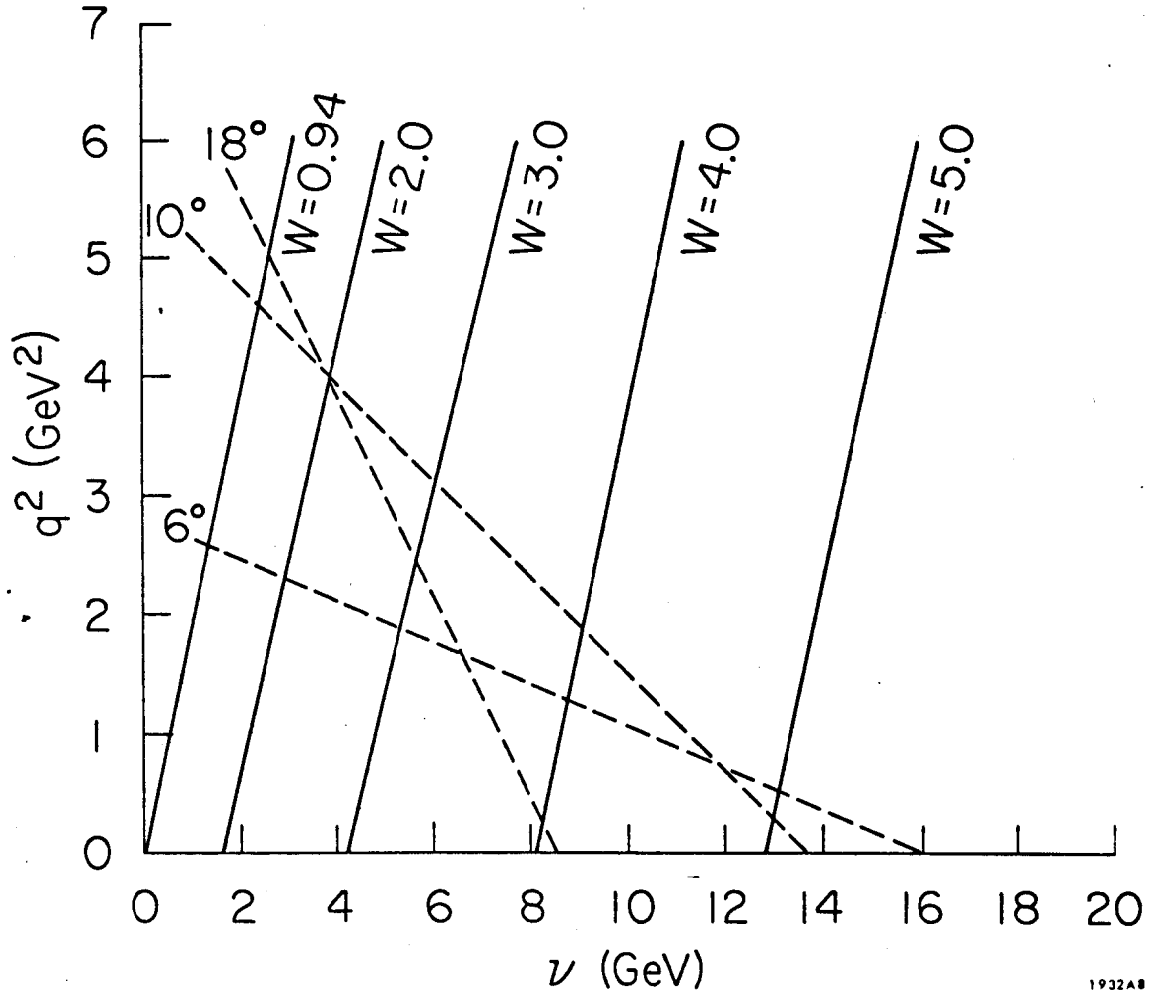
7
6
5
4
3
2
1
0
q^2 (GeV^2)
18°
10°
6°
W=0.94
W=2.0
W=3.0
W=4.0
W=5.0
0 2 4 6 8 10 12 14 16 18 20
ν (GeV)
1932A8

Fig. 10

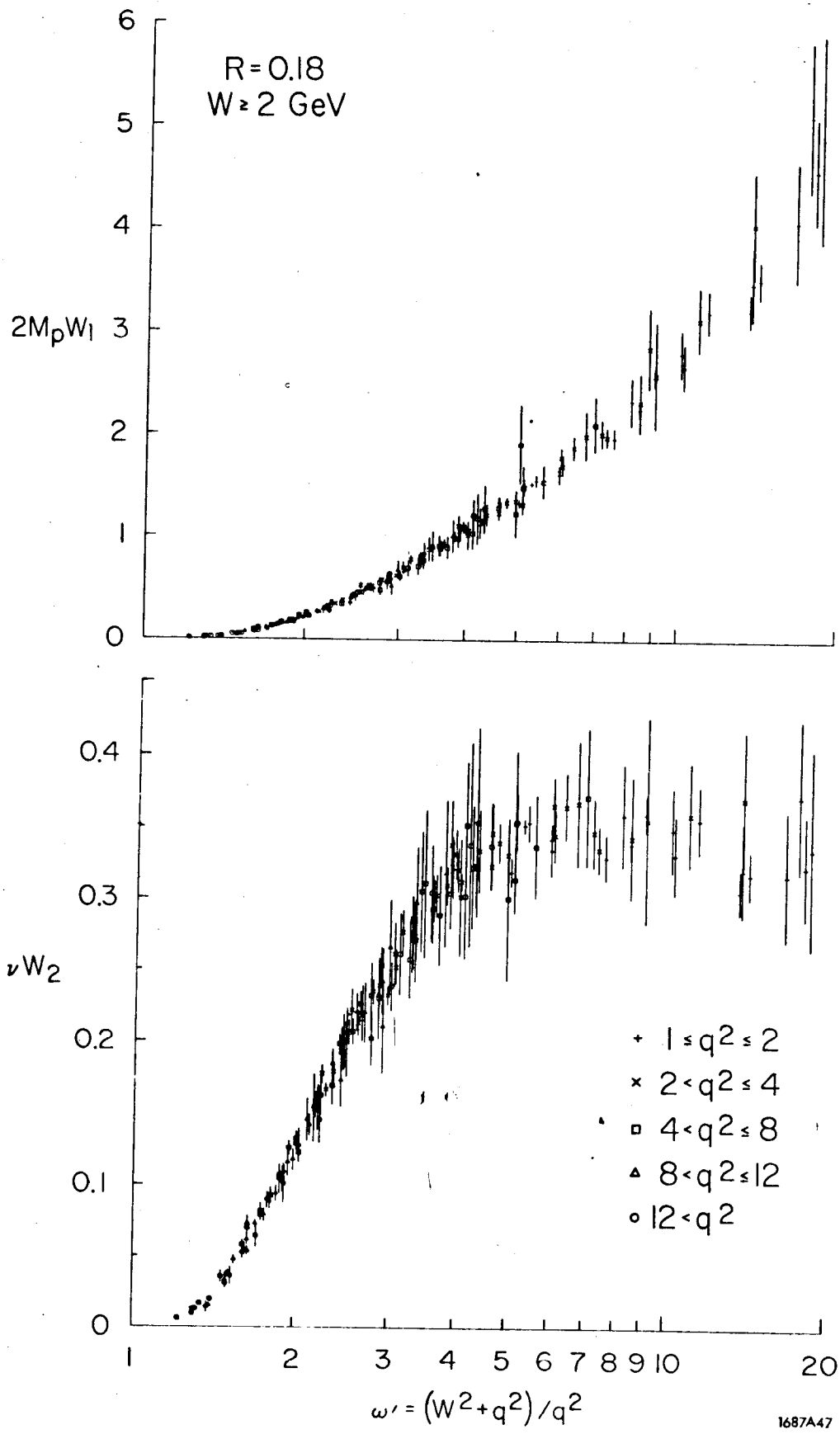
R = 0.18
W ≥ 2 GeV
2MpW1
νW2
+ 1 ≤ q2 ≤ 2
× 2 < q2 ≤ 4
□ 4 < q2 ≤ 8
△ 8 < q2 ≤ 12
○ 12 < q2
ω' = (W2+q2)/q2
1687A47

Fig. 11

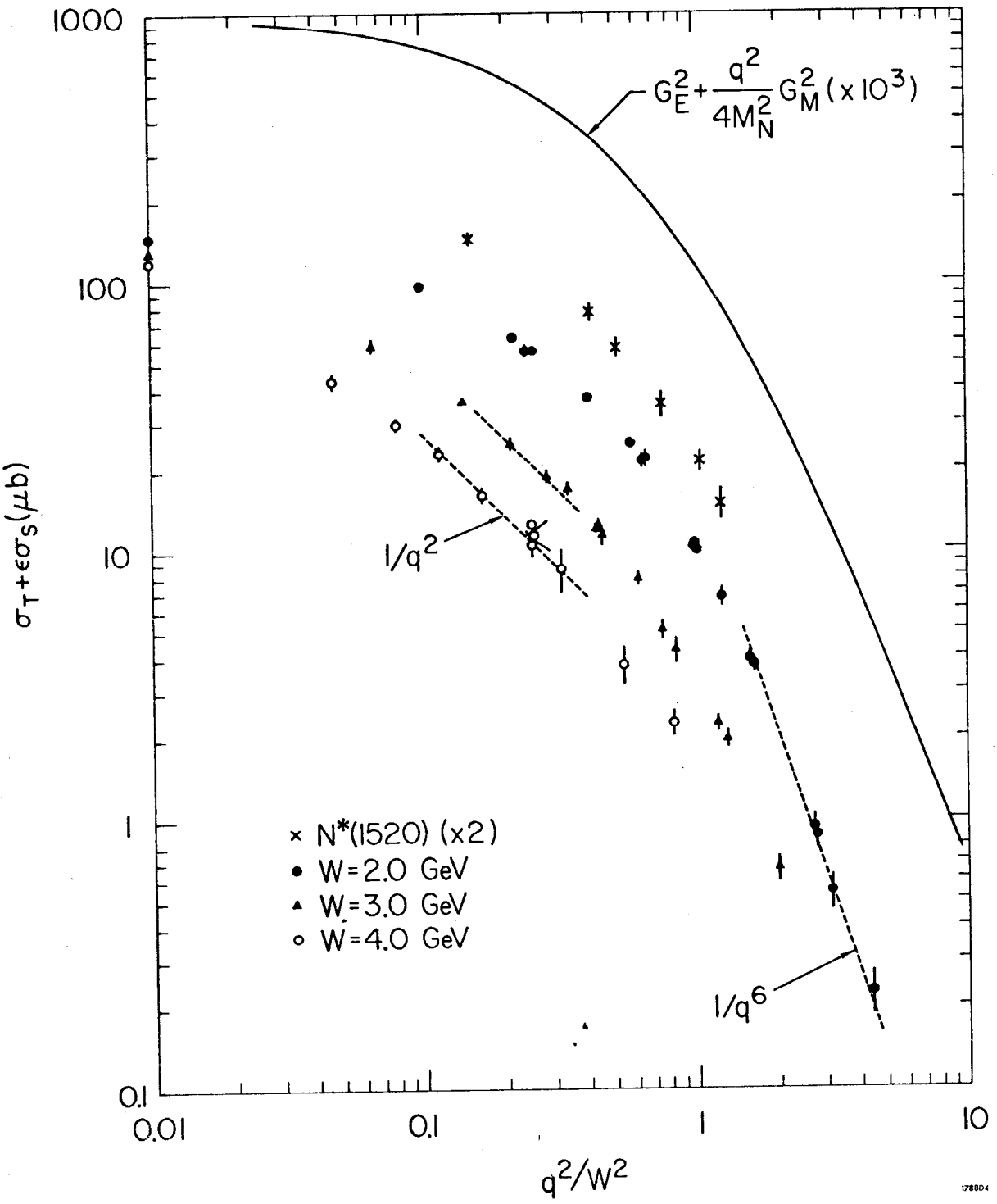
1000
100
10
1
0.1
0.01
0.1
1
10
$\sigma_T+\epsilon\sigma_S(\mu b)$
q^2/W^2
$G_E^2+\frac{q^2}{4M_N^2}G_M^2(\times 10^3)$
$1/q^2$
$1/q^6$
× N*(1520) (x2)
• W=2.0 GeV
▲ W=3.0 GeV
○ W=4.0 GeV

Fig. 12

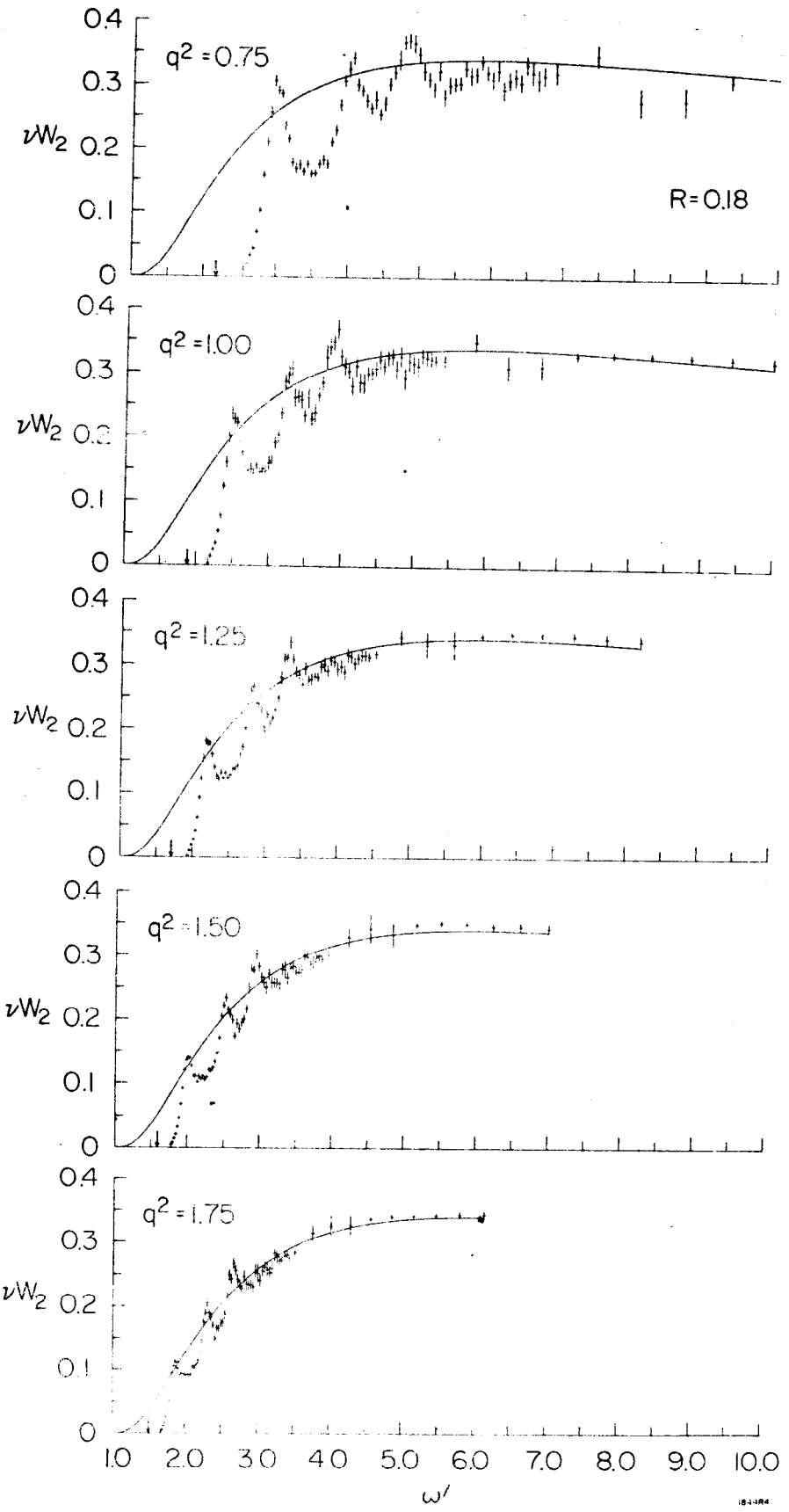
0.4
0.3
νW_2 0.2
0.1
0
$q^2 = 0.75$
R=0.18
$q^2 = 1.00$
$q^2 = 1.25$
$q^2 = 1.50$
$q^2 = 1.75$
1.0 2.0 3.0 4.0 5.0 6.0 7.0 8.0 9.0 10.0
ω'

Fig. 13

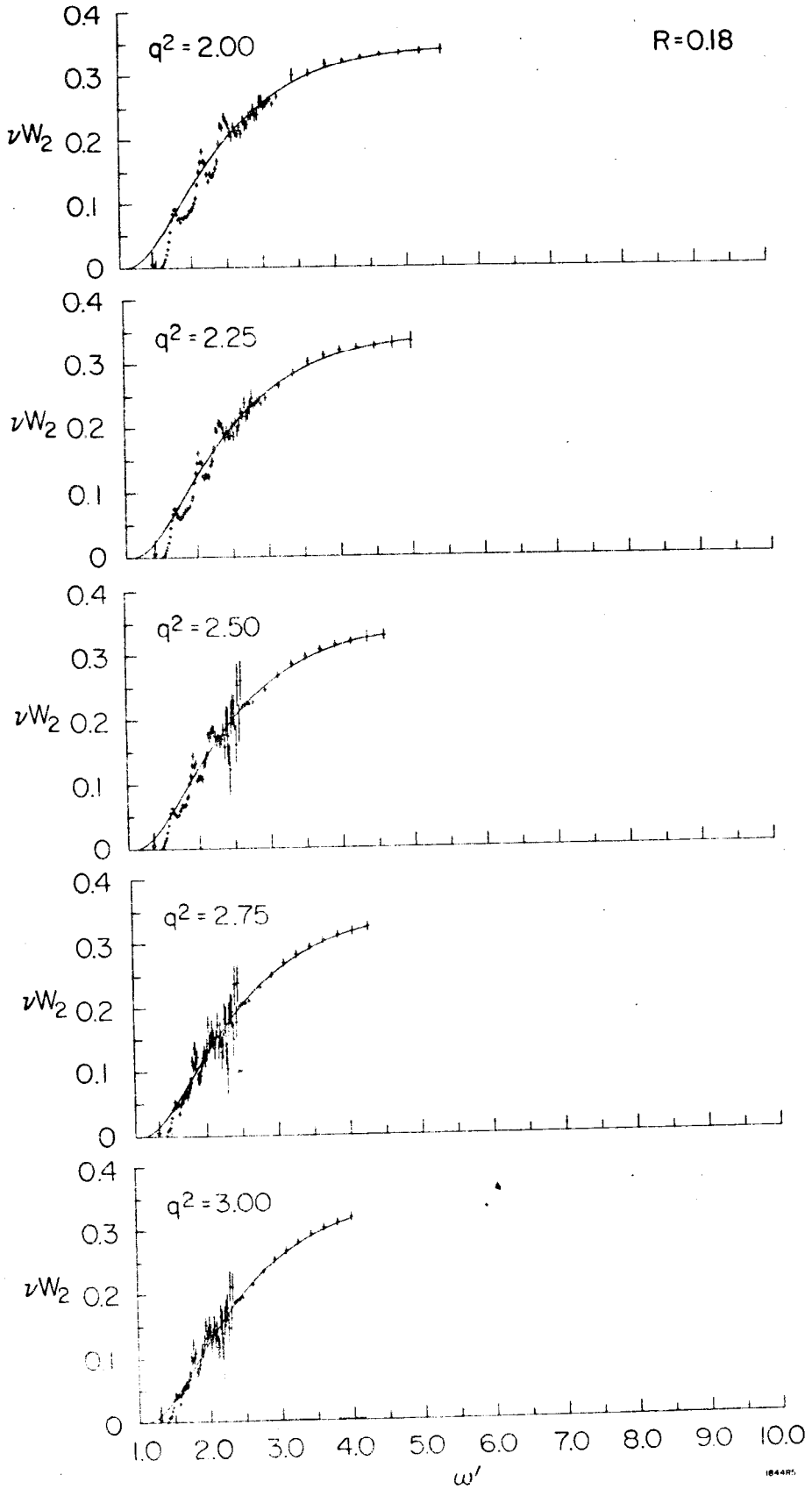
0.4
0.3
νW_2 0.2
0.1
0
$q^2 = 2.00$
R=0.18
$q^2 = 2.25$
$q^2 = 2.50$
$q^2 = 2.75$
$q^2 = 3.00$
1.0 2.0 3.0 4.0 5.0 6.0 7.0 8.0 9.0 10.0
ω'
1844R5

Fig. 14